Vibrational Spectroscopic Studies of Orientationally-Disordered Organic Cage Molecules

by

Nancy T. Kawai

A thesis submitted to the Faculty of Graduate Studies and Research
of McGill University in partial fulfillment of the requirements
for the degree of Doctor of Philosophy

March 1991
Department of Chemistry
McGill University
Montreal, Quebec, Canada

to my parents, Ted and Toshiko Kawai
and my grandmother, Nobuko Kawai

for their encouragement throughout my education

ABSTRACT

The phase behaviour of six orientationally-disordered organic cage molecules, norbornane, norbornylene, norbornadiene, quadricyclane, bicyclooctene, and fluoroadamantane, has been characterized by differential scanning calorimetry, and variable-temperature and -pressure infrared and Raman spectroscopy. All of these compounds undergo one or more solid-solid phase transitions on cooling from disordered phases to ordered, crystalline structures, except for fluoroadamantane, which forms a glass. The phases of all these solids under high pressure have been shown to be the same as those formed at low temperatures.

A method of using pressure dependences of vibrational modes to aid in making spectral assignments is proposed, which proved to be very useful in classifying C-H stretching vibrations and modes which have large contributions from skeletal stretching motions. A semiquantitative analysis of the effect of pressure on different types of stretching vibrations is described.

RÉSUME

Le comportement de phase de six molécules organiques cages d'orientations désordonnées, le norbornane, le norbornylène, le norbornadiène, le quadricyclane, le bicyclooctène, et le fluoroadamantane, a été caractérisé par calorimétrie différentielle à balayage, ainsi que par spectroscopies Raman et infrarouge à température et pression variables. En refroidissant, tous ces composés montrent une ou plusieurs transitions de phases solide-solide au passage de phases désordonnées vers des structures cristallines ordonnées, sauf pour le fluoroadamantane, qui se vitrifie. Il est démontré que les phases de tous ces solides à pression élevée sont les mêmes que celles formées à basses températures.

Une méthode d'attribution des spectres utilisant la dépendance des modes vibrationnels sur la pression est proposée et apparaît très utile dans la classification des vibrations d'étirements C-H et des modes ayant une grande contribution des mouvements d'étirements C-C. Une analyse semi-quantitative de l'effet de la pression sur les différents types de vibrations d'étirements est décrite.

ACKNOWLEDGEMENTS

I would like to express my deepest appreciation to Professors Ian Butler and Denis Gilson for their indispensible guidance and support throughout the course of this work. I am particularly grateful to Professor Gilson for his patience and encouragement during the writing of this thesis.

I am indebted to the Natural Sciences and Engineering Research Council of Canada for providing financial support in the form of a postgraduate scholarship.

I would also like to thank:

my colleagues in this line of research, Mr. Y. Huang and Dr. J. Haines, for many enjoyable and enlightening discussions;

Mr. S. M. Barnett, for proofreading this thesis, and for his assistance with the FT-Raman work;

Prof. P. G. Farrell and his co-workers for the synthesis of 1-fluoroadamantane and the cubane derivatives;

Dr. J. Britten for teaching me the practical aspects of x-ray crystallography;

Drs. E. Gabe and Y. Lepage (X-Ray Diffraction Laboratory, National Research Council of Canada, Ottawa) for collecting the x-ray diffraction data for 1,4-dibromocubane;

Prof. M. Kamal (Dept. of Chemical Engineering) for allowing me the use of his DSC-7C instrument;

Prof. D. N. Harpp and his students for the use of the gas chromatograph,

Prof. B. J. Chin and his students for access to their computer and laser printer facilities;

Messrs. R. Rossi, G. di Rudolpho, R. Gaulin, A. Kluck, and W. Bastien, for their technical expertise;

Mr. Gaetan Caron for kindly translating the abstract into French;

and all of my friends in laboratories 335 and 406 who have made my graduate-school years memorable.

Finally, I would like to thank Stephen, Stanley, and Alexandra, for their love and moral support through all stages of this thesis.

LIST OF ABBREVIATIONS

The following abbreviations have been used in this thesis:

BCO *or* bicyclooctane	bicyclo[2.2.2]octane
BCOE *or* bicyclooctene	bicyclo[2.2.2]oct-2-ene
DAC	diamond anvil cell
DSC	differential scanning calorimetry
DTA	differential thermal analysis
fluoroadamantane	1-fluoroadamantane
IQNS	incoherent quasielastic neutron scattering
IR	infrared
NBA *or* norbornane	bicyclo[2.2.1]heptane
NBD *or* norbornadiene	bicyclo[2.2.1]hepta-2,5-diene
NBE *or* norbornylene	bicyclo[2.2.1]hept-2-ene
NMR	nuclear magnetic resonance

NOTE ON UNITS

The following units have been used in this thesis for historical reasons. Their definitions and SI equivalents are given below:

physical quantity	symbol	SI unit	unit used
wavenumber	$\bar{\nu}$	m^{-1}	cm^{-1} (= 100 m^{-1})
pressure	p	Pa (N m^{-2})	kbar (= 10^8 Pa)
force constant	k	N m^{-1}	dyne cm^{-1} (= 10^3 N m^{-1})
transition volume	ΔV_t	m^3 mol^{-1}	cm^3 mol^{-1} (= 10^{-6} m^3 mol^{-1})
bond length	r	m	Å (= 10^{-10} m)

In the text of this thesis, the unit of vibrational wavenumber is often referred to as vibrational frequency (ν). These quantities are directly proportional to one another, $\nu = c\bar{\nu}$, where c is the speed of light.

TABLE OF CONTENTS

CHAPTER 5. QUADRICYCLANE

CHAPTER 6. BICYCLOOCTENE

CHAPTER 7. 1-FLUOROADAMANTANE

CHAPTER 8. A STRUCTURAL STUDY OF 1,4-DIBROMO- AND 1,4-DIIODOCUBANE IN THE SOLID STATE

CHAPTER I. ORIENTATIONALLY-DISORDERED SOLIDS

Many different types of compounds exhibit orientational disorder in the solid state.[1] It was Timmermans who began the study of a group of orientationally-disordered solids which he called "plastic crystals",[2] whose fundamental characteristic was a low entropy of fusion (< 2.5 R or 21 J K^{-1} mol^{-1}). Other attributes of plastic crystals have also been defined.[3] The molecules are often "globular" in that they possess spherical geometry or could form a sphere upon rotation about an axis. The crystal structures of plastic phases are highly symmetric, cubic or hexagonal close-packed. In terms of macroscopic properties, these solids are characterized by low entropies and volumes of fusion, but high melting and triple points. The vapour pressures are also high, causing plastic crystals to sublime readily when heated. They are highly malleable, and deform easily under their own weight. Most plastic crystals lose their orientational disorder during one or more phase transitions below the melting temperature.

The techniques that have been used to study the phases of solids which exhibit orientational disorder are diverse. Calorimetry has been the starting point of many studies; the measurement of transition temperatures and enthalpies is imperative in the study of disordered solids. Nuclear magnetic resonance (NMR) spectroscopy and neutron scattering studies are useful in investigating the molecular motions occurring in the disordered phase. Vibrational spectroscopy and x-ray diffraction can be used to study structural aspects of the various solid phases of these materials.

The number of compounds that have been classified as having plastically-crystalline phases is considerable, spanning inorganic and organic molecules; linear, non-linear, and globular shapes; and rigid and flexible structures.[4] A considerable amount of data has been collected for organic plastic crystals in particular. The upper limit on the entropy of fusion of 2.5 R applies to most of these compounds. The entropy of the phase transition is generally considerably higher than that of melting, indicating that the main disordering process occurs from ordered to disordered solid rather than from disordered solid to liquid. The phase transition is usually first order and is often accompanied by a large temperature hysteresis. Some thermodynamic data are given in Table 1.1 for a few organic plastic crystals. Within this subclass of disordered solids, a thermodynamic trend has been observed: the transition enthalpy, ΔH_t, decreases as the temperature range of the plastic phase increases.[5] Of particular interest are the rigid organic cage compounds which fit the "globular" theme. The classic example of this group is adamantane (tricyclo[3.3.1.1]decane, $C_{10}H_{16}$), many derivatives of which have previously been investigated in this laboratory.[6,7]

Table 1.1. Thermodynamic Data for Some Organic Plastic Crystals.[1]

compound	T_f K	ΔS_f J K^{-1} mol^{-1}	T_t K	ΔS_t J K^{-1} mol^{-1}
carbon tetrachloride	250	10.1	226	20.4
cyclohexane	280	9.3	186	36.0
adamantane	~543		209	16.2
bicyclo[2.2.2]octane	448	18.7	164	27.9

The motions that occur within an orientationally-disordered solid phase can be quantified by studying rotational and lattice diffusion processes. Nuclear magnetic resonance spectroscopy and radioisotope diffusion have been used to investigate translational diffusion, while NMR and quasielastic neutron scattering provide information on the rotational process. Nuclear magnetic resonance has usually been the technique chosen to study lattice diffusion in plastic crystals[8-12] since measurements can be made on the bulk solid rather than on single crystals which are needed for radiotracer experiments.[13,14] The measurement of spin relaxation rates by NMR spectroscopy can provide both rotational and lattice diffusion rates since they are typically five orders of magnitude in difference, and their contributions can be easily separated. In earlier studies of organic plastic crystals, the results have been interpreted in terms of a random-walk model for diffusion in polycrystalline samples.[8,9] The experimental results, however, were found to be consistent with this model only for plastic crystals with relatively high entropies of fusion (*e.g.* hexamethylethane and adamantane). Later studies revealed that a monovacancy diffusion mechanism,[11,13] or an isotropic diffusion mechanism[10] provided better correlation to experimental data for solids of both high and low fusion entropies. The mean jump time or correlation time for self-diffusion, τ_1, in plastically-crystalline phases is of the order of 10^{-6} to 10^{-7} s.

In a crystal, molecular rotations occur much faster than do translational motions. In plastic crystals, the reorientational correlation time, τ_2, can be up to 10^{-12} s, which is at the upper limit of NMR spectroscopic measurements. Scattering measurements are on a much faster timescale; incoherent quasielastic neutron scattering (IQNS) is most useful in characterizing motions occurring on the 10^{-11} to 10^{-13} s timescale.[15,16] Molecular reorientation within a lattice can occur by different mechanisms: (1) isotropic rotation, (2) rotational diffusion, or (3) jump reorientation. Free rotation is thought to be unlikely in solid phases due to strong intermolecular interactions. Recently, however, free or quasi-isotropic rotation has been shown to occur in the plastic phases of norbornane, norbornylene, and norbornadiene by IQNS.[15] From NMR studies, isotropic rotation was also believed to occur in high symmetry, tetrahedral or octahedral molecules.[12] However, x-ray and IQNS studies have shown that the rotational jump model is more fitting for adamantane.[17,18]

Molecular motions can also be observed by Brillouin and Rayleigh scattering techniques,[19-21] and by measuring infrared (IR) and Raman linewidths.[21-25] Rotational correlation times can be derived from linewidth measurements of the Rayleigh line or other vibrational bands, but the components of different polarizations must be separated. Brillouin lines, which arise from the interaction of the incident light with transverse and longitudinal phonons in the crystal, can be used to measure the elastic constants of a crystal. These types of measurements, however, require oriented single crystals of the plastic phases.

Structural information on disordered solids can be derived from x-ray diffraction, although the disorder results in diffuse scattering. Single crystal studies have been successfully performed on several plastic crystals.[26] Rotational models have been incorporated into the structure determination process to account for the diffuse pattern.[27] Upon cooling to the ordered phase, however, crystals of disordered solids often crack, and single crystals must be grown directly at low temperatures. Because of the difficulty in handling single crystals of volatile disordered solids, powder diffraction methods have been used extensively to determine the structure of plastic crystals.[28] Although the exact space group cannot be pinpointed, cell symmetry and unit cell parameters can be uncovered. It is clear that an easier method of obtaining structural information on disordered and ordered phases is desirable. Even more convenient is a method of analysis which divulges dynamic and structural information, and can be performed with a minimum of sample handling.

Vibrational spectroscopy has the advantage over many methods in the study of disordered phases in that the timeframe of IR and Raman measurements is between that of diffraction methods and NMR spectroscopy.[29] The degree of molecular motions can be observed by vibrational linewidths and the contour of the low-frequency region. Structural information of the ordered phase can also be derived from solid-state splitting effects which appear upon cooling through the phase transition. In addition, these studies need not be performed on single crystals.

In this thesis, several rigid organic cage compounds which form plastic crystals were analyzed by differential scanning calorimetry (DSC) and vibrational spectroscopy. The calorimetric method was employed to measure transition temperatures and thermodynamic parameters, and to observe hysteresis effects. Low-temperature IR and Raman spectra were then measured to observe the structural changes that occur as a result of the phase transition. Subsequently, the behaviour of these solids under pressure was investigated by high-pressure IR and Raman spectroscopy. The structural changes that occur at high pressures were compared to the low-temperature effects. The pressure dependences of the vibrational modes were measured in both phases, and comparisons were made between different types of vibrations and compounds. Other pressure-induced effects such as the change in vibrational coupling were also investigated.

The thesis is divided into chapters according to each compound. Chapter 2 describes the experimental methods as well as the information that can be obtained from the measured data, and Chapter 3 provides the details of the experiments performed. Three seven-carbon cages with related structures, norbornane, norbornylene, and norbornadiene, are discussed in Chapter 4, which also includes a comparison of the three molecules. The phase behaviour of another seven-carbon cage compound, quadricyclane, is presented in Chapter 5. Chapters 6 and 7 describe similar experiments on two other plastic crystals, bicyclooctene and 1-fluoroadamantane, respectively. The phase behaviour of two derivatives of cubane, 1,4-dibromo- and 1,4-diiodocubane, were also studied. These compounds were determined not be orientationally disordered, but their interesting structures warranted a single-crystal x-ray diffraction study, as well as the analysis of their solid-state vibrational spectra. These results are presented in Chapter 8. Finally, some general conclusions concerning all the disordered compounds, and, in particular, the high-pressure vibrational spectroscopic results, will be made in Chapter 9.

References

1. N. G. Parsonage and L. A. K. Staveley, *Disorder in Crystals*, Clarendon Press, Oxford, 1978.
2. J. Timmermans, J. Chim. Phys., **35**, 25 (1938).

3. G. W. Smith in *Advances in Liquid Crystals*, vol. 1, (G. H. Brown, ed.), Academic Press, New York, 1975, p. 189.

4. J. N. Sherwood, ed., *The Plastically Crystalline State (Orientationally-Disordered Crystals)*, Wiley-Interscience, Chichester, 1979.

5. C. N. R. Rao, Proc. Indian Acad. Sci., **94**, 181 (1985)

6. P. D. Harvey, Ph. D. Thesis, McGill University, Montreal, Quebec, Canada, 1986

7. R. M. Paroli, Ph. D. Thesis, McGill University, Montreal, Quebec, Canada, 1989.

8. R. Folland, S. M. Ross, and J. H. Strange, Mol. Phys., **26**, 27 (1973).

9. R. Folland, R. L. Jackson, J. H. Strange, and A. V. Chadwick, J. Phys. Chem. Solids, **34**, 1713 (1973)

10. N. Boden, J. Cohen, and R. T. Squires, Mol. Phys., **31**, 1813 (1976).

11. A. R. Britcher and J. H. Strange, Mol. Phys., **37**, 181 (1979).

12. N. Boden in *The Plastically Crystalline State*, (J. N. Sherwood, ed.), Wiley-Interscience, Chichester, 1979, Chap. 5, p. 147.

13. A. V. Chadwick and J. W. Forrest, J. Chem. Soc., Faraday Trans I., **74**, 2560 (1978).

14. J. N. Sherwood in *The Plastically Crystalline State*, (J. N. Sherwood, ed.), Wiley-Interscience, Chichester, 1979, Chap. 2, p. 39.

15. M. Bee, J. Chim. Phys., **82**, 205 (1985).

16. M. Bee, J. L. Sauvajol, A. Hedoux, and J. P. Amoureux, Mol. Phys., **55**, 637 (1985).

17. A. J. Leadbetter and R. E. Lechner in *The Plastically Crystalline State*, (J. N. Sherwood, ed.), Wiley-Interscience, Chichester, 1979, Chap. 8, p. 285.

18. J. P. Amoureux, M. Bee, and J. C. Damien, Acta Crystallogr., **B36**, 2633 (1980).

19. A. J. Hyde in *The Plastically Crystalline State*, (J. N. Sherwood, ed.), Wiley-Interscience, Chichester, 1979, Chap. 6, p. 215.

20. R. Folland, D. A. Jackson, and S. Rajagopal, Mol. Phys., **30**, 1053 (1975).

21. R. Folland, D. A. Jackson, and S. Rajagopal, Mol. Phys., **30**, 1063 (1975).

22. R. T. Bailey in *The Plastically Crystalline State*, (J. N. Sherwood, ed.), Wiley-Interscience, Chichester, 1979, Chap. 7, p. 233.

23. M. Debeau and P. Depondt, J. Chim. Phys., **82**, 232 (1985).

24. J. L. Sauvajol, J. Chim. Phys., **82**, 219 (1985).

25. J. L. Sauvajol and M. More, J. Phys. (Orsay, Fr.), **47**, 2075 (1986).

26. R. Fouret in *The Plastically Crystalline State*, (J. N. Sherwood, ed.), Wiley-Interscience, Chichester, 1979, Chap. 3, p. 85.

27. J. P. Amoureux, M. Bee, and J. C. Damien, Acta Crystallogr., **B36**, 2633 (1980).

28. W. J. Dunning in *The Plastically Crystalline State*, (J. N. Sherwood, ed.), Wiley-Interscience, Chichester, 1979, Chap. 1, p. 1.

29. H. L. Strauss, J. Mol. Struct., **126**, 177 (1985).

CHAPTER 2. METHODS USED TO STUDY DISORDERED SOLIDS

2.1 Calorimetric Measurements

Phase transitions are ordering processes for which the transition entropy, ΔS_t, can be split into contributions from several components:[1]

$$\Delta S_t = \Delta S_{pos} + \Delta S_{orien} + \Delta S_{conf} + \Delta S_{vol} \qquad [2.1.1]$$

These components are positional, orientational, and configurational entropies, and the entropy change due to a decrease in intermolecular spacing or volume change. When a liquid freezes to a crystalline solid, all forms of ordering can occur and entropy is lost. When a liquid transforms to a plastically-crystalline solid, however, positional ordering occurs, and intermolecular distances also decrease, but orientational and configurational ordering are minimal. Only at the order-disorder phase transition does the crystal lose these other forms of entropy, along with a further decrease in crystal volume. The molecules studied in this thesis are all rigid, and as such, do not have any configurational entropy contributions.

At the phase transition, the Gibbs free energies of two phases are equal at constant pressure. It then follows that, for solid phases:[1]

$$\left(\frac{\delta G}{\delta T}\right)_p = - S \qquad [2.1.2]$$

$$\left(\frac{\delta G}{\delta p}\right)_T = - V \qquad [2.1.3]$$

$$\left(\frac{\delta H}{\delta T}\right)_p = C_p \qquad [2.1.4]$$

and

$$\alpha_s = \frac{1}{Vs}\left(\frac{\delta V_s}{\delta T}\right)_p \qquad [2.1.5]$$

$$\kappa_s = - \frac{1}{V_s}\left(\frac{\delta V_s}{\delta p}\right)_T \qquad [2.1.6]$$

where α_s and κ_s are the thermal expansion and isothermal compressibility coefficients, respectively. Phase transitions have been defined as n^{th} order when the n^{th} derivative of $(\delta G/\delta T)_p$ is discontinuous.[2,3] Thus, a first-order phase transition has continuous free energy and discontinuous enthalpy, entropy and heat capacity curves. A second-order phase transition will have continuous free energy, enthalpy and entropy curves, but a discontinuous heat capacity curve. Solid-solid phase transitions are often characterized as lambda transitions due to the shape of the heat capacity versus temperature curve resembling the Greek letter, λ.[1]

An interesting phenomenon which is associated with solid-solid transitions is hysteresis, *i.e.*, when a reversible transition occurs at a higher temperature in the heating cycle than in the cooling cycle. This effect can be explained in terms of nucleation and strain effects.[1] Assume that a phase transition occurs from solid **1** to solid **2** upon cooling. At the transition point, small nuclei of solid **2** begin to form within solid **1**. Because the crystal volume of **2**, V_2, is less than that of **1**, V_1, these nucleation sites are formed under tension due to the properties of **1**. Similarly, upon heating through the transition, pockets of solid **1** are formed under tension from solid **2**. The free energies of these hybrid crystals at the transition point depend upon the internal surface energy at the boundaries between the two structures, σ_{12}, and the compressive or tensile energy caused by the matrix, χ_{12}. Consider a situation where a fraction of crystals x of solid **1** exists in a fraction of crystals (1-x) of solid **2**. This is shown pictorially in Figure 2.1.1. The free energy of a hybrid crystals is:

$$G_{hybrid} = x\, f_1(p, T, \sigma_{12}, \chi_{12}) + (1-x)\, f_2(p, T, \sigma_{12}, \chi_{12}) \qquad [2.1.7]$$

If the newly forming crystal substance is symbolized by a square bracket, [ ], while the residual substance is written without a bracket, at equal values of x, the free energies of the two hybrid crystals are:

$$G_{hybrid} = x\, f_1(p, T, [\sigma_{12}], [\chi_{12}]) + (1\text{-}x)\, f_2(p, T, \sigma_{12}, \chi_{12}) \qquad [2.1.8]$$

and

$$G_{hybrid} = x\, f_1(p, T, \sigma_{12}, \chi_{12}) + (1\text{-}x)\, f_2(p, T, [\sigma_{12}], [\chi_{12}]) \qquad [2.1.9]$$

These free energies will not be the same because of the bracketed and nonbracketed terms. Since $V_1 > V_2$, then $[\chi_{12}] > \chi_{12}$. However, differences between $[\sigma_{12}]$ and σ_{12} are more difficult to ascertain, since these depend on the interfacial area at the crystal boundaries. In any case, these differences result in hysteresis of the phase transition, the hysteresis being larger for the greatest differences between unit cell structures of **1** and **2**.

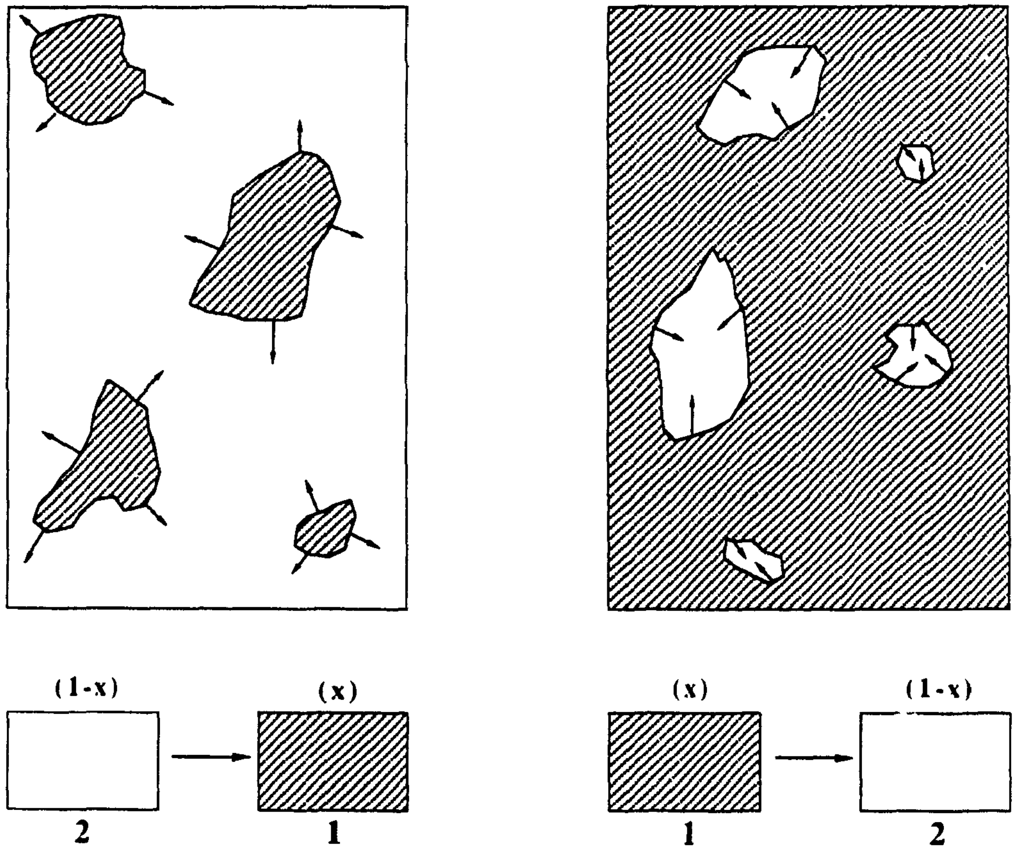

Figure 2.1.1. Hybrid single crystals of solid **1** and solid **2** at the transition point, where $V_1 > V_2$.[1]

The measurement of thermodynamic quantities can be achieved by calorimetry. Adiabatic calorimetry can be performed to measure the heat capacity of a substance, C_p, as it transforms from one phase to another. Another method is differential thermal analysis (DTA).[4] In this case, the difference in temperature between a sample and a reference under identical heating conditions is measured. The resulting thermogram is thus a difference in temperature plotted against time (or temperature of one sample). Differential thermal analysis is particularly useful in analyzing thermal stabilities of materials. The need to measure thermodynamic quantities resulted in the development of calorimetric or quantitative DTA instruments. One group of these instruments is based upon recording the energy difference required to maintain a sample and a reference at equal temperature; this technique is known as differential scanning calorimetry (DSC).[5] The main advantages of this type of apparatus are:[6]

(a) It has an extremely low inertia, and a wide range of heating rates can be used.

(b) It has high sensitivity, with reproducibility >2% and accuracy ~4%.

(c) It can also be used as a conventional DTA instrument.

(d) Both heating and cooling cycles can be employed over a wide temperature range and at subambient and ambient conditions.

A DSC thermogram plots heat flow (dq/dt) versus temperature. First-order transitions, such as melting, appear as sharp peaks. Integration of the thermogram allows the determination of the enthalpy change of the transition, ΔH_t. Different scan speeds result in negligible variations in peak and area measurements,[7] although baseline shifts must be compensated. The shape of the peak, however, changes with scan speed; a very rounded peak indicates the occurrence of a diffusion or scan-rate dependent processes.[4] Some authors quote the actual peak position as the transition temperature, while others report the onset, *i.e.*, the intercept between the baseline and the initial slope of the peak.[3] When reversible phase transitions are measured, it is customary to quote the transition temperature of the heating cycle since supercooling often occurs, while superheating is rare.

2.2 Vibrational Spectroscopy

The interaction of light with matter can produce a change in the vibrational motions of molecules. This interaction can be in the form of absorption or inelastic scattering of radiation. The former effect requires that the light be of the exact energy as a vibrational transition, *i.e.*, in the IR region; the latter effect has no such restriction, and is known as Raman scattering. These interaction processes are completely different in origin, yet they both yield vibrational energy information important in molecular structure determination.

The simplest model for a molecular vibration is a mass, m, suspended from an elastic band in the z direction.[8] A slight displacement of this mass, along the x direction, will result in simple harmonic oscillations at a frequency given by:

$$\nu_x = \frac{1}{2\pi} (k_x/m)^{1/2} \qquad [2.2.1]$$

where k_x is the force constant in the x direction. Similarly, a small displacement in the y direction will result in oscillations at a frequency:

$$\nu_y = \frac{1}{2\pi} (k_y/m)^{1/2} \qquad [2.2.2]$$

Displacement of the mass in any other direction will result in more complicated motion, however, this movement can always be described as a superposition of the two motions in the x and y directions. These latter, simple harmonic motions, are the normal modes of the mass, and the x and y coordinates are the normal coordinates of the system.

The vibrations of a molecule can be represented by a model of heavy masses joined by springs. The motions of each atom must be described in order to determine the vibrational modes of the molecule. For each nucleus, there are 3 degrees of freedom; therefore, a molecule consisting of N atoms will have 3N degrees of freedom. However, complete translation or rotation of the entire molecule are nongenuine vibrations, and there are actually 3N-6 vibrational degrees of freedom (3N-5 for a linear molecule). As with the simple mass and elastic band model, the normal vibrations of a molecule can also be broken down into less complicated motions, where each atom carries out simple harmonic motion at the same oscillation frequency. These latter vibrations are again called normal modes, and the number of these equals the number of vibrational degrees of freedom. Molecular vibrations can also be expressed in terms of normal coordinates, ξ_1, ξ_2, . . . ξ_{3N-6}, instead of in Cartesian coordinates. This facilitates the depiction of normal vibrations since the atomic motions are described in relation to the molecular geometry.

By both classical and quantum mechanics, the vibrational motion of a molecule can be described, to a first approximation, as the superposition of 3N-6 simple harmonic oscillators in 3N-6 normal coordinates. The energy levels of these oscillators are given by:

$$E_i = h\nu_i(v_i + 1/2) \qquad [2.2.3]$$

where ν_i are the classical oscillation frequencies, and v_i are vibrational quantum numbers. For each normal vibration, there is a selection rule of $\Delta v_i = \pm 1$. In the harmonic approximation, therefore, vibrational transitions can only occur between adjacent levels, and the positions of vibrational bands occur only at the classical vibrational frequencies, ν_i. However, when anharmonicity in the oscillators is considered, this selection rule breaks down, and the combinations and overtones that are observed experimentally can also be described. Since the population of energy levels with $v_i > 0$ is low at ambient temperatures, according to a Boltzmann distribution, the majority of transitions occur from $v_i = 0$ to $v_j = 1$. These are called the fundamental transitions.

In the harmonic approximation, which can only be used when displacements are very small, the potential energy of an oscillator is restricted to the quadratic terms.

$$V = 1/2 \sum_{ij} (k_{xx} x_i x_j + k_{yy} y_i y_j + k_{zz} z_i z_j) + \sum_{ij} (k_{xy} x_i y_j + k_{xz} x_i z_j + k_{yz} y_i z_j) \qquad [2.2.4]$$

When anharmonicity is considered by including cubic, quartic, and higher terms in the equation for the potential energy of the oscillator, it no longer becomes possible to reduce any vibrational motion into a combination of normal modes. The energy is not merely a sum of independent normal vibrations, but also contains cross terms with vibrational quantum numbers of two or more normal modes. The vibrational energy levels of a nonlinear triatomic molecule, for example, can be written as:

$$\begin{aligned} G(v_1, v_2, v_3) = {} & \omega_1 (v_1 + 1/2) + \omega_2 (v_2 + 1/2) + \omega_3 (v_3 + 1/2) + x_{11} (v_1 + 1/2)^2 \\ & + x_{22} (v_2 + 1/2)^2 + x_{33} (v_3 + 1/2)^2 + x_{12} (v_1 + 1/2)(v_2 + 1/2) \qquad [2.2.5] \\ & + x_{13} (v_1 + 1/2)(v_3 + 1/2) + x_{23} (v_2 + 1/2)(v_3 + 1/2) + \ldots \end{aligned}$$

where ω_1, ω_2, and ω_3 are the harmonic oscillation frequencies of the three normal vibrations (3N-6 = 3) or zero-order frequencies, x_{ij} are the anharmonicity constants, and v_1, v_2, and v_3 are the vibrational quantum numbers corresponding to each normal mode. The experimentally observed fundamental vibrations occur between levels of $v_i = 0$ and $v_j = 1$, with all other $v_k = 0$. Therefore, the three fundamentals of the triatomic molecule are:

$$\begin{aligned} v_1 &= \omega_1 + 2x_{11} + 1/2\, x_{12} + 1/2\, x_{13} \\ v_2 &= \omega_2 + 2x_{22} + 1/2\, x_{12} + 1/2\, x_{23} \qquad [2.2.6] \\ v_3 &= \omega_3 + 2x_{33} + 1/2\, x_{13} + 1/2\, x_{23} \end{aligned}$$

The x_{ij} values are usually negative, and thus the observed v_i are less than the zero-order frequencies. Anharmonicity constants are generally very small, except for very large amplitudes of the nuclei; thus, vibrations involving hydrogen atoms have the greatest anharmonicities.

The consideration of anharmonic oscillations determines not only the fundamental transitions occurring at ν_i, but also allows vibrations appearing with energies $2\nu_i$, $3\nu_i$, . . . and $\nu_i + \nu_j$, $\nu_i - \nu_j$, $2\nu_i + \nu_j$, *etc.* Since anharmonicities are generally small, however, these overtone and combination bands are much weaker than the fundamentals. In a polyatomic molecule, it is highly possible for more than one vibration, including combinations and overtones, to have similar energies. This accidental degeneracy can lead to perturbation of the energy levels, as was first recognized by Fermi.[9] In a diatomic molecule, this perturbation is caused by vibrational and electronic interactions. In a polyatomic molecule, the anharmonicity in the potential energy, *i.e.*, the interactions between different vibrations, is enough to cause the mixing of energy levels, or Fermi resonance. In order for perturbation to occur, however, the vibrational levels must be of the same symmetry. The consequences of Fermi resonance are that one of the vibrational levels shifts up in energy whereas the other shifts down, so that the separation of the transition energies is greater than expected, and the similarity in intensities of the bands reflects the degree of energy mixing.

The calculation of the normal modes of a polyatomic molecule can be facilitated by considering symmetry properties of the molecule.[10] These normal vibrations can be summarized in the form of an irreducible representation, Γ, where the symmetry of the vibrational modes is also described. Not all vibrations appear in both the IR and Raman spectra, and those which should be active can be determined by group theory. All of the observed fundamental bands and resulting overtones and combinations are called internal vibrations, since they arise from intramolecular vibrations. In the solid state, the vibrations and rotations of the molecules themselves within a crystal lattice also give rise to transitions called external modes, comprising of translational and librational motions. These and other solid-state effects will be described in section 2.2.3.

2.2.1 Infrared Spectroscopy

The concept of IR spectroscopy is straightforward. The periodic change of the dipole moment of a molecule can cause the absorption or emission of radiation of that frequency. The change in dipole moment does not have to be in its magnitude, but can also be an alteration in its direction with respect to a fixed coordinate system. Not all vibrations cause a variation in the dipole moment, and those which do are termed "IR active". Most internal vibrations occur in the mid-IR region (4000 - 200 cm^{-1}), whereas combinations and overtones can extend into the near-IR range (13000 - 4000 cm^{-1}). External vibrations generally occur below 100 cm^{-1}, which is in the far-IR region.

2.2.2 Raman Spectroscopy

When light is scattered, the majority of the radiation is emitted at the same frequency as the incident light, ν_0, in the form of Rayleigh scattering. Some of the radiation, however, is scattered inelastically in the form of Raman scattering. Bands which appear at frequencies higher than ν_0 are called anti-Stokes lines, while those at lower frequencies are called Stokes lines. The differences in energy between the Stokes (and anti-Stokes) lines and the incident light correspond to the fundamental vibrational frequencies, ν_i, as well as combinations and overtones.

Classically, Raman scattering is due to the electromagnetic field of light inducing a variable dipole moment in a molecule.[11] This dipole moment oscillates at the frequency of the incident light, and thus becomes an emitter of radiation. The induced dipole moment is given by:

$$\mu = \alpha\, E_0 \cos(2\pi\nu_0 t) \qquad [2.2.3]$$

where α is the molecular polarizability, E_0 is the amplitude of the electromagnetic wave, and ν_0 is its frequency. The intensity of the light emitted by the molecule is:

$$I = \frac{16\pi^4\nu_0{}^4}{3c^2}\, \alpha^2 E_0{}^2 \cos^2(2\pi\nu_0 t) \qquad [2.2.4]$$

This expression, however, assumes that the polarizability remains constant, which is not true for a vibrating molecule. If the molecule vibrates at a frequency ν_i, the polarizability will also oscillate according to:

$$\alpha = \alpha_0 + \alpha_i \cos(2\pi\nu_i t + \phi_i) \qquad [2.2.5]$$

where α_i is the maximum change in α during the vibration, and ϕ_i is a phase factor. Taking this into account, the intensity can be expressed as:

$$I = \frac{16\pi^4\nu_0{}^4}{3c^2}\, E_0{}^2 \left\{ \nu_0{}^4\alpha_0{}^2\cos^2(2\pi\nu_0 t) + (\nu_0+\nu_i)^4\, \frac{\alpha_i{}^2}{4} \cos[2\pi(\nu_0+\nu_i)t + \phi_i] \right.$$
$$\left. + (\nu_0-\nu_i)^4\, \frac{\alpha_i{}^2}{4} \cos[2\pi(\nu_0-\nu_i)t - \phi_i] \right\} \qquad [2.2.6]$$

The first term is the coherent scattering of light at the same frequency as the incident radiation, *i.e.*, the Rayleigh line. The second and third terms are scattering at the anti-Stokes and Stokes frequencies, respectively. These types of scattering are incoherent because the phase factor is not constant from molecule to molecule.

The classical theory correctly predicts the positions of the Stokes and anti-Stokes lines; it does not, however, accurately predict their intensities. Although these can only be described correctly by quantum mechanics, the simplicity and partial validity of the classical treatment is very useful in describing polarization of Raman bands as well.

From equation 2.2.6, the intensity of scattered light is proportional to the fourth power of the frequency of the incident light. For this reason, a high-frequency excitation source should be chosen in Raman scattering experiments. With an ultraviolet excitation source, however, electronic transitions can occur, whereas with an infrared source, simple IR absorption will complicate the spectrum. The most logical choice for an excitation source is a line in the visible region, bearing in mind that many molecules can still undergo electronic transitions in this region. Laser sources can provide high power, monochromatic visible light, and are widely used in Raman spectroscopy. The linear polarization of laser light, however, also allows the ability to measure polarization characteristics of vibrational bands.

The polarizability of a molecule, α, is a symmetric, second-order tensor rather than a scalar quantity. It can be expected, therefore, that when molecular orientations are fixed in space, scattering of a laser beam will be of unequal intensity depending on the direction of observation. Experimentally, this is achieved by placing a polarizer after the sample such that only the light of proper polarization is measured. Interestingly, band polarization is also observed in isotropic systems of liquids and gases, because the squares of the components of α average to different values over all space. The depolarization ratio of a liquid measured at 90° scattering from a laser can then be defined as:

$$\rho_l = \frac{I_T(\mathrm{obs}_\perp) - I_\parallel(\mathrm{obs}_\perp)}{I_\parallel(\mathrm{obs}_\perp)} = \frac{3\gamma^2}{25\alpha^2 + 4\gamma^2} \qquad [2.2.7]$$

where α is the mean value or isotropic part of the polarizability, equal to the trace of α, and γ^2 is the anisotropy of the polarizability ellipsoid. If γ^2 equals zero, as in the case of a highly symmetric molecule, the polarizability ellipsoid is a sphere, and $\rho_l = 0$; the line is completely polarized. Where anisotropy exists, the depolarization ratio will be a nonzero value less than 0.75. Group theoretical analysis shows that $\alpha \neq 0$ only for totally symmetric vibrations; this condition results in polarized Raman bands where $\rho_l < 0.75$. Non-totally symmetric vibrations are depolarized, with $\rho_l = 0.75$.

2.2.3 Solid-State Effects

Infrared and Raman bands are subject to inhomogeneous broadening due to the kinetic energy of the molecules in a sample. In the liquid phase, the high mobility of molecules causes vibrational bands to be broadened. The Rayleigh scattering line is also broadened, resulting in a long tail into the low-frequency region of the Raman spectrum.

In the solid state, several effects can occur. The ordered packing of molecules results in translational and librational bands appearing in the low-frequency region. In the case of an ordered crystalline phase, the external bands are sharp. Broad, librational bands superimposed upon the Rayleigh tail indicate the occurrence of anisotropic reorientation of molecules within the crystalline lattice ($\tau_2 \sim 10^{-7}$ s).[12,13] Faster reorientations ($\tau_2 > 10^{-12}$ s) result in a liquid-like low-frequency region.

A molecule in a lattice is affected by the symmetric arrangement of other molecules around it, and group theory is very useful in predicting the spectroscopic outcome of these intermolecular interactions.[14] The molecular unit belongs to a particular point group according to its symmetry elements. Each molecule is located at a position in the lattice which also has a well-defined symmetry, called the site symmetry, which must be the same as or lower in symmetry than that of the molecule. The crystallographic space group can be reduced to a subclass of symmetry elements known as a factor group; this factor group must be of equal or higher symmetry than the site group, in order for the particular site symmetry to exist within the unit cell. The normal modes of an isolated molecule can then be correlated from molecular to site to factor group symmetry, which can result in an increase in the number of observed vibrational bands known as solid-state or factor group splittings, correlation couplings, or Davydov effects.

The group-theoretical analysis of a molecular solid will be exemplified using the CH_3I molecule. Methyl iodide consists of five atoms and therefore has nine normal modes. According to the C_{3v} symmetry of the molecule, these normal modes transform according to: $\Gamma_{vib}^{int} = 3a_1 + 3e$. Since a_1 and e modes are both IR and Raman active under C_{3v} symmetry, six peaks should appear in both spectra of the liquid. Methyl iodide is known to crystallize in the space group Pnma (D_{2h}^{16}) with four molecules per unit cell, each located at a site of C_s symmetry.[15] A correlation diagram for crystalline CH_3I is shown in Figure 2.2.1.

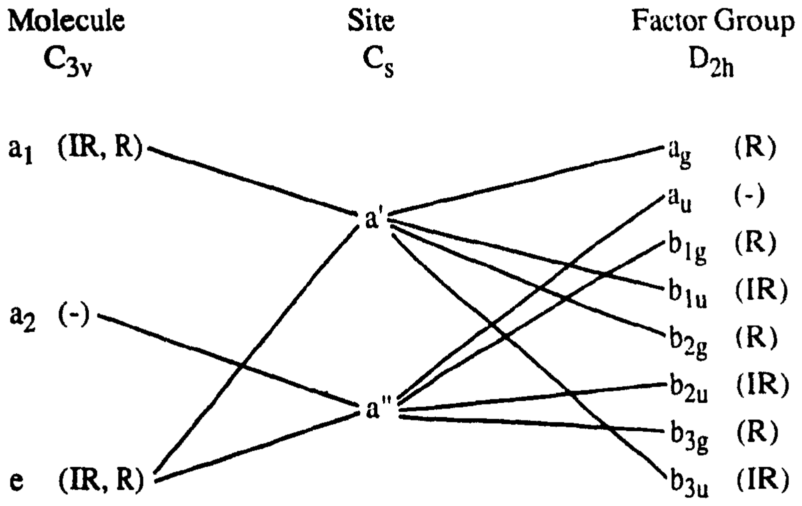

Figure 2.2.1. Correlation diagram for crystalline methyl iodide (R = Raman active, IR = IR active).

Using the correlation diagram, the solid-state splittings that occur in CH_3I can be predicted. Each a_1 mode is not affected by site splitting, since it is nondegenerate, however it should split into four modes ($a_1 + b_{1u} + b_{2g} + b_{3u}$) under the influence of the D_{2h} factor group. This would result in two Raman and two IR peaks in the solid-state spectrum for each a_1 peak originally in the liquid spectrum. Similarly, an e mode of the liquid should be split into two by site group splitting, and each should be further split into four modes by factor group splitting. Thus, in the solid, four Raman and three IR peaks should be observed for each e mode peak. Furthermore, all bands in the solid-state spectrum are mutually exclusive due to the Pnma centrosymmetric space group. The solid-state spectra reported in the literature do indeed reflect these predictions, although not all of the splittings could be observed, even at 0.5 cm^{-1} spectral resolution, and there are several coincident bands in the IR and Raman spectra.[16]

The external vibrations of CH_3I can also be calculated using group theoretical procedures. Translational and librational modes arise from vibrations of the entire molecules within the lattice structure, thus, only the site and factor group symmetries are of concern. According to the C_s site symmetry for each molecule, three rotational and three translational modes transform as $\Gamma_{tot}^{ext} = 3a' + 3a''$. Correlating once again to the D_{2h} factor group, these result in $\Gamma_{tot}^{ext} = 3a_g + 3a_u + 3b_{1g} + 3b_{1u} + 3b_{2g} + 3b_{2u} + 3b_{3g} + 3b_{3u}$. Subtracting the three acoustic modes, $b_{1u} + b_{2u} + b_{3u}$ (which are not IR or Raman active), results in $\Gamma_{vib}^{ext} = 3a_g + 3a_u + 3b_{1g} + 2b_{1u} + 3b_{2g} + 2b_{2u} + 3b_{3g} + 2b_{3u}$. Therefore, twelve Raman and six IR bands should appear in the lattice region. Experimentally, ten of the Raman and five of the IR external modes were observed, along with other combination and overtone bands appearing at higher frequencies.[16]

Group theory, therefore, is highly useful in interpreting solid-state vibrational spectra when the structure of a solid is known. When the crystal structure is not available, factor group analysis can also be used as a back-calculatation to predict the site and factor group symmetry from the solid-state splittings and the number of external modes. This type of analysis will be attempted for each of the compounds investigated in this thesis.

2.2.4 Vibrational Bands Under Pressure

When a crystal is compressed, the initial effect is a decrease in the intermolecular distances, which ultimately leads to a decrease in interatomic distances. In the harmonic approximation, this would not result in any changes in vibrational frequencies. However, since molecular bonds are anharmonic, the slight decreases in interatomic distances leads to increases in vibrational force constants, and therefore in the frequencies of the modes. Sherman and Wilkinson have developed a relation between the change in atomic spacing and the resulting change in vibrational force constant.[17] For external modes, with the energy of the system given by a Lennard-Jones potential function, they calculated that a 1% decrease in intermolecular spacing would result in a 21% increase in vibrational force constant. Internal, stretching modes were estimated as having a 6% increase in force constant with a 1% decrease in interatomic distance, according to equations for the potential energy of diatomic molecules.[18] No simplified explanation for the behaviour of other, non-stretching vibrations could be provided; however, since the force constants of bending modes do not depend as heavily upon interatomic distance as do those of stretching modes, bending vibrations should have comparitively small pressure shifts.

Internal modes can usually be fit to linear pressure dependences, the slopes of these lines being dν/dp. Structural transitions are evidenced by a discontinuity in the slope, or a change in its value upon passing through the phase transition.[17] For the purposes of comparison between modes spanning a range of frequencies, the logarithmic pressure dependence, dlnν/dp, provides a parameter which accounts for the different energies of vibrations. The volume change of the crystal must also be removed in order to compare values between different solids. The mode Grüneisen parameter, γ_i, has been defined as:[19]

$$\gamma_i = \frac{-V\,d\nu_i}{\nu_i\,dV} = \frac{-d(\ln\nu_i)}{d(\ln V)} \qquad [2.2.8]$$

where ν_i is the frequency of a vibrational mode, and V is the crystal volume. This relation can be more conveniently written as:

$$\gamma_i = - \frac{1}{\kappa_S} \frac{d\ln\nu_i}{dp} \qquad [2.2.9]$$

where κ_S is the isothermal compressibility of the crystal given in equation 2.1.6. Values of γ_i for IR and Raman bands of molecular crystals are typically 0.03 to 3.

References

1. A. R. Ubbelohde, *Melting and Crystal Structure*, Oxford University Press, London, 1965.
2. E. F. Westrum Jr. and J. P. McCullough in *Physics and Chemistry of the Organic Solid State*, (D. Fox, M. M. Labes, and A. Weissberg, eds.), Wiley-Interscience, London, 1963, Chap. 1, p. 1.
3. W. Gutt and A. J. Majumdar in *Differential Thermal Analysis*, (R. C. Mackenzie, ed.), Academic Press, London, 1972, Chap. 29, p. 79.
4. P. D. Garn, *Thermoanalytical Methods of Investigation*, Academic Press, New York, 1965.
5. E. E. Sidorova and L. G. Berg in *Differential Thermal Analysis*, (R. D. Mackenzie, ed.), Academic Press, London, 1972, Chap. 2, p. 3.
6. J. Rouquerol and P. Boivinet in *Differential Thermal Analysis*, (R. D. Mackenzie, ed.), Academic Press, London, 1972, Chap. 27, p. 23.
7. W. P. Brennan, B. Miller, and J. C. Whitwell, Ind. Eng. Chem. Fundam., **8**, 314 (1967).
8. G. Herzberg, *Molecular Spectra and Molecular Structure. Vol. II. Infrared and Raman Spectra of Polyatomic Molecules*, D. Van Nostrand Company, Princeton, 1945.
9. E. Fermi, Z. Physik, **71**, 250 (1931).
10. F. A. Cotton, *Chemical Applications of Group Theory*, 2nd ed., Wiley-Interscience, New York, 1971.
11. S. Califano, *Vibrational States*, Wiley-Interscience, London, 1976.
12. M. Debeau and P. Depondt, J. Chim. Phys., **82**, 232 (1985).
13. J. L. Sauvajol, J. Chim. Phys., **82**, 219 (1985).
14. W. G. Fateley, F. R. Dollish, N. T. McDevitt, and F. F. Bentley, *Infrared and Raman Selection Rules for Molecular and Lattice Vibrations*, Wiley-Interscience, New York, 1972.
15. T. Kawaguchi, M. Hijikigawa, Y. Hayafiyi, M. Ikeda, R. Fukushima, and Y. Tomiie, Bull. Chem. Soc. Jpn., **46**, 53 (1973).
16. O. S. Binbrek, A. Anderson, B. Andrews, and B. H. Torrie, J. Raman Spectrosc., **15**, 406 (1984).
17. W. F. Sherman and G. R. Wilkinson in *Advances in Infrared and Raman Spectroscopy*, vol. 6, (R. J. H. Clark and R. E. Hester, eds.), Heyden and Son, London, 1980, Chap. 4, p. 158.
18. G. Herzberg, *Molecular Spectra and Molecular Structure. Vol. I. Spectra of Diatomic Molecules*, 2nd ed., Van Nostrand Reinhold Company, New York, 1950, p. 457.
19. R. Zallen, Phys. Rev., **B9**, 4485 (1974).

CHAPTER 3. EXPERIMENTAL

3.1 Samples

Sublimed crystals of 1-fluoroadamantane were provided by Ms. K. Khougaz and Prof. P. G. Farrell (McGill University). Proton NMR analysis (200 MHz) did not reveal the presence of any impurities, and the sample was used without additional purification. Purchased samples of norbornane, norbornylene, bicyclooctene (Wiley Organics) and norbornadiene (Aldrich Chemical Co.) were analyzed by gas chromatography, and were determined to be > 99.5% pure. No further purification was attempted. Quadricyclane was also purchased from Aldrich Chemical Co.; chromatographic analysis revealed 98% purity. However, simple distillation (b.p. 108°C at 740 mm Hg) resulted in decomposition of the sample. Preparatory gas chromatography was attempted, but the sample and impurity peaks could not be separated. Since the DSC thermograms revealed very sharp peaks, and little fluorescence was observed in the Raman spectra, the sample was utilized in its original state. It is possible that the impurity peak present in the gas chromatogram was due to decomposition of the sample along the column.

3.2 Differential Scanning Calorimetry

Differential scanning calorimetric measurements were made on a Perkin-Elmer DSC-7 calorimeter with liquid nitrogen as the coolant. The minimum temperature attainable by the instrument was 103 K (-170°C). Both the temperature and enthalpy of the calorimeter were calibrated by using the phase transition of cyclohexane (Aldrich, Gold Label). All samples, typically 5-10 mg, were weighed on a Cahn electrobalance and hermetically sealed in aluminum pans. Subsequent weighings were performed to ensure that complete sealing of the pans had been achieved.

All samples were scanned in both cooling and heating directions, at 5 or 2.5 K min^{-1}. Solids were cycled repeatedly at 20 K min^{-1} prior to measurement to ensure homogeneity of the sample. Because calorimetric data for quadricyclane and 1-fluoroadamantane were not available in the literature, these samples were scanned, then cycled, and scanned once again to determine any memory effects associated with these samples.

Phase transition temperatures were recorded as the onset of the peak. Enthalpies were measured by determining the area under each peak; division by the transition temperature resulted in the transition entropies.

3.3 Infrared Spectroscopy

Infrared spectra were recorded on a Nicolet 6000 FT-IR spectrometer with an MCT(B) detector cooled with liquid nitrogen. The low-temperature spectra were scanned typically 100 times at a resolution of 1 cm^{-1}. High-pressure spectra were usually recorded at a resolution of 2 or 4 cm^{-1}, coadding 500 to 1000 scans. Low-temperature IR spectra of norbornane were obtained on an Analect AQS-18 FT-IR spectrometer, at a resolution of 2 cm^{-1}. Unless otherwise stated, the IR spectra throughout this thesis are reported in absorbance units versus wavenumbers (cm^{-1}).

3.4 Raman Spectroscopy

Raman spectra were recorded on an Instruments S.A. spectrometer with a Jobin-Yvon Ramanor U-1000 double monochromator, interfaced to an IBM PS/2 Model 60 computer for data collection and processing. The excitation source was usually the 514.532-nm line of a Spectra Physics model 164, 5-W argon ion laser, although the 487.987-nm line (Ar^+) or the 530.865-nm line of a Coherent Innova 100-K3, 15-W krypton ion laser were also used. Variable-temperature spectra were recorded at 2 cm^{-1} resolution for most spectra, with one spectrum of each solid phase recorded at 1 cm^{-1}

resolution. Laser power at the sample was typically 300 mW. Polarization measurements were made at 90° scattering, of either CCl_4 or CS_2 solutions, or on the neat liquid. High-pressure Raman spectra were recorded at 4 cm^{-1} resolution, with the laser power at the sample 30-50 mW. All Raman spectra are reported in units of total counts versus wavenumbers (cm^{-1}).

3.5 Low-Temperature Spectra

A Cryodyne Cryocooler model 21 cryostat (Cryogenics Technology Inc.) attached to a Cryophysics model 4025 controller was used to maintain and measure the sample temperature in the variable-temperature spectroscopic measurements. The cryostat could be equipped with either glass windows for Raman measurements, or KBr windows for IR spectroscopy.

For the IR measurements, a KBr window was mounted onto the cold finger of the cryostat, and a valved tube containing the sample was attached to the chamber. The sample chamber was then evacuated and cooled to a temperature below the phase transition. Sublimation of the sample onto the window occurred immediately upon opening the valve. Subsequently, the sample was heated and cooled repeatedly through the phase transition until the spectra of both phases were consistent.

Samples were sealed in glass capillary tubes for Raman measurements, which were mounted onto the cold finger in the cryostat with indium foil as a conducting junction. Spectra were measured at a 90° scattering angle.

Infrared and Raman spectra were measured every 10 K near the phase transition, both on cooling and on heating. The accuracy of the temperature reading was ±5 K, while the precision was typically ±1 K.

3.6 High-Pressure Spectra

Two different diamond anvil cells (DAC) were used in the experiments. The IR cell was from High Pressure Diamond Optics (Tucson, Arizona), equipped with type IIA diamonds. This type of diamond is the most IR transparent, with complete absorption occurring only in the 2600-1800 cm^{-1} region. The pressure calibrant chosen was $NaNO_3$ diluted in a NaBr matrix (0.1-0.3 wt. %), which has a strong, single peak assigned as the antisymmetric stretching mode of NO_3^- at 1401.3 cm^{-1}. The equation used to calculate the pressure of the sample was:[1]

$$p = 1.775\ \Delta\bar{\nu} - 0.7495\ \Delta\bar{\nu}\ \exp(-\Delta\bar{\nu}/78) \qquad [3.6.1]$$

where $\Delta\bar{\nu}$ is the measured peak shift at each pressure. The calibrant was pressed into a thin pellet, and then broken into small pieces and dried at ~180°C. For solid samples, a stainless-steel gasket, 200 μm in thickness, was seated firmly on one of the diamond anvils using small pieces of plasticine. A chip of calibrant only slightly smaller than the gasket hole (400 μm in diameter) was positioned into the hole and pressed in the DAC to form a thin, uniform layer of calibrant. The cell was then opened, and a piece of solid sample was put over the hole. Quickly, the cell was reassembled, and enough pressure was applied to keep the volatile sample from escaping the gasket. For liquid samples, a piece of calibrant was placed into the hole of a 100 μm thick gasket, and a drop of the sample was then placed on top. The cell was then assembled and enough pressure was applied so that the sample and calibrant formed a transparent layer. The pressure was then released, and the system was allowed to equilibrate for several hours. The DAC was mounted onto an XYZ stage which was aligned on a Spectra-Bench 4X beam condenser (Spectra-Tech). Infrared spectra were obtained upon compression and decompression at 1-3 kbar intervals.

High-pressure Raman spectra were obtained using a DAC from Diacell Products, Leicester, England, equipped with type IIA diamonds. The sample, together with a ruby chip as a pressure calibrant, was placed into the 300 μm hole of a 380 μm thick stainless steel gasket between the diamonds. The DAC was placed under the 4X objective of the Nachet optical microscope coupled to the Raman spectrometer, with the scattered light being collected at a 180^{o} angle. Spectra were measured every 1-3 kbar upon compression only, due to the design of the cell. The pressure of the sample was calculated using the equation:[2]

$$p = -1.328\ \Delta\bar{\nu} + 0.0003\ (\Delta\bar{\nu})^2 \qquad [3.6.2]$$

where $\Delta\bar{\nu}$ is the observed shift in the ruby R_1 fluorescence band from its initial position of 694.178 nm (5029.6 cm^{-1} away from the 514.532 nm Ar^+-laser line).

The use of a gasket in the DAC serves to both contain the sample and to maintain even pressure throughout the sample.[3] Hydrostatic pressure, however, is completely ensured when a pressure-transmitting fluid is also placed into the cell along with a solid sample. Various types of fluids have been reported; one of the more popular has been a 4:1 methanol-ethanol mixture. Gases such as He, Ar, and N_2 have also been used, but in the solid phase. The difficulties associated with using the methanol-ethanol mixture, as well as other organic liquids such as n-octane,[4] are that the sample must be insoluble in the fluid, and in any case, the vibrational spectrum becomes complicated with its bands. Solid gases are difficult to employ since these require special cell-loading techniques at cryogenic temperatures. The method of using these gases was developed to maintain hydrostatic pressures up to several hundred kbar. Since all of the compounds investigated in this thesis are organic, and highly soluble in organic solvents, and because relatively moderate pressures were achieved (generally up to 25 kbar), no pressure-transmitting fluids were employed in any of the high-pressure vibrational spectroscopic experiments.

The linear pressure dependences (dv/dp) of all vibrational modes measured were calculated by linear least-squares analyses of plots of peak positions, in cm^{-1}, versus pressure, in kbar. The phase transition point was chosen where the majority of spectral changes occurred, and the plotted lines were broken at that pressure. In cases where the phase transition was sluggish, *i.e.*, where the transition did not occur sharply between measured pressures, the data obtained during the phase transition were omitted from the calculation of the pressure dependences. In all the tables of high-pressure data given, lines with a correlation coefficient, r^2, of greater than 0.95 are reported with two significant digits, whereas lines with $0.80 < r^2 < 0.95$ are reported with one significant digit. When the r^2 values are less than 0.80, slopes are listed only if more than ten data points have been measured, because these values still reflect the general trend of the vibrational peak.

References

1. D. D. Klug and E. Whalley, Rev. Sci. Instrum., 54, 1205 (1983).
2. G. J. Piermarini, S. Block, J. D. Barnett, and R. A. Forman, J. Appl. Phys., 46, 2774 (1975).
3. J. R. Ferraro, *Vibrational Spectroscopy at High External Pressures. The Diamond Anvil Cell*, Academic Press, Orlando, 1984, p. 46.
4. V. Benham, G. Lord, I. S. Butler, and D. F. R. Gilson, Appl. Spectrosc., 41, 915 (1987).

CHAPTER 4. THE NORBORNANE SERIES

4.1 Introduction

The seven-carbon, bicyclic hydrocarbons are well known to exhibit orientational disorder in the solid state.[1] This family of compounds includes bicyclo[2.2.1]heptane (norbornane), bicyclo[2.2.1]hept-2-ene (norbornylene), and bicyclo[2.2.1]hepta-2,5-diene (norbornadiene), the structures of which are shown in Figure 4.1.1. Henceforward, they will be referred to as NBA, NBE, and NBD, respectively.

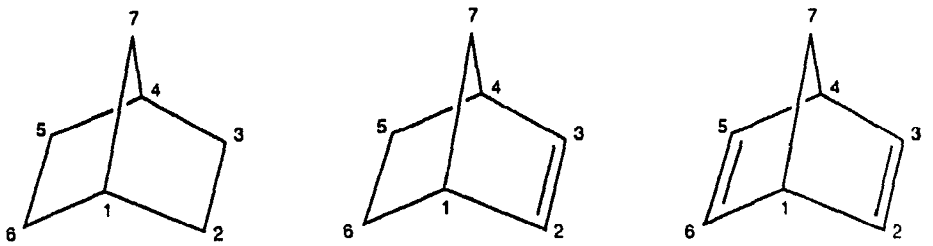

NBA **NBE** **NBD**

Figure 4.1.1. Structures of norbornane (NBA), norbornylene (NBE), and norbornadiene (NBD)

At ambient temperature and pressure, NBA and NBE exist as orientationally-disordered solids while NBD is a liquid. Upon cooling below the melting temperature, the diene also forms a disordered solid. Norbornane has an additional disordered phase (phase I) which exists over a short temperature range above room temperature. Adiabatic calorimetry has been performed by Westrum;[2] the data are shown in Table 4.1.1. A powder x-ray diffraction study[3] determined the structures of these disordered solids, and in each case, the phase which exists at temperatures above the crystalline phase is hexagonal close-packed. The crystal dimensions were determined to be: a = 6.17 and c = 10.03 Å for NBA, a = 5.89 and c = 9.51 Å for NBE, and a = 6.08 and c = 9.81 Å for NBD. The second disordered phase of NBA, existing at a higher temperature, was determined to be body-centred cubic with a = 8.73 Å. These findings make this family of

Table 4.1.1. Adiabatic Calorimetric Data for Some Seven-Carbon Bicyclic Hydrocarbons.[2]

Transition		T_t (K)	ΔS_t ($\mathrm{J\ K^{-1}\ mol^{-1}}$)
norbornane	III → II	131	31.5
	II → I	306	0.3
	I → liq.	360	12.7
norbornylene	II → I	129	37.5
	I → liq.	320	10.9
norbornadiene	II → I	202	44.2
	I → liq.	254	6.6

compounds particularly interesting in that they all have hexagonally close-packed disordered phases, while most other organic cage-compounds have cubic disordered phases.[1]

A considerable amount of data has been collected for the various solid phases of these three compounds. Extensive proton NMR studies under variable-temperature and -pressure conditions have been performed on all three.[4,5] The rotational activation enthalpies in the disordered phases of NBA, NBE, and NBD were determined to be 5.4-8.8, 6.3-10.5, and 8.0 kJ mol^{-1}, respectively. Ranges were given for NBA and NBE since the plots of $\ln\tau_2$ versus 1/T were not linear. In addition, only a marginal change in ΔH^*_{rot} was observed between the two disordered phases of NBA. This is consistent with the occurrence of rapid endospheric rotation in both disordered phases. An IQNS study confirmed that isotropic rotation occurs in both plastic phases of NBA, with no change detected at the hexagonal to cubic phase transition.[6] Similar results were obtained for NBD; the authors also claimed to have discovered a metastable, cubic close-packed phase which forms upon slow cooling of the liquid.[7] No other evidence for the existence of this phase was given, and the exact cooling conditions needed to obtain this metastable phase were not reported. For the diffusion process, the activation enthalpies for NBA (phase II and phase I), NBE, and NBD were determined to be 54.5, 64.8, 48.6, and 39.9 kJ mol^{-1}, respectively, by NMR spectroscopy.[4,5] Radiotracer studies on NBA and NBE were consistent with the NMR data, confirming that self-diffusion occurs via a monovacancy mechanism.[8] Deuterium NMR of NBA-d_4 and NBA-d_2 showed the hexagonal to cubic phase transition to occur 25 K and 9 K higher than in NBA, respectively.[9] The slower rotations and translational diffusion of NBA-d_4 were suggested to be at least partially responsible for the observed isotope effect.

The disordered phase of NBE, in particular, has been the focus of several studies. Brillouin, Rayleigh, and Raman scattering have been undertaken showing no discontinuities at the melting transition.[10,11] The Raman measurements, however, were limited to a study of only the 837 cm^{-1} peak in the disordered and liquid phases. A muonium adduct radical of NBE was investigated, and the rotational regime of the molecules in the disordered phase was determined to be isotropic at room temperature, with anisotropy setting-in at about 160 K.[12]

Several vibrational spectroscopic studies have been reported on these compounds, evoked by the interesting geometry and strain of these bicyclic structures, as well as the ability for NBD to serve as a bidentate ligand in organometallic complexes. Infrared spectra have been recorded of the gas phase, and liquid phase IR and Raman spectra have also been published.[13-17] Solid phase IR and Raman spectra of NBA and NBD have been measured at liquid nitrogen temperatures.[13,15,18] The vibrational spectra have been calculated by several authors, including normal coordinate calculations for NBA,[19] and NBA and NBD,[13] and more recently, scaled *ab initio* STO-3G and 3-21G harmonic force fields for all three compounds have been computed.[16] An extensive vibrational study of NBA alone has been reported including IR, Raman, and neutron inelastic scattering measurements, as well as a normal coordinate analysis.[18] None of these studies, however, has addressed the phase transitions which occur in these compounds, as the solid state spectra have been confined to the crystalline phases. Furthermore, no solid state spectra of NBE have been reported at all. In this chapter, variable-temperature IR and Raman spectroscopy have been undertaken in order to gain structural information on the solid phases of NBA, NBE, and NBD. In addition, high-pressure Raman spectroscopic studies have been performed to investigate the pressure behaviour of these materials. The results will be presented for each compound separately, followed by a general discussion concerning all three related solids.

4.2 Norbornane

Figure 4.2.1 shows a typical thermogram of NBA measured by differential scanning calorimetry. Since the DSC instrument was equipped for subambient use, only the phase II → phase III transition could be measured precisely, occurring at 130 K on heating and 129 K on cooling, with average enthalpy and entropy changes of 4.1 kJ mol^{-1} and 32.0 J K^{-1} mol^{-1}. The thermograms obtained at 2.5 and 5 K min^{-1} agree in both onset temperature and enthalpy, and thus the shape of the thermogram was not caused by too fast a scan rate, but was inherent to the transition. The negligible hysteresis was surprising since the majority of order-disorder transitions of organic cage molecules are often associated with very large hystereses, *i.e.*, up to 50 K.[20] The phase I → phase II transition occurred at 313 K on heating and 305 K on cooling, but due to its very small enthalpy change, could not be measured with much precision. These DSC results agree with adiabatic calorimetric measurements reported by Westrum.[2]

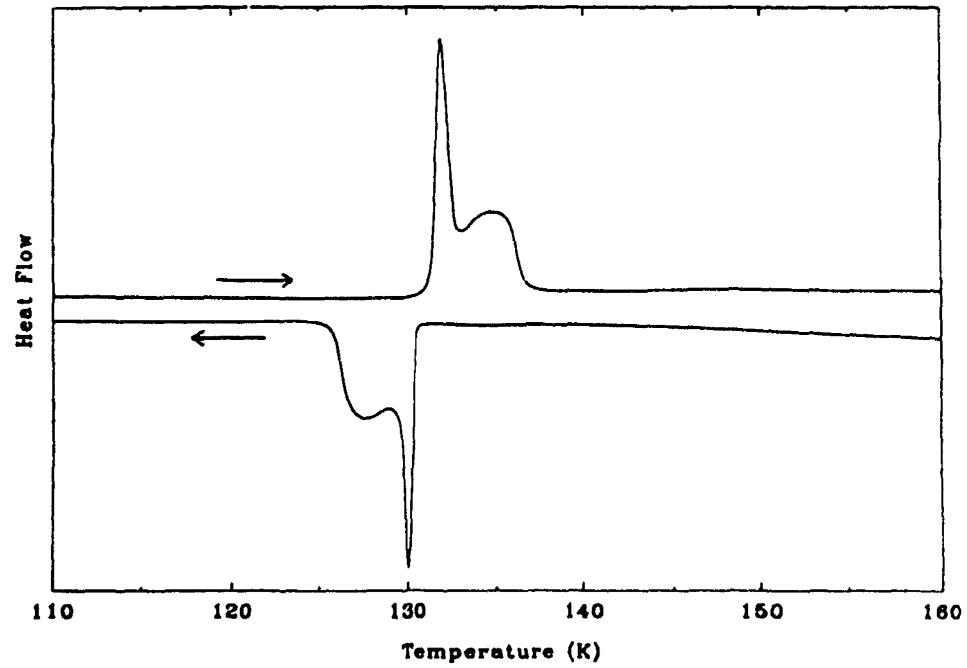

Figure 4.2.1. Differential scanning calorimetric thermogram of norbornane, scanning at 5 K min^{-1}.

The phase II → phase III transition was observed quite clearly in the low-temperature IR and Raman experiments, characterized by sudden line narrowing and the appearance of at least two external modes. Figures 4.2.2 and 4.2.3 show representative IR and Raman spectra of these two phases. The broad bands in the spectra of phase II are similar to those of a liquid, which is expected for a rapidly reorienting molecule. Norbornane (C_7H_{12}), having C_{2v} symmetry, has 51 normal modes, $\Gamma_{vib}{}^{int} = 15a_1 + 11\ a_2 + 13\ b_1 + 12\ b_2$. All vibrations are Raman active while all but the a_2 modes are IR active. A summary of the observed IR and Raman peaks is given in Table 4.2.1. The assignments of the skeletal modes were transferred directly from Brunel *et al.*[18] However, their C-H stretching band frequencies did not agree with those observed in this study, and these latter modes were assigned according to Levin and Harris.[13] The structure of phase III is certainly fully ordered since two sharp lattice modes were observed in the Raman spectrum. Not even one clear instance of factor group splitting in either the IR or Raman spectrum was detected for phase III. From this observation, the unit cell structure of the ordered phase can be postulated according to the method of analyzing site and factor group splittings of solid state spectra.

Norbornane cannot exhibit site splittings since all modes are nondegenerate under the molecular symmetry. However, factor group splittings are indeed possible under certain conditions. The site symmetry of the NBA molecules can be C_{2v} or less, *i.e.*, C_2, C_s or C_1. About half the bands are coincident in the IR and Raman spectra, and the possibility of a centrosymmetric space group should not be ruled out. A set of combinations of site and factor group symmetries which will not result in any splittings in either the IR or Raman spectrum occurs when the site and factor groups are identical. These possibilities all allow only one molecule per unit cell, which is consistent with the observation of two Raman lattice modes. The other possibility is a D_{2h} factor group with a C_{2v} site; this combination allows for two molecules in the centrosymmetric unit cell.

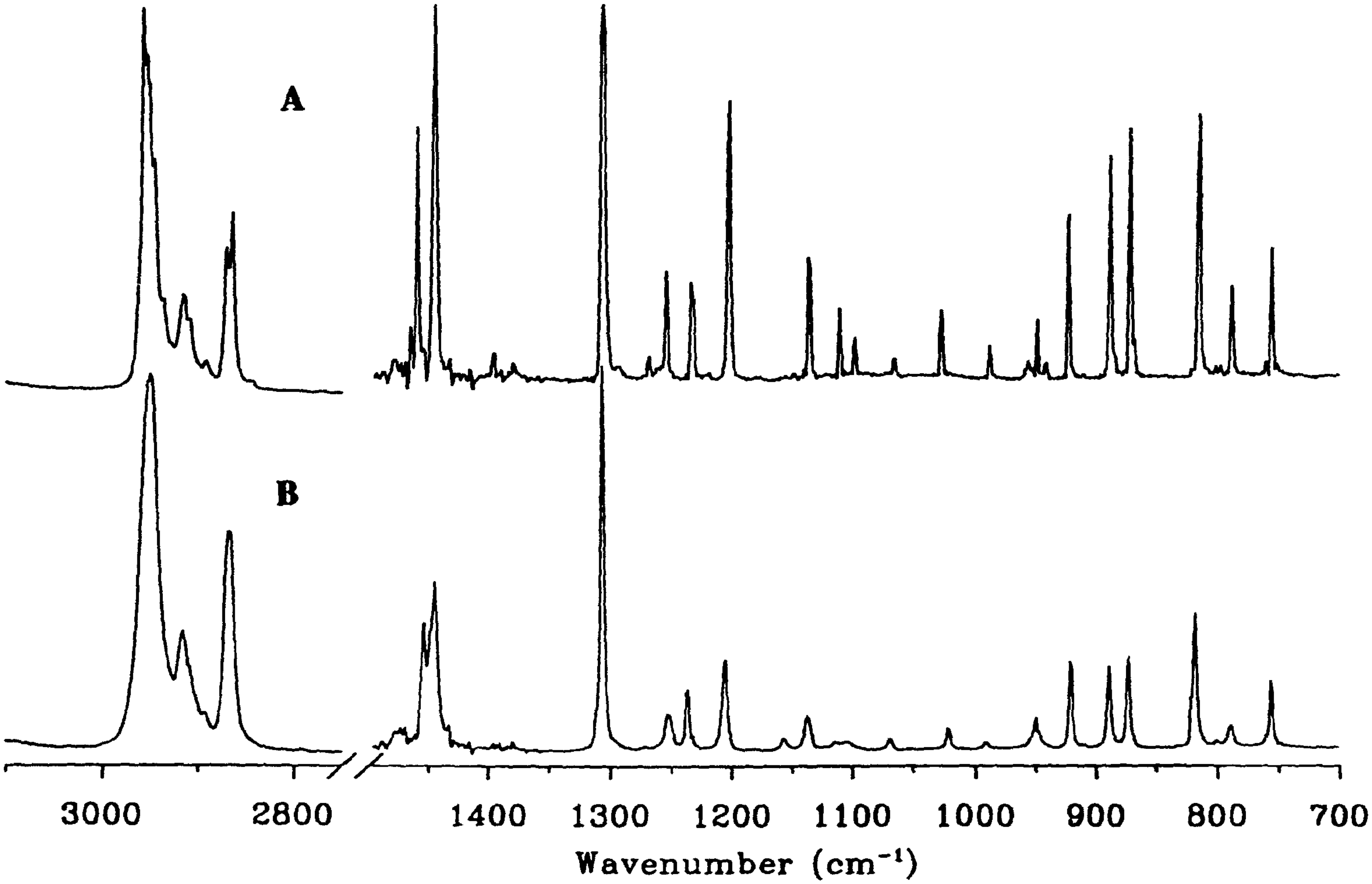

Figure 4.2.2. Infrared spectra of norbornane at (A) 115 K and (B) 155 K The n(C-H) region is actually 4x more intense than the skeletal vibration region

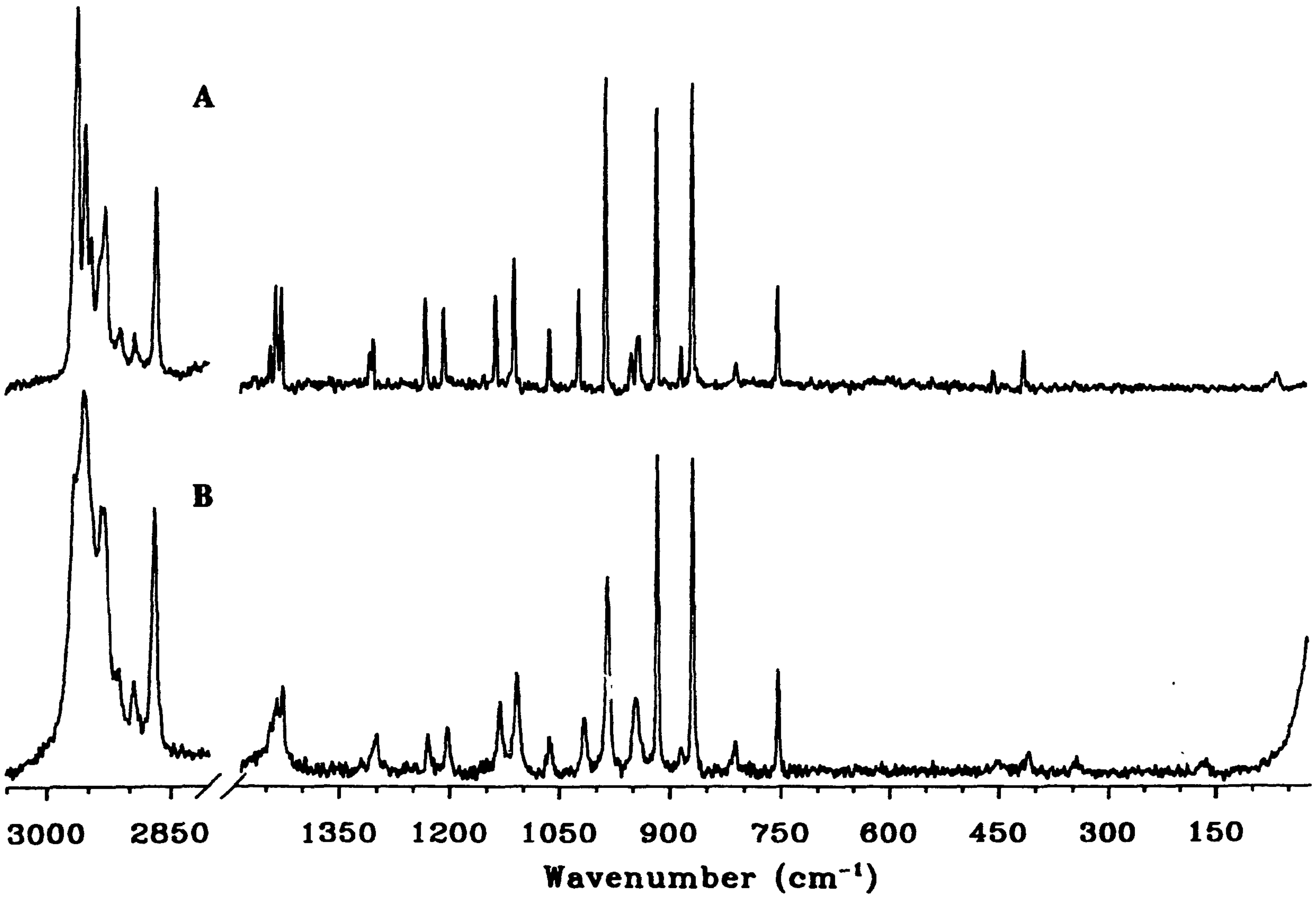

Figure 4.2.3. Raman spectra of norbornane at (A) 75 K and (B) 200 K.

Table 4.2.1. Vibrational Data (cm^{-1}) for Norbornane.

phase II		phase III		
Raman (200 K)	IR (155 K)	Raman (75 K)	IR (115 K)	assignment[a]
		60 w		lattice modes
		67 w, sh		
165 vw				ν_{26}
342 vw		342 vw		ν_{39}
409 w		414 w		ν_{15}
452 vw		456 w		ν_{51}
757 m	755 m	757 m	755 m	ν_{14}
	788 w		788 m	ν_{50}
	800 vw		797 vw	
			801 vw	
817 w	818 s	815 w	816 s	ν_{13}
	821 w, sh		821 w	
			869 m, sh	ν_{49}
875 s	874 s	875 w	873 s	ν_{12}
			886 w, sh	
891 w	890 s	891 m	890 s	ν_{37}
924 s	921 s	924 s	925 s	ν_{11}
948 w, sh	948 w, sh		943 w	
	951 m	950 m	950 m	ν_{48}
954 m	955 vw, sh	960 m	958 vw	ν_{24}
993 m	992 vw	995 s	990 w	ν_{10}, ν_{23}
1025 m	1023 w	1032 m	1030 m	ν_{36}
1073 w	1072 vw	1072 m	1069 vw	ν_{35}, ν_{47}
	1107 vw, br		1103 w	
1118 m	1117 vw, br	1121 m	1115 m	ν_{22}
1142 m	1141 w	1147 m	1140 m	ν_9, ν_{46}
	1160 vw			ν_{34}
1214 w	1209 m	1218 m	1207 s	ν_{33}
	1236 vw, sh	1232 vw	1236 m	ν_{21}
1241 w	1240 m	1244 m	1238 m	ν_{45}
	1256 w, br		1259 m	ν_8
	1274 vw		1273 w	ν_{20}
1313 w	1312 s	1317 m	1312 s	ν_7
1319 w, sh	1316 w, sh	1321 w		ν_{19}, ν_{44}
1442 m		1443 m		ν_{43}
1450 m	1450 s	1451 m	1451 s	ν_6
	1453 m, sh			ν_{30}
1459 w	1459 m	1460 w	1465 m	ν_{18}
2867 s	2867 vs	2865 s	2864 vs	
			2870 vs	
2893 m	2893 m	2891 m	2892 m	ν_{17}
2910 m	2910 s, sh	2909 m	2908 s	ν_4, ν_{29}
	2915 s		2915 s	
		2928 s	2927 m, sh	ν_3, ν_{42}
2931 s		2934 s, sh	2937 s	
		2945 m	2947 s, sh	ν_2, ν_{28}, ν_{41}
			2955 s, sh	
2953 vs	2951 vs	2952 s	2958 vs	
2966 s		2963 vs		ν_1, ν_{16}, ν_{27}, ν_{40}

[a] From references 18 (skeletal modes) and 13 (C-H stretches).

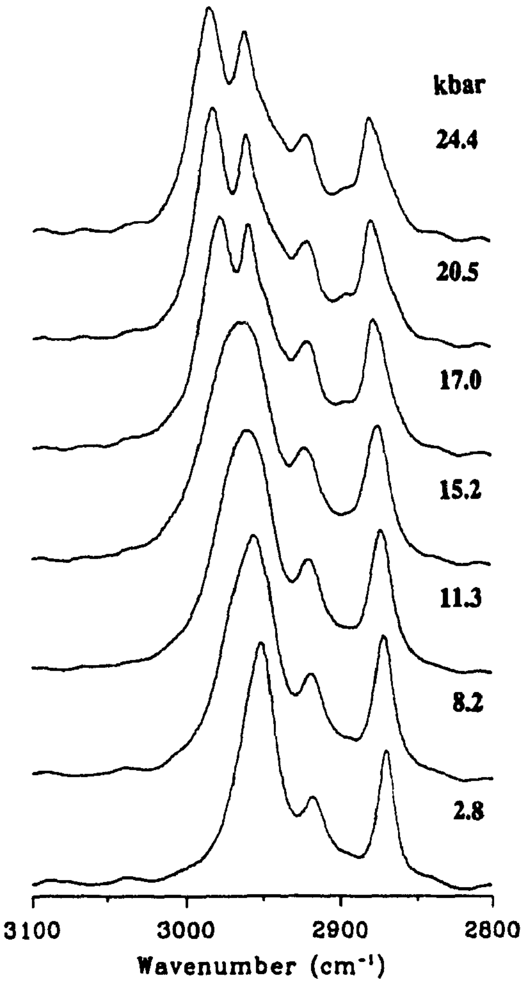

Figure 4.2.4. Infrared spectra of norbornane at the indicated pressures upon compression.

The space group of phase III, according to the interpretation of the low-temperature spectra, is either orthorhombic (C_{2v}^1, C_{2v}^{11}, C_{2v}^{14}, C_{2v}^{18}, C_{2v}^{20}, D_{2h}^1, D_{2h}^5, D_{2h}^{13}, D_{2h}^{17}, D_{2h}^{19}, D_{2h}^{21}, D_{2h}^{23}, D_{2h}^{25}, or D_{2h}^{28}), monoclinic (C_s^1, C_s^2, C_s^3, C_s^4, C_2^1, C_2^2 or C_2^3), or triclinic (C_1^1).

The behaviour of a material under pressure can be easily monitored by high-pressure IR spectroscopy. Figure 4.2.4 shows the C-H stretching region at various pressures. Upon compression, the peaks shift to higher frequency due to compression of the intramolecular bonds. At 16.4 ± 1.0 kbar, the peaks suddenly narrow, indicating that the transition to the ordered phase (phase III) has occurred. The application of pressure to the ordered phase causes the vibrational bands to continue to shift to higher energy. Representative plots of the frequencies of IR bands versus pressure are given in Figure 4.2.5. The pressure behaviour of vibrational peaks can be summarized by the slopes of linear fits of the band positions versus applied pressure, with the phase transition characterized by a discontinuity in these lines. A compilation of the available high-pressure IR data is given in Table 4.2.2. Comparison of the pressure dependences of the peaks is possible by calculating the logarithmic dependence of the bands, dlnv/dp, or (1/v)(dv/dp). These are also listed in the table, along with vibrational assignments according to the literature. The main features to note are, within each phase, the lower

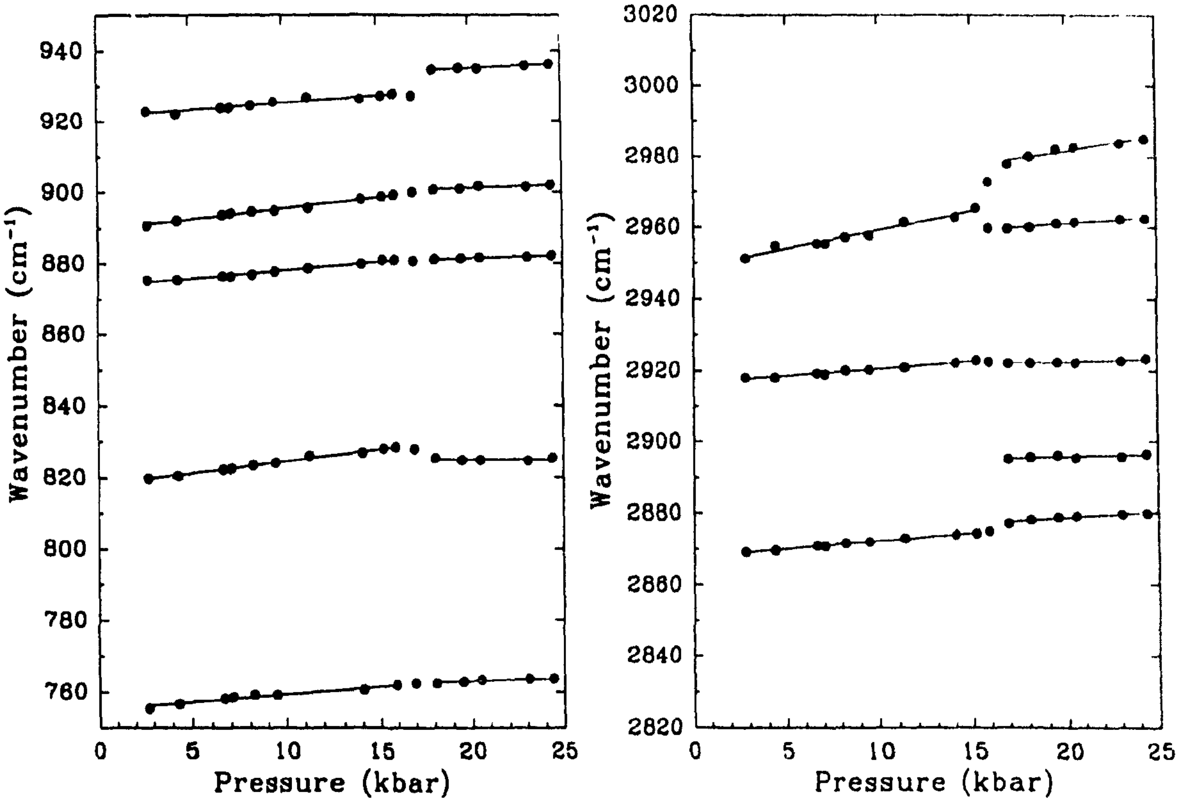

Figure 4.2.5. Pressure dependences of selected IR peaks of norbornane.

Table 4.2.2. Pressure Dependences of Infrared Peaks of Norbornane.

phase II			phase III			
ν (cm^{-1})	$d\nu/dp$ ($cm^{-1}kbar^{-1}$)	$dln\nu/dp$ ($kbar^{-1} x 10^4$)	ν (cm^{-1})	$d\nu/dp$ ($cm^{-1}kbar^{-1}$)	$dln\nu/dp$ ($kbar^{-1} x 10^4$)	assignment[a]
755	0.43	5.7	755	0.19	2.4	a_1, skeletal def.
818	0.66	8.0				a_1, CH_2 rock
874	0.47	5.3	873	0.16	1.8	a_1, C-C str.
890	0.62	6.9	890	0.2	3	b_1, C-C str.
921	0.40	4.3	925	0.25	2.7	a_1, C-C str.
			1140	0.088	0.77	a_1, CH_2 twist + b_2, CH def.
1209	0.2	2	1207	0.080	0.66	b_2, CH_2 twist
1256	0.4	3	1259	0.13	1.0	a_1, CH def. + CH_2 twist
1312	0.18	1.4	1312	0.2	1	a_1, C-C str.
1450	0.17	1.2	1451	0.11	0.76	a_1, CH_2 scissor
1459	0.19	1.3	1465	0.04	0.3	a_2, CH_2 scissor
2867	0.41	1.4	2864	0.3	1	
2915	0.40	1.4	2915	0.2	0.5	2-C-bridge CH_2 str.
2951	1.1	3.6	2955	0.35	1.2	bridgehead CH str. + 2-C-bridge CH_2 str.
			2958	0.87	2.9	bridgehead CH str. + 2-C-bridge CH_2 str.

[a] From references 18 (skeletal modes) and 13 (C-H stretches).

pressure dependences of certain modes, such as those at 1209 (b_2, CH_2 twist) and 1450 cm^{-1} (a_1, CH_2 scissor). Since the force constants of bending modes depend upon interatomic distance to a lesser extent compared to stretching modes, it follows that peaks assigned to these modes exhibit lesser pressure shifting. The pressure dependences of almost all the modes are lower in phase III than in phase II; this is an indication of lower compressibility of the ordered, high-pressure phase. Among the C-H stretching modes of phase III, there is a wide variation in dlnν/dp values. These can be attributed to the different types of C-H bonds due to the high strain that exists in the NBA molecule, and will be discussed in conjunction with NBE and NBD in the general discussion to follow.

The high-pressure IR experiments were performed in the decompression direction as well as upon compression. The spectral peaks reverted to their original appearance in phase II, with the phase transition occurring at 16.1 ± 0.5 kbar. Within experimental error, therefore, there is no significant pressure hysteresis associated with the phase II → phase III transition, which is in agreement with the DSC results.

4.3 Norbornylene

Differential scanning calorimetry was performed in both the cooling and heating directions at 5 and 2.5 K min^{-1}. The heating thermograms showed a sluggish phase transition at 127 K with accompanying enthalpy and entropy changes of 4.3 kJ mol^{-1} and 35.9 J K^{-1} mol^{-1}. These results are in agreement with adiabatic calorimetric measurements.[2] Like many first-order transitions, hysteresis was associated with this phase transformation, the onset on cooling occurring at 114 K. The different heating and cooling rates showed that the sluggish nature of the phase transition was not caused by too fast a scan rate, but was inherent to the transition. Figure 4.3.1 shows a typical thermogram of norbornylene in both heating and cooling directions.

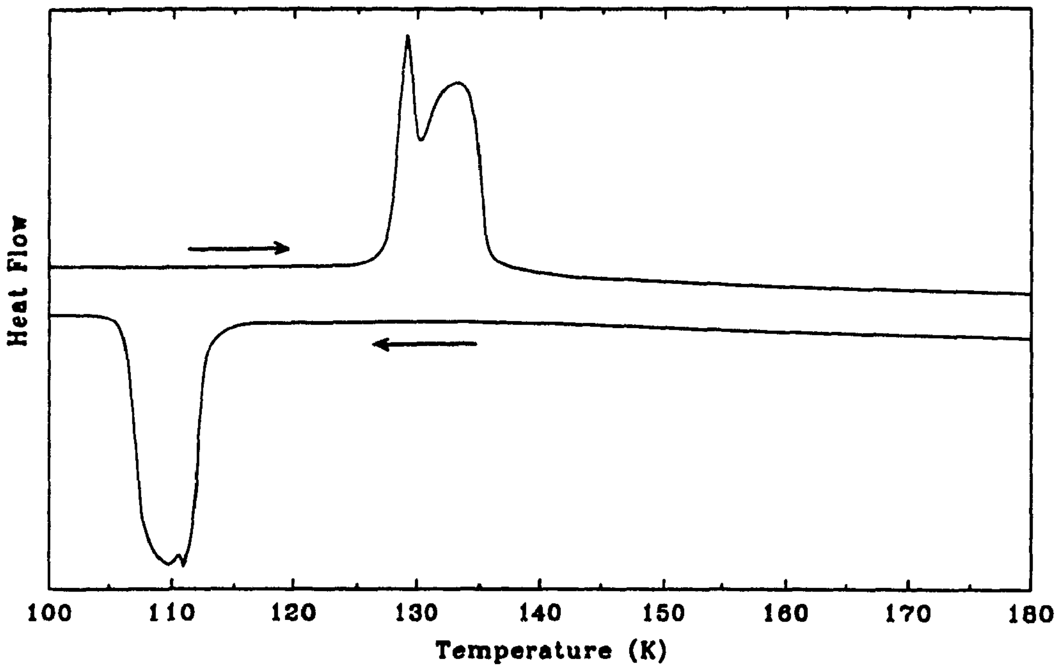

Figure 4.3.1. Differential scanning calorimetric thermogram of norbornylene, scanning at 5 K min^{-1}.

Variable-temperature IR and Raman spectroscopic studies were used to characterize structural changes occurring during the phase transition. Figures 4.3.2 and 4.3.3 show representative spectra of each phase. No evidence of a metastable phase was detected in the vibrational spectra. Phase I, the disordered phase of norbornylene, exhibited liquid-like features in both the IR and Raman spectra. No lattice modes were observed in the low-frequency Raman spectra, only the broad tail of the Rayleigh line. This confirms that the molecules in this phase undergo rapid tumbling in the hexagonal close-packed lattice, which is expected since, upon melting, no change in correlation times were observed by either NMR[4,5] or Raman spectroscopy.[11] All modes are both IR and Raman active, which would be expected for the disordered phase of a molecule with C_s symmetry ($\Gamma_{vib}{}^{int}$ = 23a' + 22 a"). The low-temperature structure, phase II, was formed immediately upon cooling through the transition temperature. Many changes in both spectra occurred at this point, including line narrowing and peak splitting. In addition, nine external modes suddenly appeared in the low-frequency Raman spectrum, indicating that an ordered, crystalline solid had been formed (Figure 4.3.4). Table 4.3.1 summarizes the vibrational peaks observed for both solid phases of norbornylene, with assignments of the skeletal bands according to STO-3G force-field calculations.[16] The C-H stretching modes have been left unassigned at the present time.

Analysis of the vibrational spectra showed that several peaks of phase I, regardless of symmetry, split into doublets in phase II throughout the spectral region. These splittings can be attributed to solid-state effects occurring in phase II which were not present in phase I due to the disordered nature of the latter solid. The spectra of phase I resemble those of a liquid, *i.e.*, the observed IR and Raman peaks are governed by the molecular symmetry, whereas the peaks of phase II are influenced by the site and crystal symmetry. No site splitting occurs since all modes are nondegenerate under C_s molecular symmetry; therefore, any splitting effects are due to correlation coupling.

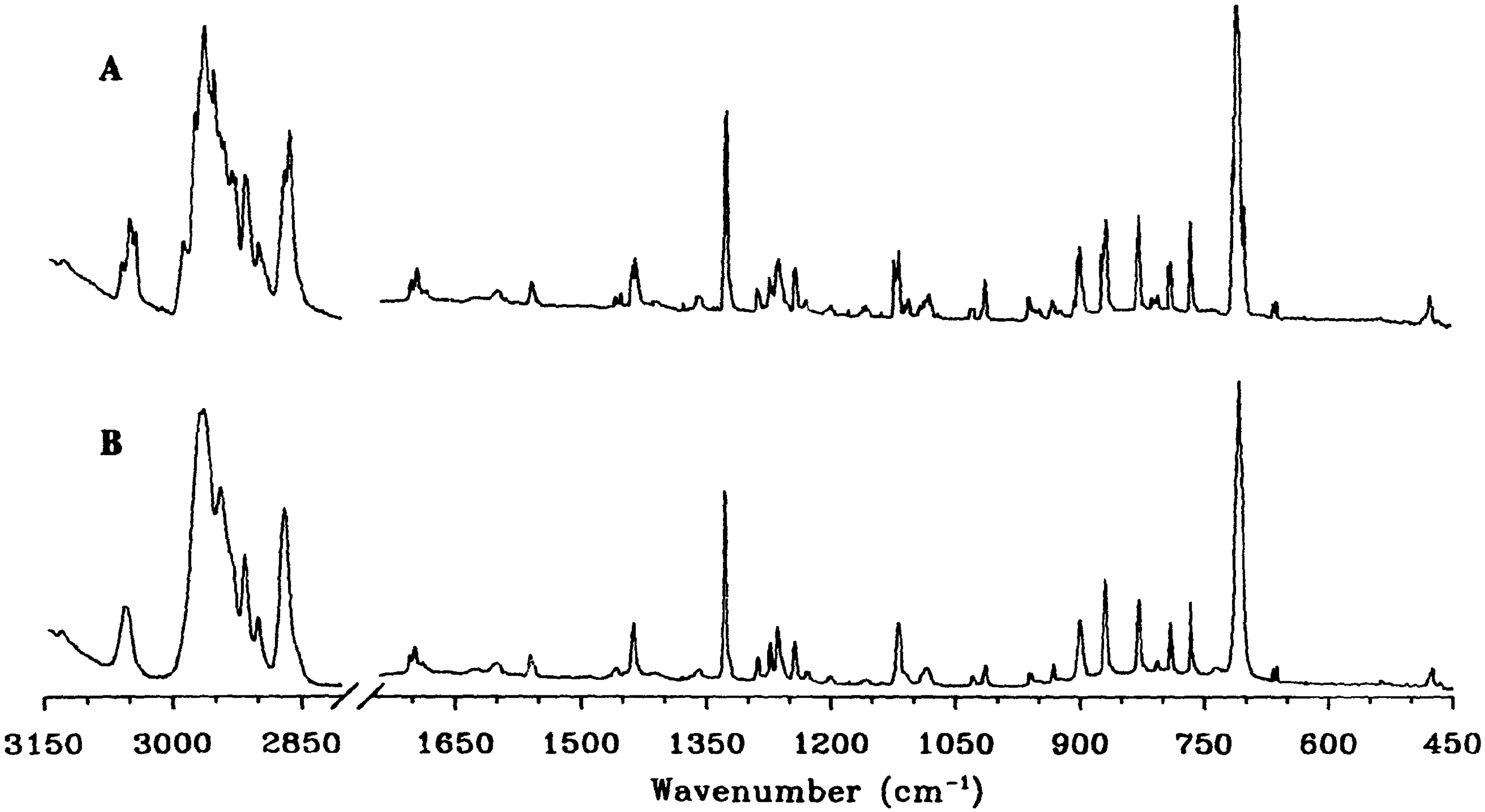

Figure 4.3.2. Infrared spectra of norbornylene at (A) 58 K and (B) 145 K.

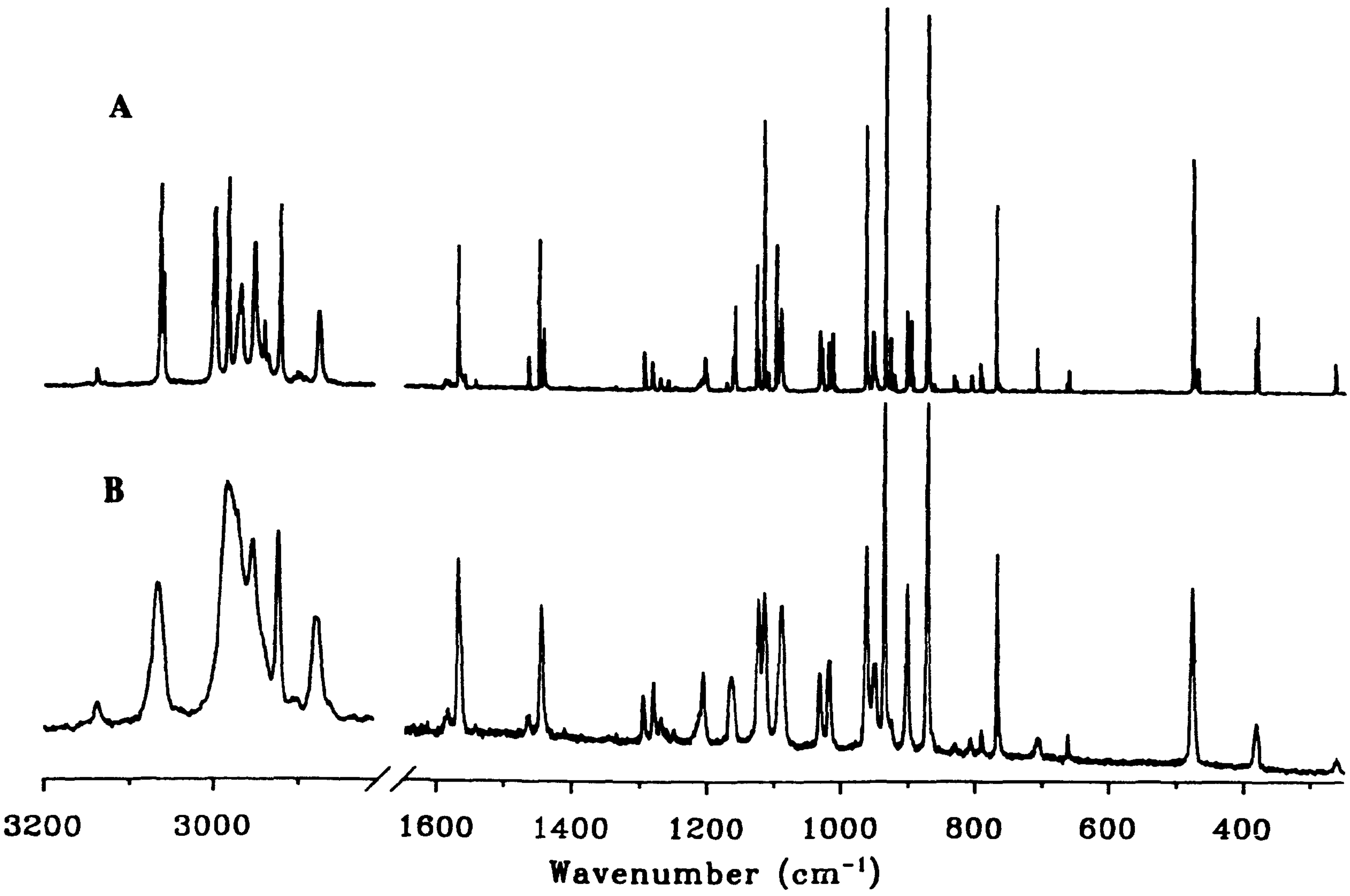

Figure 4.3.3. Raman spectra of norbornylene at (A) 48 K and (B) 135 K:

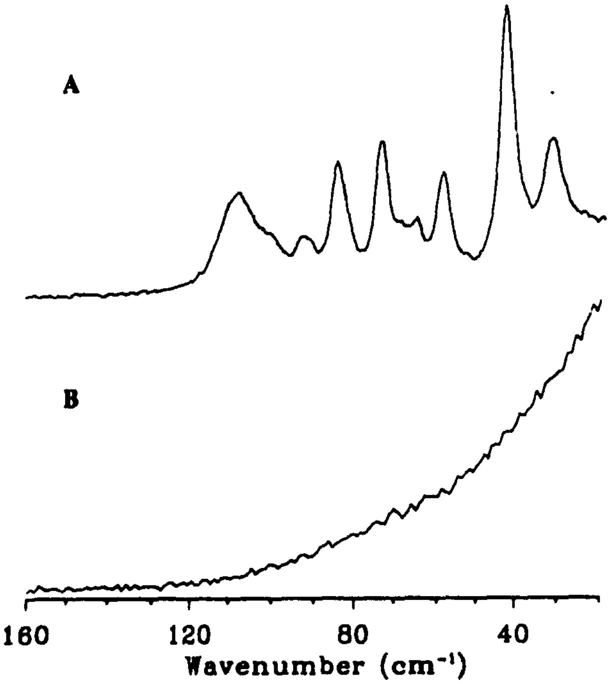

Figure 4.3.4. Low-frequency Raman spectra of norbornylene at (A) 48 K and (B) 135 K.

Since more than half of the observed fundamentals of phase II coincide in the Raman and IR spectra, the crystal symmetry is almost certainly noncentrosymmetric. The possible lattice sites that a molecule of C_s symmetry can occupy are C_s and C_1. Considering the first case, the crystal can have any noncentrosymmetric factor group which has C_s as a subset. Of these, only C_{2v} and C_{4v} will result in doubling of all the modes due to factor group splitting. In the second case, *i.e.*, if the molecules occupy general positions, only the C_2 and C_s factor groups can give rise to the observed splitting effects. All four of these possibilities can account for the nine external modes which were observed in the Raman spectrum. The unit cell of phase II, therefore, is monoclinic or orthorhombic containing two molecules, or tetragonal containing four molecules.

Table 4.3.1. Vibrational Data (cm^{-1}) for Norbornylene

phase I		phase II		
Raman (135 K)	IR (145 K)	Raman (48 K)	IR (58 K)	assignment[a]
		30 w		lattice modes
		39 m		
		53 w		
		59 vw		
		66 w		
		75 w		
		82 vw		
		89 vw		
		95 w		
261 w		264 w		a'', ν_{45}
382 m		380 m		a', ν_{24}
		383 w		
		469 w		
		472 w		
477 s	474 w	477 s	476 w	a', ν_{23}
664 w	664 vw	663 w	663 vw	a'', ν_{43}
	668 vw	665 vw	668 vw	
			703 m	a', ν_{22}
708 w	709 s	710 w	712 s	
			717 m	
		764 vw		
769 s	769 m	767 vw	768 m	a', ν_{21}
		771 s		
793 w	793 m	792 w	793 m	a'', ν_{42}
		794 w		
810 w	809 w	807 w	808 w	a', ν_{20}
		809 w		
		815 w		
832 w	832 m	830 vw		a'', ν_{41}
		833 w	832 m	
867 w		864 vw		
		868 vw		
873 vs	873 m	871 m	871 m	a', ν_{19}
		874 vs	876 m	
		896 w, sh		
		897 m	899 w, sh	
903 s	903 m	901 m	902 m	a', ν_{18}
		904 s	905 m	
			911 w	
927 w	927 vw	923 w		a'', ν_{40}
		928 m	926 vw	
		931 w		
938 vs	937 w	936 vs	936 w	a', ν_{17}
952 m	952 vw	950 w		a'', ν_{38}
		954 m	952 vw	
964 s	964 w	962 w	958 vw	a', ν_{16}
		965 vs	965 w	
1019 m	1019 w	1015 m		a', ν_{15}
		1020 m	1019 m	
1034m	1033w	1030 m	1033 w	a'', ν_{37}
		1034 m	1035 w	
			1085 w, sh	
			1087 w	
1090 s, br	1090 w, br	1091 s	1093 w, sh	a', ν_{14}
		1099 s	1098 w	
1116 s	1116 w, sh	1111 w	1112 w	a'', ν_{36}
		1117 s	1115 w	
1125 s	1125 m	1125 w	1124 m	a', ν_{13}
		1128 s	1127 m	
			1130 m	
	1144 vw		1145 vw	

Table 4.3.1. (cont'd.)

phase I		phase II		
Raman (135 K)	IR (145 K)	Raman (48 K)	IR (58 K)	assignment[a]
		1160 s		
1165 m, br	1164 w	1162 w 1164 w,sh	1161 vw, sh 1164 w	a'', ν_{12}
		1173 vw		
	1184 vw		1185 vw	a'', ν_{35}
1207 m	1207 w	1204 w	1207 w	a'', ν_{34}
1213 w, sh		1210 vw		
	1235 w		1238 w	
1250 vw	1250 m	1247 vw	1250 m	a'', ν_{33}
1262 vw	1266 w, sh	1260 vw		
		1268 vw	1265 w, sh	
1270 w	1271 m	1271 vw	1270 m	a'', ν_{32}
1280 m	1280 m	1282 w	1278 w 1282 m	a', ν_{11}
1296 m	1295 m	1294 w	1297 w	a', ν_{10}
	1329 m, sh		1329 w, sh	
1336 vw	1335 s	1337 vw	1334 s	a'', ν_{30}
	1366 w		1368 w	
	1386 vw		1386 vw	
	1418 w		1420 w	A', 2 x 709 cm^{-1}
1447 s	1445 m	1443 m 1445 m	1444 m 1447 m	a', ν_9
		1450 s		
1466 w	1466 w	1465 w	1461 w 1468 w	a', ν_8
1544 vw		1545 vw		A', 2 x 769 cm^{-1}
		1561 vw		
1566 m, sh		1565 w, sh		
1570 s	1570 w	1570 s	1569 w	a', ν_7
1585 w		1585 vw		
1590 vw, sh		1589 vw	1600 vw	
	1611 w, br		1611 w, br	
			1626 vw	
	1634 vw, br		1634 vw	
	1699 w		1697 w	
	1709 w		1708 w	
	1716 w		1715 w	
2852 w				
2869 m	2868 s	2866 s	2863 s 2869 s	a'
		2883 vw		
		2889 vw		
2891 vw		2892 vw		a'
2897 vw	2899 m	2896 vw	2900 m	
2915 s	2916 m	2913 s	2916 s	a'
2934 m, sh	2931 m, sh	2928 w 2932 m	2929 s 2932 s	a''
2947 s	2946 s	2944 s	2942 s 2947 s	
			2954 s	
2966 s, sh	2966 s, br	2961 m 2965 m,sh	2958 s, sh 2966 s	a''
			2971 s, sh	
2976 s, br		2976 s	2977 s	a'
		2992 s	2991 m	
		3055 m	3048 m 3055 m	a'', vinyl CH str.
3061 s	3059 m	3058 s	3064 m	a', vinyl CH str.
3135 w	3135 w	3136 w	3134 w	A', 2x1570 cm^{-1}

[a] Skeletal modes from reference 16.

The phase transition in norbornylene was also observed to occur by high-pressure IR spectroscopy. Figure 4.3.5 shows two IR spectral regions at various pressures. At 14.9 ± 0.3 kbar, the band profiles changed suddenly, along with a shift of frequencies. The band shapes and frequencies continued to change up to 16 kbar, but then remained essentially constant up to 26 kbar except for pressure-induced frequency shifts. Upon decompression, the phase transition occurred more slowly, broadened-out between 15 and 13 kbar, with the bulk of the spectral changes occurring at 13.3 ± 0.4 kbar.

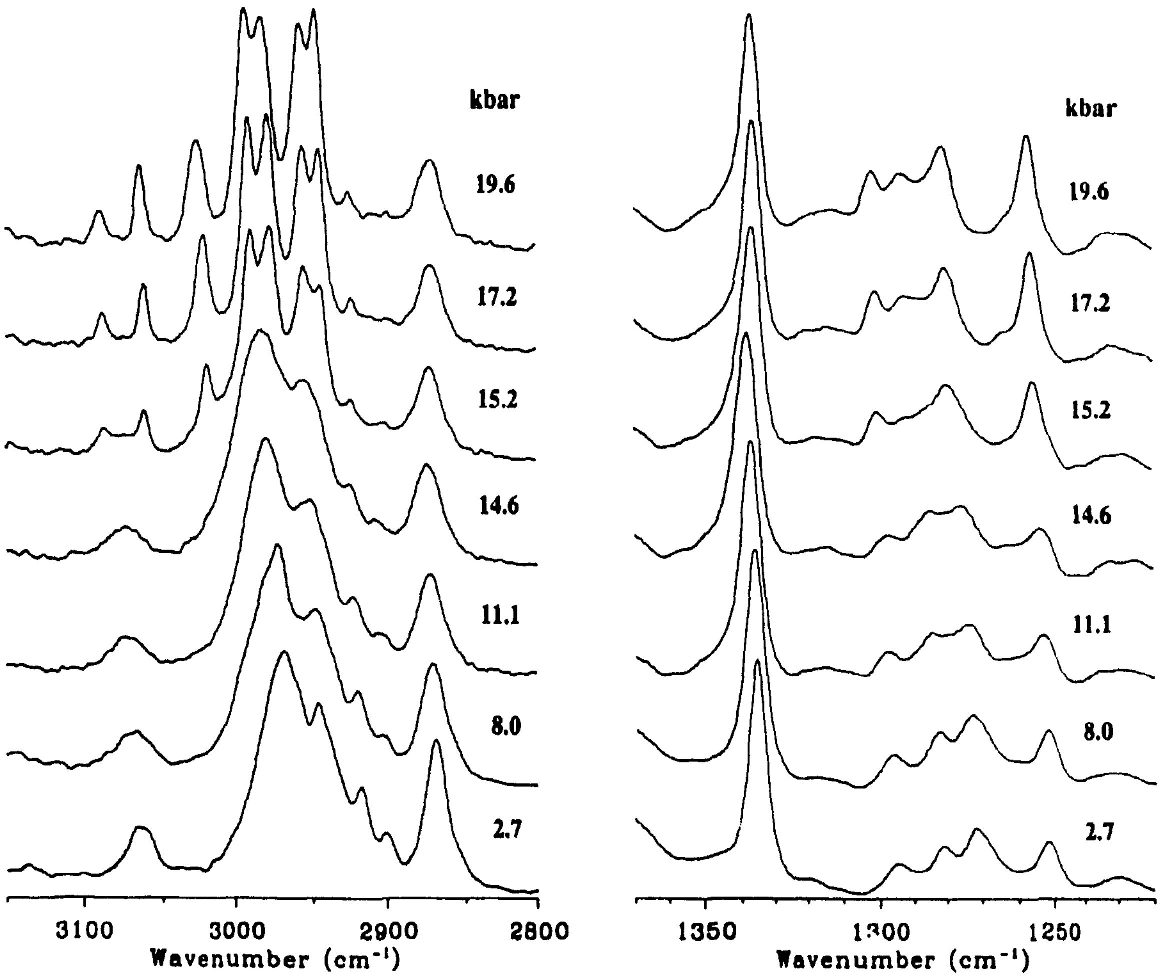

Figure 4.3.5. Two regions of the IR spectrum of norbornylene at the indicated pressures upon compression.

Figure 4.3.6 shows a detailed measurement of one mode, the vinyl CH deformation (1335 cm^{-1} at atmospheric pressure), in both compression and decompression directions. On compression, the band position dropped suddenly at the phase transition, whereas on decompression, the phase transition occurred more slowly about the phase transition point. The 13 K temperature hysteresis is therefore manifested as a 1.6 ± 0.7 kbar pressure hysteresis.

No pressure-volume data have been reported for norbornylene. However, from our measurement of the temperature and pressure hysteresis of the phase transition, the volume change at the transition can be calculated using Equation 4.3.1:

$$\Delta S_t \Delta T_h = \Delta p_h \Delta V_t \qquad [4.3.1]$$

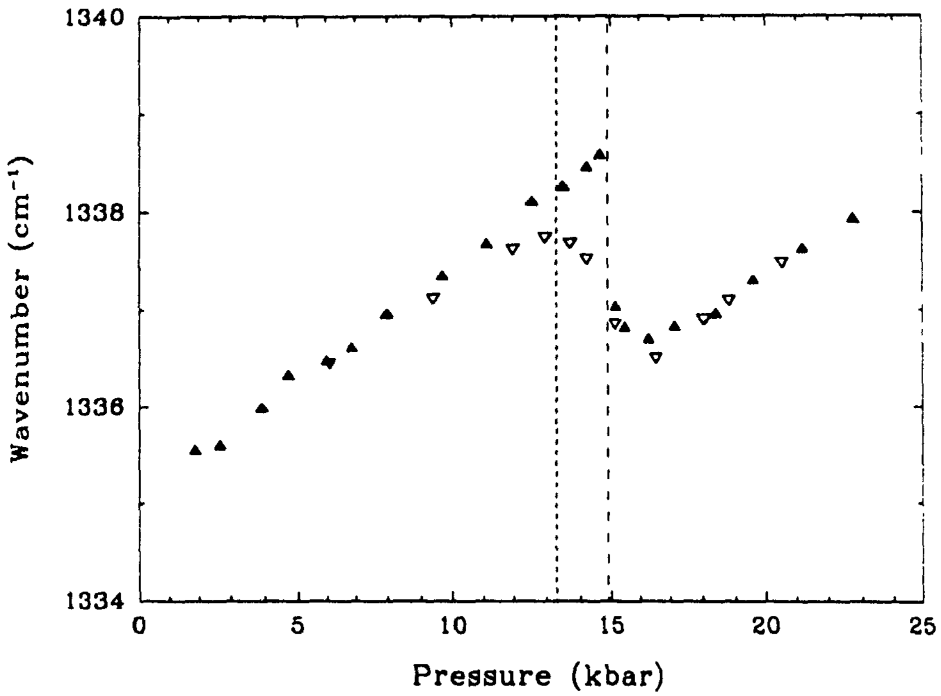

Figure 4.3.6. Infrared peak position of the vinyl CH deformation mode upon compression (▲) and decompression (▽). The lines indicate the phase transition point, *i.e.*, where the majority of spectral changes occur, upon compression (····) and decompression (----).

where ΔS_t and ΔV_t are the entropy and volume changes at the transition, respectively, and Δp_h and ΔT_h are the pressure and temperature hystereses associated with the transition.[21] The volume change at the transition, ΔV_t, is, therefore, 3.1 ± 1 $cm^3 mol^{-1}$, which is comparable with values obtained for other disordered cage hydrocarbons, adamantane (2.3 $cm^3 mol^{-1}$) and 2-methyladamantane (2.8 $cm^3 mol^{-1}$).[22]

Figure 4.3.7 shows the frequencies of several IR peaks plotted against applied pressure; the frequency shifts of the peaks in both phases are summarized in Table 4.3.2. There are several effects that are apparent from these data. As was observed in the case of NBA, there is a definite decrease in pressure dependence of most of the modes in phase II compared to phase I due to the lower compressibility of the ordered phase. The

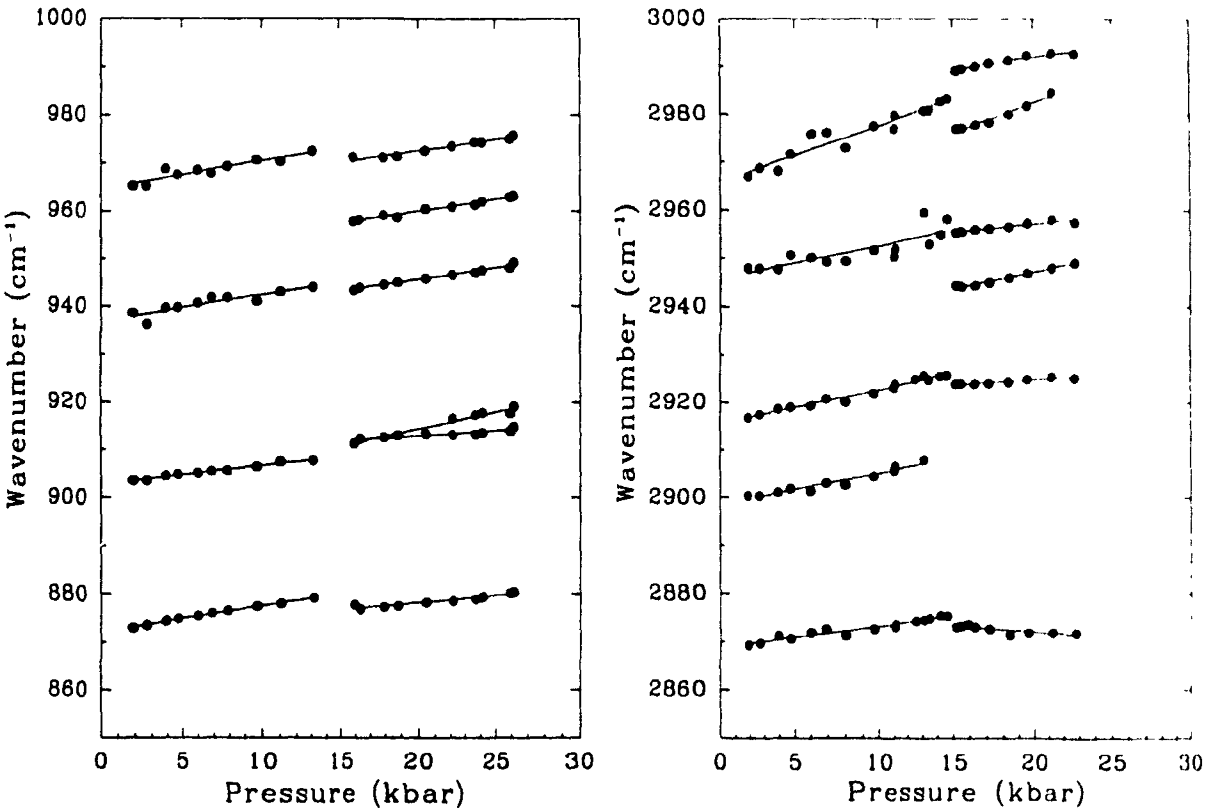

Figure 4.3.7. Pressure dependences of selected IR peaks of norbornylene. Note the factor group splitting displayed in phase II by the 903 cm^{-1} peak.

Table 4.3.2. Pressure Dependences of Infrared Peaks of Norbornylene.

phase I			phase II			
ν (cm^{-1})	dν/dp (cm^{-1}kbar^{-1})	dlnν/dp (kbar^{-1}x10^{4})	ν (cm^{-1})	dν/dp (cm^{-1}kbar^{-1})	dlnν/dp (kbar^{-1}x10^{4})	assignment[a]
708	0.3	4	712	0.3	4	a', sp^2 CH def. o/p
769	0.32	4.2	768	0.1	1	a', CH$_2$ rock + C-C str.
793	0.34	4.3	793	0.29	3.6	a", ring def. i/p
			808	0.22	2.7	a', CH$_2$ rock
832	0.43	5.1	832	0.37	4.4	a", C-C str.
873	0.54	6.2	871	0.29	3.4	a', C-C str.
903	0.40	4.4	902	0.2	2	a', 1-C-bridge C-C str.
			905	0.71	7.9	
937	0.6	6	936	0.49	5.2	a', C-C str.
			952	0.50	5.3	a", C-C str. + ring def. i/p
964	0.6	6	965	0.47	4.9	a', C-C str. + ring def. i/p
1019	0.34	3.4	1019	0.33	3.3	a', 1-C-bridge CH$_2$ rock
1033	0.2	2	1035	0.70	6.8	a", CH$_2$ rock
1090	0.2	2	1093	0.23	2.1	a", CH$_2$ rock
			1115	0.42	3.8	a", 1-C-bridge CH$_2$ twist
1125	0.4	3	1127	0.50	4.5	a', CH$_2$ twist
1250	0.11	0.92	1250	0.29	2.3	a", 1-C-bridge CH$_2$ wag
1271	0.30	2.3	1270	0.28	2.2	a", sp^2 CH def. i/p + sp^3 CH def. i/p
1280	0.26	2.0	1282	0.58	4.5	a', sp^3 CH def. o/p
1295	0.26	2.0	1297	0.32	2.5	a', CH$_2$ wag + sp^3 CH def. i/p
1335	0.23	1.8	1334	0.1	1	a", sp^2 CH def. i/p
1445	0.12	0.85	1444	0.1	0.7	a', 1-C-bridge CH$_2$ scissor
			1461	0.25	1.7	a', CH$_2$ scissor
1570	0.24	1.5	1569	0.1	0.8	a', C=C str.
2868	0.44	1.5	2869	-0.2	-0.8	a', 2-C-bridge CH$_2$ str.
2899	0.67	2.3				a", 2-C-bridge CH$_2$ str.
2916	0.71	2.4	2916	0.21	0.73	a', 2-C-bridge CH$_2$ str.
			2932	0.67	2.3	a", 1-C-bridge CH$_2$ str.
2946	0.7	2	2947	0.33	1.1	a", 2-C-bridge CH$_2$ str.
2966	1.2	4.0	2958	1.2	4.2	a", bridgehead CH str.
			2977	0.52	1.7	a', 1-C-bridge CH$_2$ str.
			2991	1.3	4.5	a', bridgehead CH str.
			3048	0.58	1.9	a", vinyl CH str.
3059	1.1	3.6	3064	0.44	1.4	a', vinyl CH str.
3135	0.8	3	3134	0.87	2.8	A', 2 x 1570 cm^{-1}

[a] Skeletal modes from reference 16.

C=C stretching mode at 1570 cm^{-1} has a particularly low pressure dependence in both phases compared to the C-C stretching modes, due to the lower compressibility of the double bond. Some of the peaks of phase II, such as those at 1035 (a", CH$_2$ rock) and 905 cm^{-1} (a', 1-C-bridge C-C stretch), have particularly high pressure dependences. These peaks are the higher frequency components of modes split by correlation coupling. The application of pressure causes an increase in intermolecular interactions, and, therefore, the large pressure shifts of these particular peaks.

4.4 Norbornadiene

Differential scanning calorimetry at 5 K min^{-1} determined the melting and transition temperatures of NBD to be 254 and 175 K on cooling, and 254 and 201 K on heating. The melting and transition enthalpies were 1.5 and 7.8 kJ mol^{-1}, respectively, and the corresponding entropies were 5.8 and 41.6 J K^{-1} mol^{-1}. These results are again in agreement with those obtained by adiabatic calorimetry.[2]

Figures 4.4.1 and 4.4.2 show IR and Raman spectra of NBD in each of its solid phases. The spectra of phase II are in agreement with the low-temperature spectra reported in the literature.[13,15] The band positions for both solid phases, along with the assignments[13-16] are presented in Table 4.4.1. Little change occurred in the spectra on going from the liquid to phase I, except for line narrowing, but considerable changes occurred at the transition to phase II when the internal modes decreased in bandwidth, and many peaks were observed to shift and split. Furthermore, lattice vibrations characteristic of an ordered crystal appeared in phase II, whereas in phase I only the broadening of the Rayleigh line was apparent, indicating the occurrence of extensive molecular reorientation in a disordered lattice (Figure 4.4.3). This is not unexpected, since the NMR studies showed that lattice diffusion and reorientation occur in the high-temperature phase, and the entropy of transition is very high compared to that of melting, indicating that the major disordering process occurs at the phase transition and not upon melting.

Various possibilities for the factor group of phase II can be postulated by examining the solid state splitting effects. Norbornadiene (C_7H_8) has 39 internal vibrational modes ($\Gamma_{vib}^{int} = 12\ a_1 + 8\ a_2 + 9\ b_1 + 10\ b_2$). All of these are Raman active, while only the a_1, b_1 and b_2 modes are IR active. Several Raman peaks were observed to split into doublets in the Raman spectrum upon cooling from phase I to phase II. In addition, at least seven external modes were observed for phase II in the low-frequency Raman spectrum. From

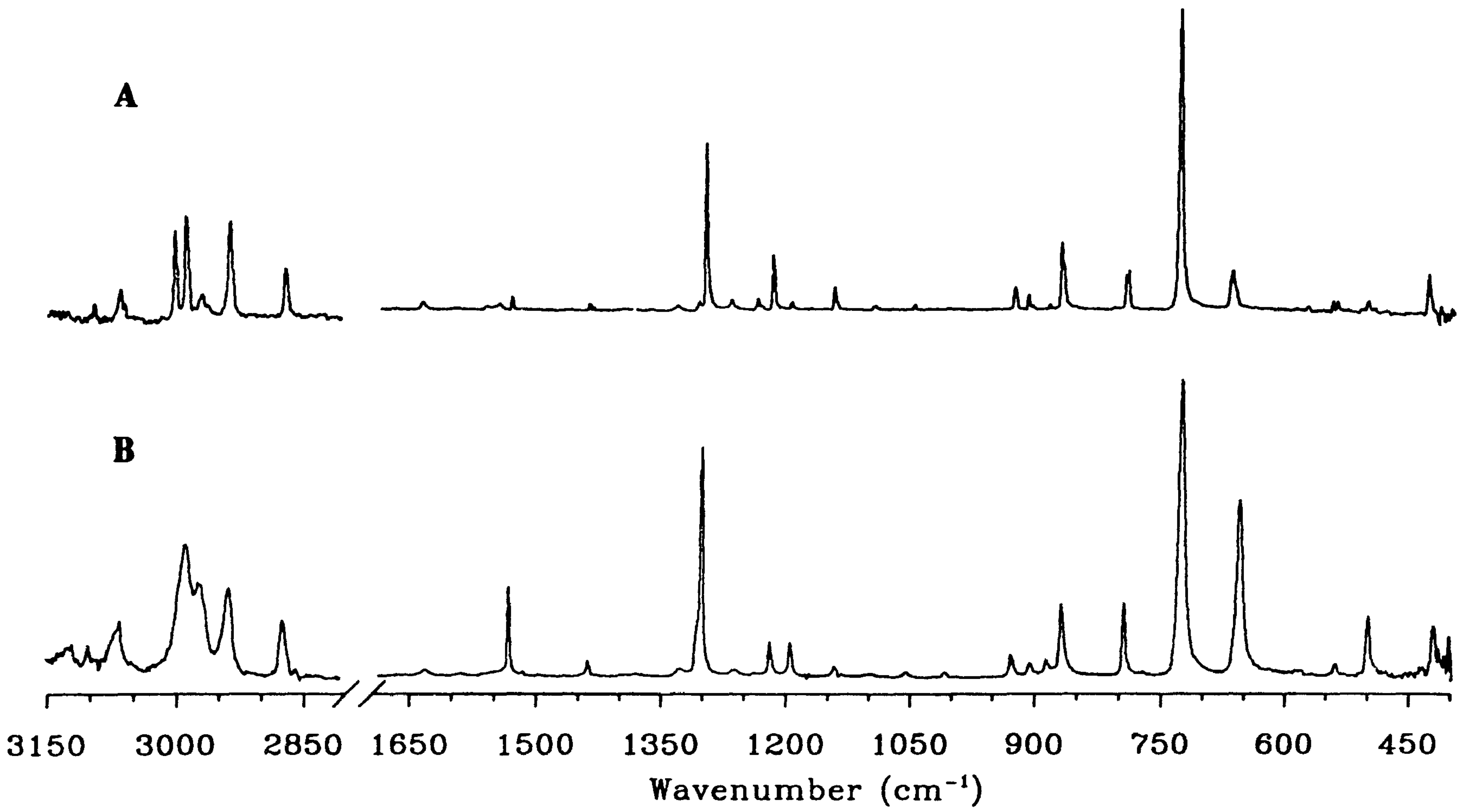

Figure 4.4.1. Infrared spectra of norbornadiene at (A) 160 K and (B) 210 K

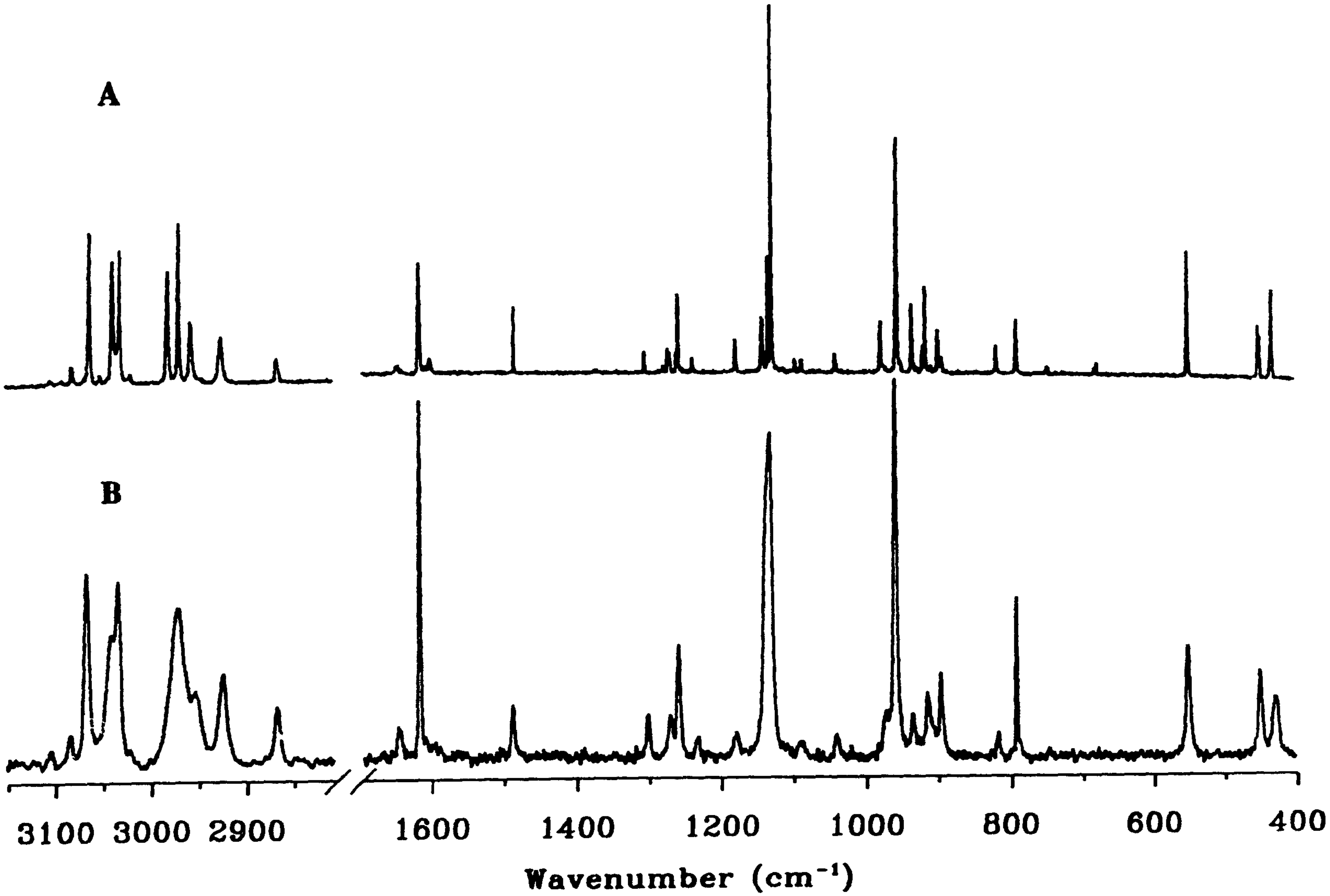

Figure 4.4.2. Raman spectra of norbornadiene at (A) 150 K and (B) 200 K.

Table 4.4.1. Vibrational Data (cm^{-1}) for Norbornadiene.

phase I		phase II		
Raman (200 K)	IR (210 K)	Raman (150 K)	IR (160 K)	assignment[a]
		27 m		lattice modes
		43 w		
		46 w, sh		
		59 m		
		72 m		
		78 m		
		97 s		
425 m	422 m	429 s	431 m	a_1,ν_{12}
446 m		445 m 447 m		a_2,ν_{20}
	502 m		505 w	b_2,ν_{39}
543 m	542 w	543 s	542 w	b_1,ν_{30}
		548 w	547 w	
	668 s	666 w 669 w	671 m	b_2,ν_{38}
		710 vw		
731 vw	728 vs	732 w	733 vs	a_1,ν_{11}
		737 vw		a_2,ν_{19}
775 m		774 m		a_1,ν_{10}
800 w	800 m	801 m	797 m	b_1,ν_{29}
877 w	875 m	874 w	874 w, sh	a_1,ν_9
		879 m	878 m	b_1,ν_{28}
		889 w		a_2,ν_{18}
895 w	894 w	896 m 899 m	893 vw	b_2,ν_{37}
		905 vw 908 w		a_2,ν_{17}
915 w	914 w	914 m	913 vw	b_1,ν_{27}
			918 vw	
938 s	937 w	930 w 934 vw	935 w	a_1,ν_8
950 w		951 w,sh 956 m		b_1,ν_{26}
1017 w	1017 vw	1017 m		b_2,ν_{36}
1066 vw	1062 w	1062 m 1070 m	1057 w	b_2,ν_{35}
		1087 w		
		1095 w		
1107 s	1107 vw	1102 vw 1107 s	1103 w	a_1,ν_7
1111 m, sh		1115 m		a_2,ν_{16}
1152 w	1151 w	1151 m	1154 m	b_1,ν_{25}
1204 w	1204 m	1209 w	1206 w	b_2,ν_{34}
		1222 vw	1222 w, sh	
1229 m	1228 m	1228 m 1229 m, sh	1227 m	a_1,ν_6
1240 w		1239 m 1242 m	1241 w, sh	a_2,ν_{15}
	1246 vw	1249 w	1246 w	
1270 w	1270 w	1273 m	1277 w	a_2,ν_{14}; b_1,ν_{24}
	1312 s		1308 s	b_1,ν_{23}
			1317 w	
	1338 w		1343 w	
1450 w	1449 w	1447 m	1449 vw	a_1,ν_5
		1525 vw		
	1543 m	1541 vw	1543 w	b_2,ν_{33}
1556 vw	1561 w, sh	1560 w	1558 w	

Table 4.4.1. (cont'd.)

phase I		phase II		
Raman (200 K)	IR (210 K)	Raman (150 K)	IR (160 K)	assignment[a]
1568 w		1567 w	1572 vw	
1575 s		1574 s		a_1,ν_4
1602 w	1602 vw	1603 w	1608 vw	
	1645 w		1651 w	
	2853 vw			
2868 w	2868 w	2867 m	2866 m	a_1,ν_3; F.R. 2x1450 cm^{-1}
2935 w	2934 m	2936 m	2934 s	a_1,ν_3; F.R. 2x1450 cm^{-1}
		2960 w	2963 m	
2970 w	2970 m	2973 m	2968 w, sh	b_1,ν_{22}
2990 m	2987 m	2987 s	2987 s	a_1,ν_2
2995 w, sh		3001 s	3000 s	b_2,ν_{32}
3050 vw		3048 w		a_2,ν_{13}
3064 m	3065 w	3060 s	3059 w, sh	a_1,ν_1, F.R. 2x1543 cm^{-1}
3073 m	3070 w, sh	3069 s	3067 m	b_1,ν_{21}
3090 w		3085 w		
3102 m	3102 w	3097 s	3096 w	a_1,ν_1; F.R. 2x1543 cm^{-1}
3123 w	3122 w	3119 m		b_2,ν_{31}
		3132 w		
3146 w		3146 w		A_1; 2x1575 cm^{-1}

[a] From references 13-15 (C-H stretching region) and 16 (skeletal modes).

the symmetry assignments according to force field calculations,[13,16] splittings of the a_1 internal modes are particularly apparent, but the splittings of the a_2, b_1 and b_2 modes are not as clearly defined (Table 4.4.1). None of the IR bands seems to split upon passing through the phase transition. Since the point group symmetry of NBD is C_{2v}, the site symmetry in the ordered phase must be the same, or lower. No site splitting is possible since all modes under C_{2v} symmetry are nondegenerate; however, the site group is important in determining the factor group splittings which were observed. If the molecule occupied a C_1 site, different types of effects could be observed depending on the crystal symmetry. The C_1 and C_i factor groups, with a C_1 site, would not result in any splittings in both the Raman and IR spectra, so the triclinic space groups can be ruled out. Assuming the symmetry of the unit cell is less than cubic, which is reasonable for an ordered phase, any other factor group would result in correlation splitting of all bands in both spectra. Since no IR splittings were observed, the site symmetry must be one of the remaining subsets of C_{2v} symmetry, *i.e.*, C_{2v}, C_s or C_2. Less than half of the vibrational modes coincide in the IR and Raman spectra; therefore, the possibility of a centrosymmetric space group exists. Furthermore, the appearance of at least seven lattice modes in the Raman spectrum suggests that the cell be occupied by at least two molecules. Under the requirement that the a_1 modes must double in the Raman spectrum, but no modes split in the IR, the more likely factor groups can be proposed. The choices are C_{4v}, D_{4h} or D_{2d} with a C_{2v} site; C_4, C_{4h} or S_4 with a C_2 site; or the C_{4h} factor group with a C_s site. The structure of phase II is, therefore, tetragonal, with either two or four molecules per unit cell.

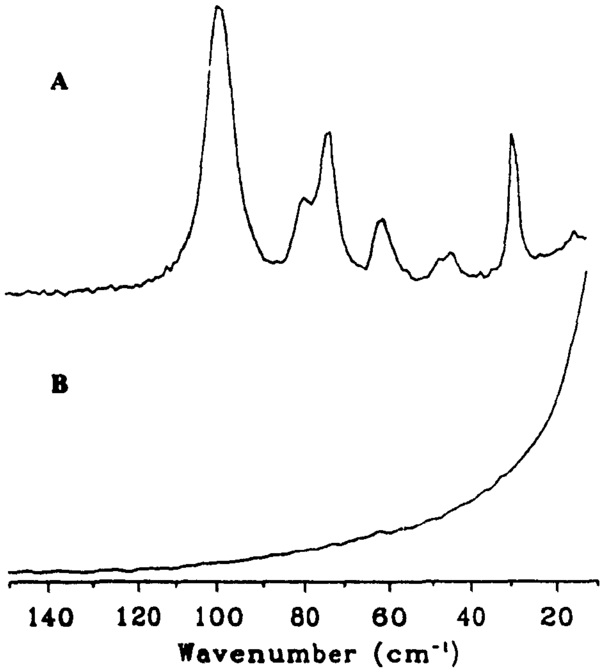

Figure 4.4.3. Low-frequency Raman spectra of norbornadiene at (A) 150 K and (B) 200 K.

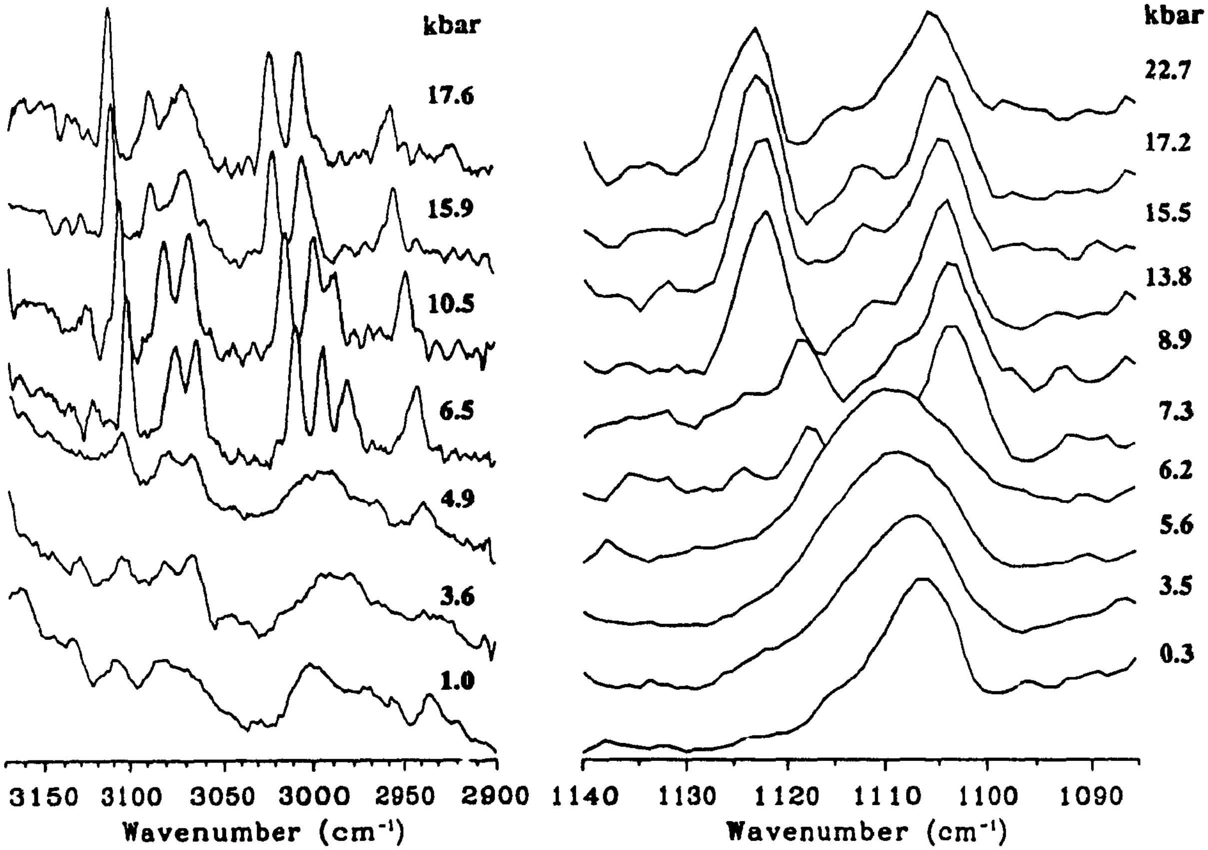

Figure 4.4.4. Two regions of the Raman spectrum of norbornadiene at the indicated pressures upon compression. Note that the shoulder that should appear at 1111 cm^{-1} in phase I was not observed due to the decreased resolution of the variable-pressure experiments.

Raman spectroscopy can also be useful in determining the pressure behaviour of any material. Figure 4.4.4 shows two regions of the Raman spectrum of NBD, the C-H stretching region and the vinyl CH out-of-plane deformation mode, at various pressures. The most obvious changes that occur as a result of the application of high-pressure are the gradual increases in frequencies, and the sudden change at 6.4 ± 1.0 kbar, where a splitting of peaks occurs. The splittings are similar to those observed in the variable-temperature experiments at the transition from phase I to phase II, and the ordered phase obtained by high-pressure thus has the same structure as the low-temperature phase.

Figure 4.4.5 shows the pressure dependences of the frequencies of these same vibrations. A summary of the pressure dependences of all the peaks observed is given in Table 4.4.2. Each mode has a different pressure dependence in the two phases, since the

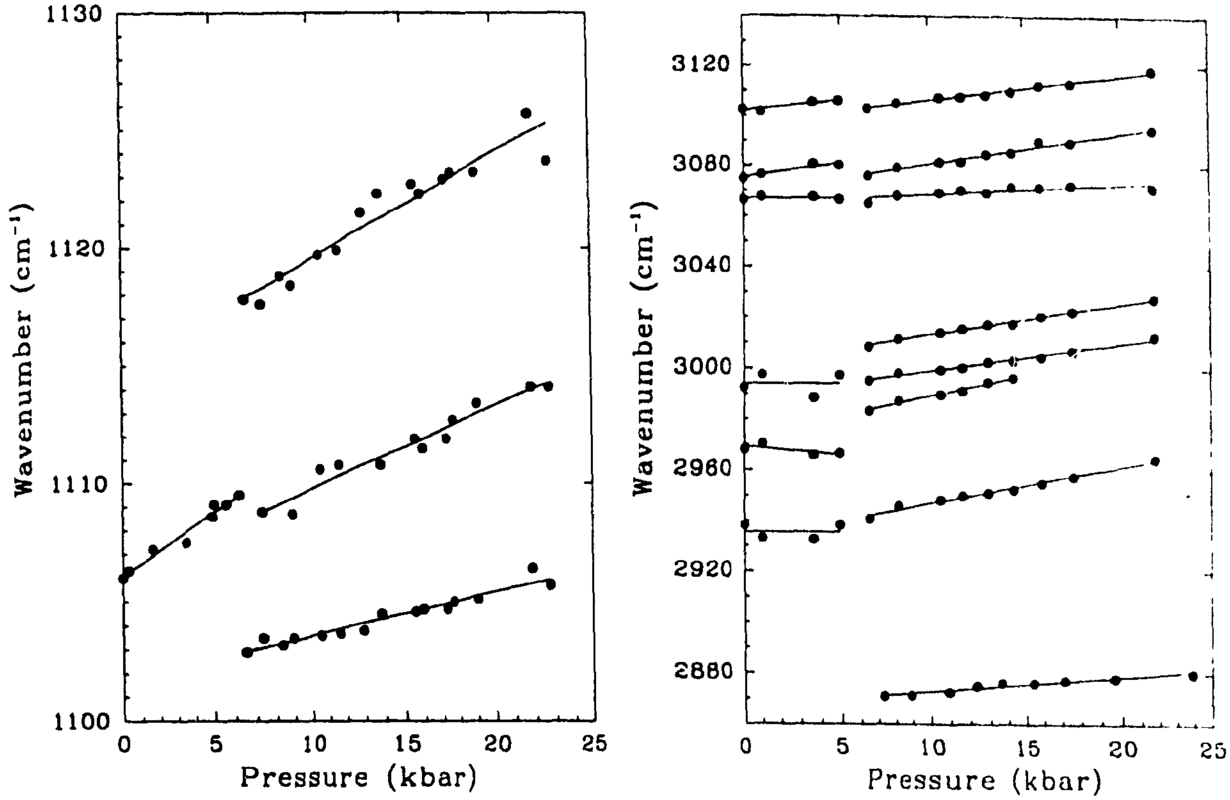

Figure 4.4.5. Pressure dependences of the Raman peaks shown in Figure 4.4.4 The 2868-cm^{-1} peak in the disordered phase was too weak to be measured.

compressibilities of the two crystal forms are not the same. The peaks of the C-H modes in phase I are broad and weak, and therefore, their pressure dependences could not be determined with accuracy. In phase II, however, the C-H modes clearly undergo greater pressure shifting than do the skeletal modes.

A previously unknown case of Fermi resonance was observed in the course of this work. In the low-temperature Raman spectrum of phase II, peaks appear at 1574 and 1560 cm^{-1} (Table 4.4.1). The former is the strong a_1 ν(C=C) mode, while the latter weak peak had been left unassigned,[14] attributed to solid-state splitting,[15] or assigned as a combination.[13] Since this weak vibration was also observed in phase I, it cannot be a result of factor group splitting. The correct assignment of these two modes is now possible as a result of the high-pressure Raman experiments. Figure 4.4.6 shows how the

Table 4.4.2. Pressure Dependences of Raman Peaks of Norbornadiene.

phase I			phase II			
ν (cm^{-1})	$d\nu/dp$ ($cm^{-1}kbar^{-1}$)	$d\ln\nu/dp$ ($kbar^{-1} x 10^4$)	ν (cm^{-1})	$d\nu/dp$ ($cm^{-1}kbar^{-1}$)	$d\ln\nu/dp$ ($kbar^{-1} x 10^4$)	assignment[a]
1107	0.54	4.9	1102	0.19	1.7	a_1, vinyl CH def.
			1107	0.36	3.2	
			1115	0.46	4.1	
			1447	0.091	0.63	a_1, CH_2 scissor
1574	0.35	2.2	1560	0.49	3.1	a_1, C=C str., F.R.
			1574	0.43	2.7	
			2867	0.59	2.0	a_1, methylene CH str., F.R.[b]
			2936	1.4	4.9	a_1, methylene CH str., F.R.[b]
			2973	1.6	5.4	b_1, bridgehead CH str.
			2987	1.1	3.6	a_1, bridgehead CH str.
			3001	1.2	4.1	b_2, methylene CH str.
			3060	0.4	1	a_1, vinyl CH str., F.R.[c]
3073	1.2	3.9	3069	1.2	4.0	b_2, vinyl CH str.
3102	0.9	3	3097	0.99	3.2	a_1, vinyl CH str., F.R.[c]

[a] From references 13-16.

[b,c] Fermi resonance pairs (see text for explanation).

relative intensity of these modes shifts from the higher- to the lower-frequency component with increasing pressure. This effect is highly indicative of Fermi resonance.[23-26] Following the method of Sherman and Lewis,[23] the theoretical energies of the unmixed vibrational modes (ν_a and ν_b) were calculated from the observed Raman peaks (ν_+ and ν_-) using Equation 4.4.1.

$$(\nu_a \text{ and } \nu_b) = 1/2\,(\nu_+ + \nu_-) \pm (\Delta^2 - \delta^2)^{1/2} \qquad [4.4.1]$$

$$\text{where } \Delta = 1/2\,(\nu_+ - \nu_-)$$

$$\delta = \text{minimum value of } \Delta$$

The resulting curves are shown in Figure 4.4.7. Here, the second-order curve fit gave better correlation coefficients to the pressure dependences of both sets of experimental frequencies than did a linear fit. The point of maximum resonance, *i.e.*,

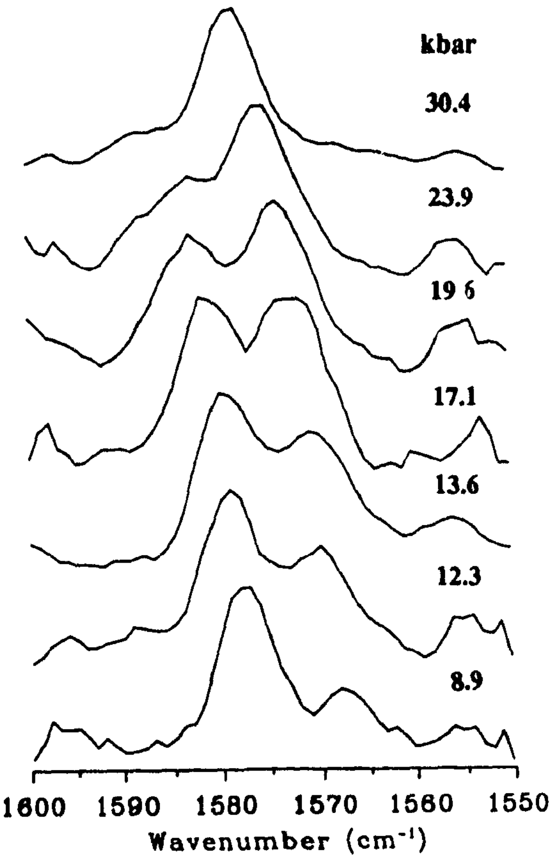

Figure 4.4.6. Raman spectra of the Fermi resonance doublets, ν_+ and ν_-, at the indicated pressures.

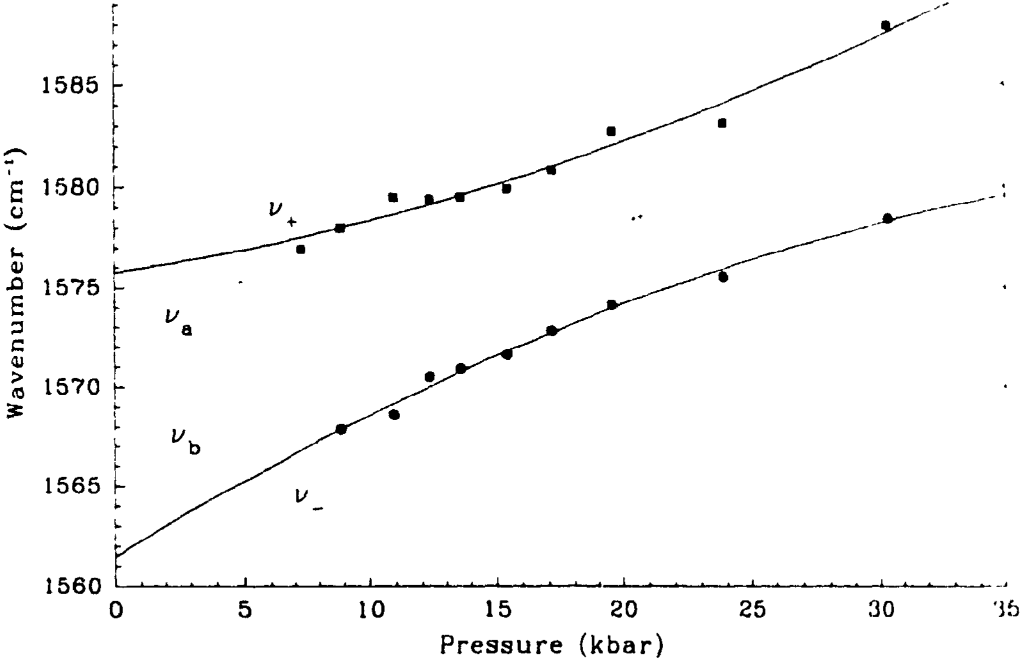

Figure 4.4.7. Pressure dependences of the observed Fermi resonance doublets, ν_+ and ν_-, and the calculated unmixed modes, ν_a and ν_b.

where the intensities of the two peaks should be equal, was calculated to be at 20.6 kbar. Experimentally, this "crossover" point was observed to occur at approximately 17 kbar, which is in agreement with the predicted pressure, and the two unperturbed modes were calculated to occur at 1574 and 1563 cm^{-1} at atmospheric pressure. Two possible combinations could be involved in this resonance effect, that given by Levin and Harris (800 + 775 cm^{-1}),[13] or a combination of the 1152 and 425 cm^{-1} modes. In either case, the combination is the higher frequency component of the pair (1574 cm^{-1}), and involves a vibrational mode which has the same symmetry as the fundamental, a_1. If no mixing of energies occurred, the C=C stretch would be observed at 1563 cm^{-1}.

Examination of the various C-H modes shows that two of the C-H stretching frequencies, occurring at 2867 and 3060 cm^{-1}, are much less sensitive to pressure than the remaining C-H stretches. The two vinyl modes are also Fermi resonance doublets, split by $2\nu_{33}$, the totally symmetric ν(C=C) mode (seen in the IR at 1543 cm^{-1}).[14,15] Similarly, the a_1 methylene C-H stretch is in Fermi resonance with the first overtone of the methylene a_1 bending mode, ν_5, appearing at 1447 cm^{-1}.[13-15] In these cases, the energy levels cannot be decomposed easily as in the previous case. The frequency shifts of these peaks can be seen as the resultant of two opposing effects. Both members of the resonant pair are rapidly increasing in frequency due to the application of pressure, while at the same time, they are being pushed further apart due to a decrease in the Fermi resonance effect at higher pressures. The net result of these effects is that the frequencies of both peaks have positive pressure dependences, but the lower frequency component lags behind. However, because the relative intensities of the resonant peaks do not change by a large amount at higher pressures, this decreased resonant effect is minimal, and the pressure at which Fermi resonance can be broken is much higher than the conditions of the present experiments. The more complicated behaviour of these modes may be due to the location of the C-H bonds on the outer surface of the molecule.

On the basis of variable-pressure DSC measurements, Wenzel and Schneider[27] developed an equation of state for the phase diagram of NBD. The temperature range investigated was limited to 200-225 K, and therefore the maximum transition pressure observed in these studies was only 1.25 kbar. Extrapolation of the data, however, predicts a transition pressure of 7.5 kbar at 295 K, which is in reasonable agreement with the present 6.4 ± 1.0 kbar value observed.

4.5 Discussion

There are several observations of note upon comparison of the high-pressure data for the three related compounds, NBA, NBE, and NBD. Unfortunately, calculation of the mode Grüneisen parameters is not possible since the isothermal compressibilities of any of the solid phases of these compounds are not known. However, since the relation between dlnv/dp and γ_i is linear, the trends of the former values within a given phase of one compound can be analysed in a manner similar to γ_i values. Also, since the compressibilities of disordered phases of organic molecules are typically about 0.02 kbar^{-1}, and κ_s for the ordered phases should also be similar between NBA, NBE and NBD, one can make limited comparisons concerning the three compounds.

It is apparent that the pressure dependences of the peaks of the ordered phases (phase II for NBE and NBD, phase III for NBA) are lower than those of the disordered phases. This is due to the lower compressibilities of the former. Once the transition to the ordered phase has occurred, the crystalline lattice becomes less compressible and the molecules can better resist the application of pressure. The resultant effect is a decrease in the pressure dependences of all vibrational modes compared to those in the disordered phase. The dlnv/dp values for the skeletal modes for all three disordered phases are comparable, ranging in general from 1 to 5 x 10^{-4} kbar^{-1}. These values for the ordered phases, however, are not as similar. In NBE and NBD, neglecting the higher-frequency components of peaks split by correlation coupling, the ordered phases have dlnv/dp values ranging from 1 to 4 x 10^{-4} kbar^{-1}, whereas the majority of skeletal modes of NBA have much lower pressure dependences, ranging from 0.5 to 3 x 10^{-4} kbar^{-1}. This confirms the assumption that the disordered phases of NBA, NBE, and NBD have similar compressibilities, while also revealing that the compressibility of the ordered phase of NBA is lower than those of NBE and NBD.

For some inorganic systems, the γ_i values have been shown to increase systematically according to the decrease in frequency of the vibrational modes, due to the greater ease of distortion of weaker bonds.[28,29] However, these conclusions were based on high-pressure Raman experiments on As_4S_4, S_4N_4, As_2S_3, and S_8. This trend in γ_i, or rather, in dlnv/dp, is certainly not observed with NBA, NBE and NBD, due to the many different types of bonds within each molecule. Still, there are some general trends which occur within a given phase of each compound. Firstly, within the carbon skeleton, the pressure dependences of the stretching modes are generally higher than those of the bending modes. This is because the force constants of bending modes do not depend as heavily upon interatomic distance as do those of stretching modes. Secondly, the components of modes affected by factor group splitting diverge with increasing pressure due to increases in intermolecular interactions. This is exemplified in both NBE (902 and 905 cm^{-1}) and NBD (1102 and 1107 cm^{-1}). The assignment of factor group splittings in Table 4.2.1 was both aided and confirmed by the very high dlnv/dp values of certain modes of the ordered phase. The lack of any peaks with particularly high pressure dependences in phase III of norbornane (Table 4.1.2) also supports the observation of the absence of solid-state splittings in the low-temperature spectra.

The behaviour of the C-H stretching modes has proven difficult to interpret in the high-pressure vibrational spectroscopic studies. Adding to the difficulty is the lack of assignments in the literature of these modes in particular. Only one study has explicitly assigned the C-H stretching modes by symmetry and general description in NBA and NBD.[13] Several authors have stated that the possibility for Fermi resonance in this region is very high, and assignments have been made to this effect. However, it has been clearly observed in the case of NBD that these high-frequency stretches do not exhibit the characteristic Fermi resonance effect documented in the literature[23-26] and observed in the present study between the 1560 and 1574 cm^{-1} peaks in phase II of NBD. One explanation that can be attributed to this anomalous behaviour is the location of the C-H bonds on the outsides of the molecular cages. The sensitivity to pressure varies greatly among the C-H stretching modes, even within the same molecule. The pressure dependences, however, can be qualitatively explained in terms of the C-H bond length and strength as determined by the strain on each carbon atom of the cage.

Table 4.5.1. Carbon Skeletal Geometries of Norbornane, Norbornylene, and Norbornadiene According to *Ab Initio* Calculations.[36]

bond angle*	NBA	NBE	NBD
C_1-C_7-C_4	94.6	93.7	92.0
C_1-C_6-C_5	103.2	102.9	
C_1-C_2-C_3		107.9	107.4
C_2-C_1-C_6	107.7	105.4	106.3
C_6-C_1-C_7	101.6	99.8	
C_2-C_1-C_7		100.8	98.3

*Refer to Figure 4.1.1 for atom numbering.

Norbornane, norbornylene, and norbornadiene all have the same basic cage structure. Several molecular structural studies have been performed on these compounds, including electron diffraction,[30-32] microwave spectroscopy,[33] x-ray diffraction,[34] and *ab initio* computations.[35-37] An analysis of several sources of experimental data, combined with molecular mechanics calculations, has been reported for NBA.[38,39] Two *ab initio* studies address all three compounds at once, arriving at very similar structures and, for this reason, the structural parameters resulting from these investigations will be used in the present discussion.[35,36] Table 4.5.1 compares the bond angles of the structures of NBA, NBE, and NBD, according to the atom numbering given in Figure 4.1.1. The idea that lower frequency peaks exhibit greater pressure shifting[28,29] can now be extended to the cage hydrocarbons. The discussion will confine itself to the ordered phases of these solids for which a greater amount of pressure data has been collected. In NBA, the bridgehead carbons (C_1 and C_4) are highly strained and hence have the strongest C-H bonds. Next, the 1-C-bridge methylene carbon (C_7) is the most distorted, followed by the 2-C-bridge methylene carbons (C_2, C_3, C_5, and C_6). The more strained carbons should have stronger C-H bonds with shorter bond lengths, and therefore should have lower pressure dependences. However, this was not observed because there are actually two opposing effects which are involved. The effect of decreasing interatomic distance upon force constant was discussed in section 2.2.5, where a 1% decrease in bond length would result in approximately a 6% increase in vibrational force constant. Thus, if two bonds of equal length having different force constants are subjected to compression, the weaker bond would be more sensitive to pressure since it is easier to deform. However, when examining different bonds within a molecule, not only do bonds of different strength have to be considered, but bonds of very different lengths as well. It has been observed that C-H stretching modes often have higher pressure dependences than C-C stretching bands. Although C-H bonds are much stronger, and hence more difficult to compress, they are also much shorter, and a small decrease in bond length would be high in terms of a percent decrease. Another contribution to these large pressure dependences is that vibrations involving hydrogens are the most anharmonic, and thus these force constants depend even more upon interatomic distance.

Returning to the discussion concerning the different C-H stretching modes in NBA, as assigned by Levin and Harris,[13] the pressure dependences of the two ν(C-H) peaks which involve the bridgehead carbon are higher than the value for the pure 2-C-bridge C-H stretching band. This is in accordance with the order of lessening strain on each carbon atom (Table 4.1.2). Thus, it follows that the decrease in bond length has a more significant effect than does the increase in bond strength. In the case of NBD, the most strained is again the bridgehead carbon, even more so than in NBA due to the shorter, 2-carbon bridges. Next is the methylene carbon (1-C-bridge), and finally, the olefin carbons. These vinyl C-H bonds, however, have a much shorter bond length and a much higher force constant than do the bonds of saturated carbons, and they should be treated separately. The trends of dlnv/dp values of Table 4.3.2 follow the prediction somewhat, neglecting the effects of Fermi resonance. The vinyl C-H stretches seem to have pressure dependences similar to the methylene stretches, but still lower than the bridgehead C-H stretches. The case of NBE ties the other two cases together in that it incorporates the structures of both. No assignments of any C-H modes have been reported for NBE in the literature, and the results of the high-pressure IR experiments can now be used to assign this region of the spectrum.

In the NBE molecule, the most strained carbon is again the bridgehead atom, followed by the 1-C-bridge methylene carbon, the olefin carbons, and finally the 2-C-bridge methylene carbons. Simply from their positions, the vinyl C-H stretches are clearly those at 3048 and 3064 cm^{-1} (in phase II), and they exhibit moderate dlnv/dp values. The peaks at 2958 and 2991 cm^{-1}, due to their large pressure dependences, are most likely bridgehead C-H stretches. The 2-carbon bridge methylene C-H stretches should have the lowest pressure dependences, and may include the peaks at 2869, 2916 and 2947 cm^{-1}. Finally, the peak with a moderately high pressure dependence, occurring at 2932 cm^{-1}, can be assigned to the 1-C-bridge methylene C-H stretch. The remaining peak at 2977 cm^{-1} may be either of the methylene stretches. These assignments, however speculative, are quite reliable in light of the large range of dlnv/dp values within the C-H stretching region, and the reasoning used to make these assignments will be continued in each of the chapters to follow.

References

1. N. G. Parsonage and L. A. K. Staveley, *Disorder in Crystals*, Clarendon, Oxford, 1978.
2. E. F. Westrum in *Molecular Dynamics and Structure of Solids*, (R. S. Carter and J. J. Rush, eds.), National Bureau of Standards, Washington, D. C., 1969, p. 459.
3. R. L. Jackson and J. H. Strange, Acta Cryst., **B28**, 1645 (1972).

4. R. Folland, R. L. Jackson, J. H. Strange, and A. V. Chadwick, J. Phys Chem. Solids, **34**, 1713 (1973).
5. R. Folland, S. M. Ross, and J. H. Strange, Mol. Phys., **26**, 27 (1973).
6. A. V. Chadwick and J. W. Forrest, J. Chem. Soc., Faraday Trans I, **74**, 2560 (1978).
7. M. Bee, H. Jobic, and C. Caucheteux, J. Chim. Phys., **83**, 623 (1986).
8. M. Bee, J. Elkhamkhami, and H. Jobic, J. Phys., Condens. Matter, **2**, 1945 (1990).
9. R. E. Wasylishen, S. Peiris, and D. R. Arnold, Chem. Phys. Lett., **114**, 31 (1985).
10. R. Folland, D. A. Jackson, and S. Rajagopal, Mol. Phys., **30**, 1053 (1975).
11. R. Folland, D. A. Jackson, and S. Rajagopal, Mol. Phys., **30**, 1063 (1975).
12. M. Ricco, C. Bucci, R. De Renzi, G. Guidi, P. Podini, R. Tedeschi, and C. A. Scott, J. Chem. Phys., **86**, 4198 (1987).
13. I. W. Levin and W. C. Harris, Spectrochim. Acta, **29A**, 1815 (1973).
14. D. M. Adams and W. S. Fernando, Inorg. Chim. Acta, **7**, 277 (1973)
15. I. S. Butler and G. Barna, J. Raman Spectrosc., **1**, 141 (1973).
16. R. A. Shaw, C. Castro, R. Dutler, A. Rauk, and H. Wieser, J. Chem. Phys., **89**, 716 (1988).
17. R. P. Carlile, T. L. Smithson, and H. Wieser, J. Mol. Struct., **96**, 283 (1983).
18. Y. Brunel, C. Coulombeau, C. Coulombeau, M. Moutin, and H. Jobic, J. Am. Chem Soc., **105**, 6411 (1983).
19. Z. Meic, M. Randic and A. Rubcic, Croat. Chem. Acta, **46**, 25 (1974).
20. R. M. Paroli, N. T. Kawai, I. S. Butler, and D. F. R. Gilson, Can. J. Chem., **66**, 1973 (1988).
21. E. B. Smith, J. Phys. Chem. Solids, **9**, 182 (1959).
22. K. Hara, Y. Katou, and J. Osugi, Bull. Chem. Soc. Jpn., **54**, 687 (1981).
23. W. F. Sherman and S. Lewis, Spectrochim. Acta, **35A**, 613 (1979).
24. A. Tartag and D. Fabre, J. Chim. Phys., **84**, 981 (1987).
25. P. T. T. Wong, T. E. Chagwedera, and H. H. Mantsch, J. Chem. Phys., **87**, 4487 (1987).
26. H. Olijnyk, H. Daufer, H.-J. Jodl, and H. D. Hochheimer, J. Chem. Phys., **88**, 4204 (1988).
27. U. Wenzel and G. M. Schneider, Thermochim. Acta, **109**, 111 (1986)
28. R. Zallen, Phys. Rev., **B9**, 4485 (1974).
29. R. Zallen and M. L. Slade, Phys. Rev., **B18**, 5775 (1978).
30. Y. Morino, K. Kuchitsu, and A. Yokozeki, Bull. Chem. Soc. Jpn., **40**, 1552 (1967).
31. J. F. Chiang, C. F. Wilcox, Jr., and S. H. Bauer, J. Am. Chem. Soc., **90**, 3149 (1968).
32. A. Yokozeki and K. Kuchitsu, Bull. Chem. Soc. Jpn., **41**, 2356 (1971).

33. J. F. Chiang, R. Chiang, K. D. Lu, E.-M. Sung, and M. D. Harmony, J. Mol. Struct., **41**, 67 (1977).

34. L. Doms, D. Van Hemelrijk, W. Van de Mieroop, A. T. H. Lenstra, and H. J. Geise, Acta Cryst., **B41**, 270 (1985).

35. K. B. Wiberg, G. Bonneville, and R. Dempsey, Isr. J. Chem., **23**, 85 (1983).

36. C. R. Castro, R. Dutler, A. Rauk, and H. Wieser, J. Mol. Struct. (Theochem), **37**, 241 (1987).

37. G. Wipff and K. Morokuma, Tetrahedron Letters, **21**, 4445 (1980).

38. L. Doms, L. Van den Enden, H. J. Geise, and C. Van Alsenoy, J. Am. Chem. Soc., **105**, 158 (1983).

39. N. L. Allinger, H. J. Geise, W. Pyckhout, L. A. Paquette, and J. C. Gallucci, J. Am. Chem. Soc., **111**, 1106 (1989).

CHAPTER 5. QUADRICYCLANE

5.1 Introduction

Quadricyclane, tetracyclo[3.2.0.0^{2,7}.0^{4,6}]heptane, is a structurally interesting cage molecule having a high degree of strain within its hydrocarbon skeleton. Consisting of only seven carbon atoms, the molecule contains two cyclopropane, one cyclobutane, and two cyclopentane rings. The synthesis of the quadricyclane skeleton was first reported by Cristol and Snell in 1958, who irradiated a dicarboxylated NBD derivative to form a dicarboxylated quadricyclane.[1] The first synthesis of the pure hydrocarbon was reported separately by two groups in 1961, as the irradiation product of NBD.[2,3] This reaction was discovered to be reversible, with quadricyclane reverting back to NBD either when heated to 140°C or when irradiated with ultraviolet light in the presence of a catalyst:

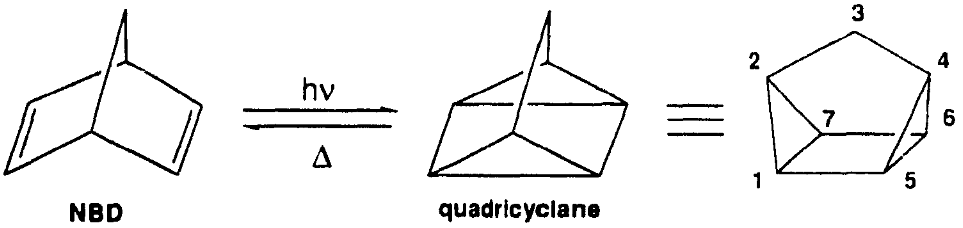

The photochemical synthesis of quadricyclane has been investigated by many authors, encouraged by the possibility of storing solar energy in the strained carbon-carbon bonds. The premise is to transform NBD to quadricyclane using sunlight, and then to convert the product back again with an appropriate catalyst resulting in the release of heat. The main problem with this system is the almost total lack of overlap between the electronic absorption spectrum of NBD and the solar radiance spectrum. Many studies have been undertaken to develop and evaluate suitable catalysts that will absorb sunlight and sensitize the conversion process, including various aromatic ketones, alone[4,5] or polymer-bound,[6] and copper(I) charge-transfer complexes of di-2-pyridyl ketone.[7] Another approach has been the synthesis of larger molecules containing the NBD moiety.[8] Another difficulty that must be overcome is the development of a suitable catalyst that will quantitatively convert quadricyclane back to NBD. Many inorganic and organometallic catalysts have been proposed,[9] for example, cobalt porphyrin derivatives used in the conversion of water soluble quadricyclane derivatives.[10] The advantage of using an aqueous system is that the flammability, toxicity, and expense of organic solvents are avoided. Another interesting approach has been the development of an electrochemical single-electron-transfer "switch" that can be used to start and stop the conversion of quadricyclanes to NBD's.[11]

The other main area of interest in quadricyclane has been from the molecular structural point of view. A standard heat of formation of quadricyclane of 339.1 ± 2.3 kJ mol^{-1} was measured by bomb calorimetry,[12] and the heat of isomerization of quadricyclane to NBD was measured by temperature-programmed calorimetry[13] as -92 ± 4 kJ mol^{-1}. Microwave spectroscopy[14] has revealed a small dipole moment in quadricyclane of 0.0199(2) D. The molecular structure has been investigated experimentally by gas electron diffraction,[15] resulting in the conclusions that the cyclobutane ring is planar and the molecular symmetry is C_{2v}. In this determination, however, some of the bond lengths had to be constrained to the lengths of those in either cyclopropane or NBA, resulting in different models. More recently, the structure of quadricyclane has been the subject of computational analyses. In an examination of several cyclopropane derivatives, MM2 calculations were determined to be more suitable than *ab initio* and semi-empirical MNDO methods for these highly strained structures.[16] The structure of quadricyclane, however, proved difficult to determine with any of these methods, since none of them could accurately predict the heat of isomerization of quadricyclane to NBD. Another *ab initio* study, employing force relaxations on a 4-21G basis set,[17] determined the structures of several strained hydrocarbons, with the authors' claim that structural trends can be predicted more reliably by this type of calculation over experimental methods. Trends in C-C and C-H bond distances were discussed, the latter bond lengths being difficult to obtain experimentally. In a later study by these same authors, the gas electron diffraction data were reinvestigated under constraints taken from these *ab initio* calculations to form a molecular orbital constrained electron diffraction (MOCED) model.[18] While this model did not improve the fit to the original data, the method was thought to be superior due to intrinsic consistency. Vibrational frequencies were also calculated from the *ab initio* force constants.

No vibrational spectra have been reported for quadricyclane, except for a few ν(C-H) fundamentals and overtones measured in the gas phase.[19] An investigation of the phase transition(s) in quadricyclane has not been performed either. Due to its interesting "globular" framework, and its structural similarities and differences with the norbornane series of disordered compounds, a calorimetric and vibrational spectroscopic study was undertaken to probe the temperature- and pressure-induced phase behaviour of quadricyclane.

5.2 Variable-Temperature Studies

The phase behaviour of quadricyclane was completely unknown; therefore, DSC measurements were performed to measure the transition temperatures, and to observe the presence of memory effects in the sample. A sample of quadricyclane was analyzed at 5 K min^{-1} to the lower temperature limit of the calorimeter, revealing the melting transition at 227 K and a single, sharp phase transition at 153 K on cooling (180 K on heating). The sample was cycled repeatedly at 20 K min^{-1}, and in each scan, the same two peaks were observed, broadened somewhat due to the faster scan rate. Immediately after, the thermogram was repeated at 5 K min^{-1}, and no anomolous effects were observed (Figure 5.2.1). The average enthalpy and entropy changes of the melting transition were determined to be 1.0 kJ mol^{-1} and 4.5 J K^{-1} mol^{-1}. The phase transition enthalpy was 6.9 kJ mol^{-1} on cooling and 7.2 kJ mol^{-1} on heating (average ΔH_t = 7.0 kJ mol^{-1}), and the

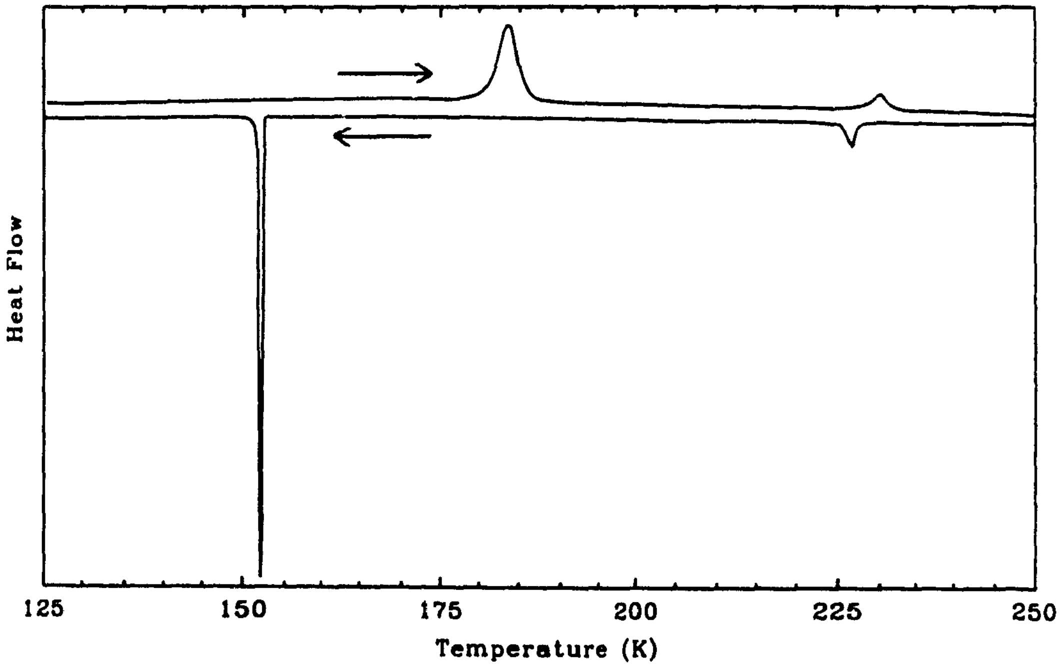

Figure 5.2.1. Differential scanning calorimetric thermogram of quadricyclane, scanning at 5 K min^{-1}.

transition entropy was 45.0 J K^{-1} mol^{-1} on cooling and 40.0 J K^{-1} mol^{-1} on heating (average $\Delta S_t = 42.5$ J K^{-1} mol^{-1}). Simply from the low entropy of melting and the very high entropy of transition, quadricyclane exists as an orientationally-disordered solid falling under the classification of a plastic crystal.

Quadricyclane has a very high entropy of transition, even compared to other plastic crystals, and its disordered phase exists over only a small temperature range of 47 K. These results are consistent with thermodynamic data for other organic plastic crystals, *i.e.*, the smaller the temperature range of the plastic phase, the higher the transition entropy. There have been attempts to quantitatively relate thermodynamic data with symmetry properties. The Guthrie-McCullough method[20] combines symmetry elements of the lattice and the molecule to determine the number of equivalent, distinguishable molecular orientations in each solid phase. The entropy of transition is then given by:

$$\Delta S_t = R \ln (N_1/N_2) \qquad [5.2.1]$$

where N_1 and N_2 are the number of molecular orientations allowed in the disordered and ordered phases (usually 1), respectively. This equation fails, however, since it does not account for the volume change at the phase transition, which is a large contributor to the transition entropy. Clark *et al.* have proposed an equation relating the entropy of transition, ΔS_t, with the number of distinguishable orientations of the molecule in the disordered lattice (hexagonal or cubic), and the temperature range of the disordered phase.[21] By fitting the data for five disordered hydrocarbons (including NBA and adamantane), the entropy of transition was defined as:[22]

$$\begin{aligned} \Delta S_t &= R \ln (N_1/N_2) + \Delta S_\tau \\ &= R \ln (N_1/N_2) + [10.3 + 71.6 \exp -\{0.01968[T_m - T_t]\}] \qquad [5.2.2] \end{aligned}$$

where ΔS_τ is the "excess entropy" resulting from the volume change, and $[T_m\text{-}T_{Tr}]$ is the temperature range of the disordered phase. The relation between molecular dimensions and temperature range of the disordered phase was also derived from data from five compounds, and is given by:

$$[T_m\text{-}T_t] = 367\text{-}130(|D_2\text{-}D_1|) \qquad [5.2.3]$$

where $|D_2\text{-}D_1|$ is the difference in molecular dimensions. It should be noted that the second term of ΔS_τ is small compared to 10.3. In the second of their two papers,[22] the authors tested equation 5.2.2 with several methyl- and halo-substituted adamantane derivatives. The data could not be described correctly by the theory, however, and they concluded that the complications arise from the introduction of substituent groups.

Quadricyclane is a pure hydrocarbon with the same symmetry as NBA, and it should agree with equation 5.2.2 very well. Clark *et al.* positioned the NBA molecule into a body-centred cubic lattice, with the C_2 axis of the molecule coincident with the C_4 axis of the crystal.[21] Thus, there are twelve equivalent, distinguishable orientations of the NBA molecule in the lattice, and this N_1 value and the experimental ΔS_t of 31.4 J K^{-1} mol^{-1} were used in the determination of equation 5.2.2. However, if the experimental ΔS_t and $[T_m\text{-}T_t]$ data for quadricyclane are substituted, the equation results in an N_1 value of 1. Since there is a large temperature hysteresis associated with the phase transition, the data obtained in the cooling direction results in a higher N_1 value of 9. In either case, however, the predicted N_1 value of 12 cannot be calculated.

Low-temperature IR and Raman spectra were recorded to observe structural characteristics of the quadricyclane phases. As expected, no obvious changes were observed upon cooling through the fusion temperature, and the spectra remained liquid-like throughout the disordered phase. The lack of any lattice modes in the plastic phase suggest that the phase I is isotropic, similar to the disordered phases of NBA, NBE, and NBD. At the phase transition temperature, sudden and dramatic changes occurred in both spectra, with many peaks splitting throughout the spectral region. Typical IR and Raman spectra of both phases are shown in Figures 5.2.2 and 5.2.3, respectively. In the low-frequency Raman spectrum, a forest of at least thirteen peaks appeared (Figure 5.2.4). Cooling further resulted only in sharpening of these bands, and no other transitions were observed as low as 45 K. This is not surprising since the sharp lattice modes indicate that phase II is completely ordered, and no further transitions would be expected. The vibrational frequencies of quadricyclane in both solid phases are summarized in Table 5.2.1., as well as some general assignments. Quadricyclane, C_7H_8, has 39 normal modes given by $\Gamma_{vib}^{int} = 12a_1 + 8a_2 + 10b_1 + 9b_2$ under C_{2v} molecular symmetry. Due to the high ring strain in the molecule, the C-H stretching bands ($\Gamma_{v(C-H)} = 3a_1 + a_2 + 2b_1 + 2b_2$) can be assigned more definitively. The three polarized Raman bands at 2858, 2929, and 3080 cm^{-1} all have a_1 symmetry, and can be attributed to the methylene, the C_2-H and C_4-H, and the four cyclobutane C-H (C_1-H, C_5-H, C_6-H, and C_7-H) stretches, respectively. The three other higher-frequency bands, occurring at 3050, 3059, and 3071 cm^{-1}, are also cyclobutane C-H stretches. The band at 2942 cm^{-1} can be assigned as the antisymmetric $C_{2(4)}$-H stretch, while the final band at 2910 cm^{-1} is the antisymmetric methylene stretch.

In phase I, the quadricyclane molecules reorientate extensively and no other structural information can be deduced simply from the vibrational spectra. Its lattice may have hexagonal symmetry like the norbornane series, or it may be cubic, which is more common for organic cage molecules. The structure of phase II, however, can be examined more thoroughly in light of the many peaks that split as a result of correlation coupling. Upon cooling through the phase transition, many bands in both the IR and Raman spectra were observed to split into two in phase II, resulting in far more peaks than the number of normal modes anticipated. Furthermore, there are possibilities that some of the Raman peaks are split into triplets rather than doublets. For example, the

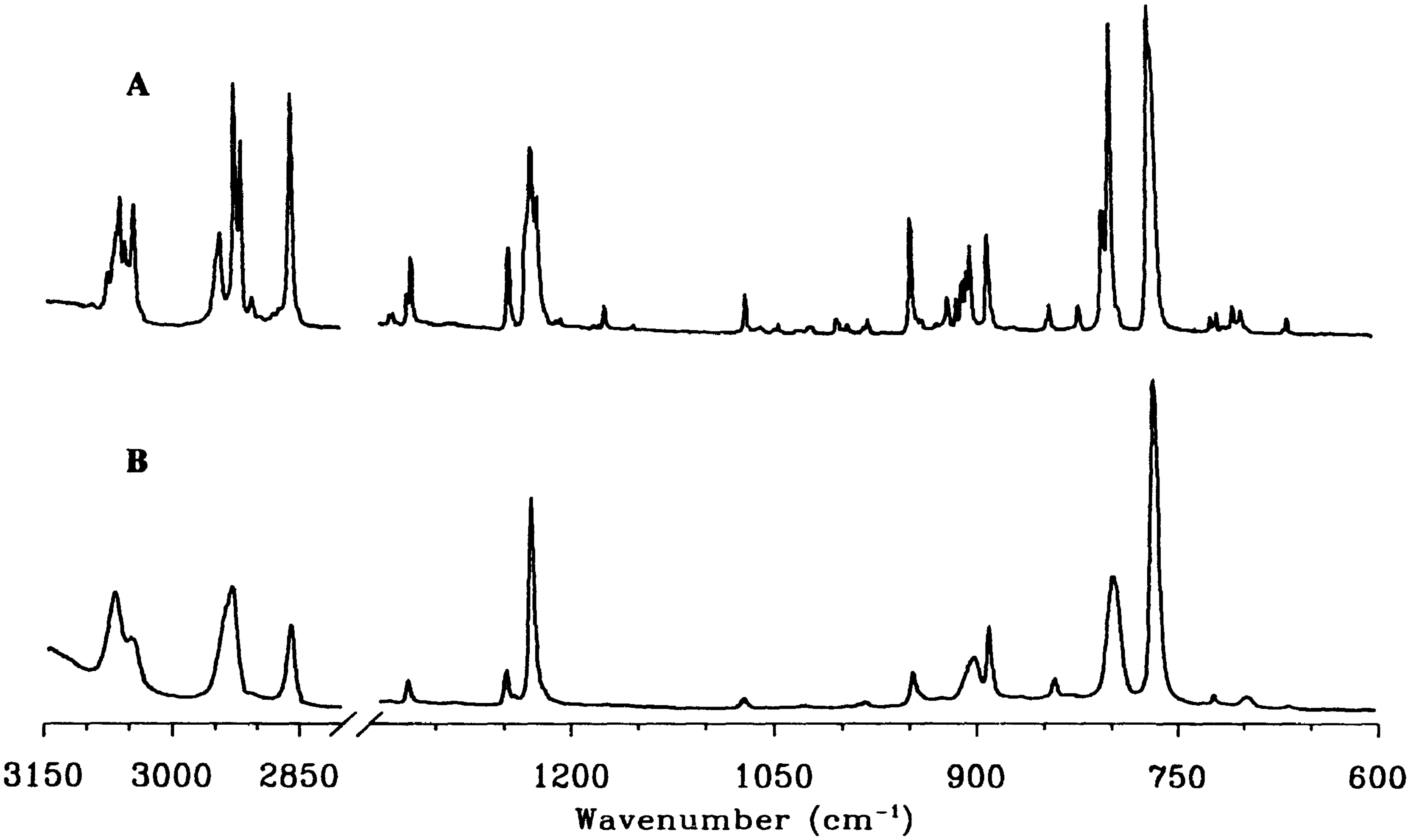

Figure 5.2.2. Infrared spectra of quadricyclane at (A) 45 K and (B) 180 K

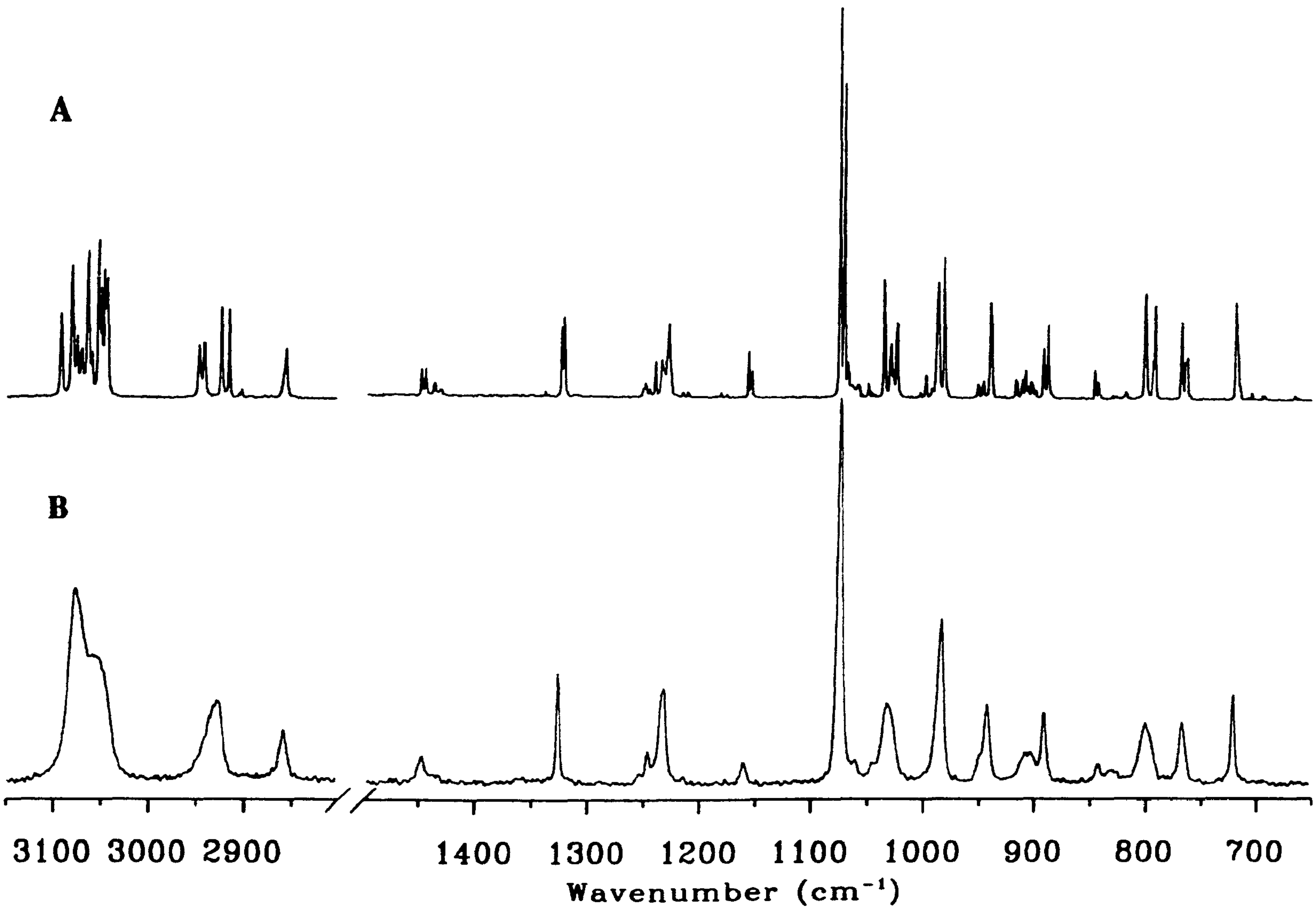

Figure 5.2.3. Raman spectra of quadricyclane at (A) 43 K and (B) 185 K

Table 5.2.1. Vibrational Data (cm^{-1}) for Quadricyclane.

liquid	phase I		phase II			
Raman[a] (295 K)	Raman (185 K)	IR (180 K)	Raman (43 K)	IR (45 K)		assignment
			31 w			lattice modes
			39 w			
			43 w			
			49 w			
			55 m			
			63 w			
			69 w			
			75 w			
			80 w,sh			
			82 w			
			93 w			
			101 m			
			116 w, br			
398 dp	398 vw, br		391 w			skeletal deformations
			400 w			
	534 vw		531 vw			
		664 vw	665 w	664 w		
			668 w	666 vw		
		696 w, br	695 w			
			697 w	699 w		
			707 vw	705 w		
			710 vw	712 vw		
721 pp	721 m	721 w	719 m, sh	717 w		
			721 s	722 w		
			765 m			
768 dp	768 m	766 vs	767 m, sh	767 vs		
			770 s	768 vs		
			794 s	792 m, sh		
800 dp	801 m, br	797 s, br	797 m	798 vs		
			803 s	804 s		
			821 w	823 m		
828	831 vw					
841 dp	843 w	843 w	846 w	845 m		
			849 m	847 w, sh		
894 pp	892 m	892 m	891 s	891 s		
			895 m			
			902 w			skeletal stretches
906	905 w	903 m, br	905 m	904 s		
			908 w	907 m		
908 dp	909 w		911 m	911 m		
			914 m	915 m		
			920 m	922 m		
		927 vw		930 w		
944 p	943 m	945 w, sh	943 s	941 w	a_1	
948 dp	951 w, sh	950 w	949 m	950 s		
			953 m			
987 p	985 s	985 vw	985 s	983 w	a_1	
			990 s	986 vw		
			996 w	998 w		
			1001 m			
			1006 vw	1006 w		
1030 dp	1034 m, br	1032 vw	1027 m	1025 w		
			1031 w	1027 vw		
			1033 m	1033 vvw		
			1039 s	1036 vw		

Table 5.2.1. (cont'd.)

liquid	phase I		phase II		
Raman[a] (295 K)	Raman (185 K)	IR (180 K)	Raman (43 K)	IR (45 K)	assignment
				1050 w	
	1047 w	1046 vvw	1053 w	1053 vw	
1059	1063 w	1062 vvw	1063 w		
			1068 w		
			1072 m		
1077 p	1078 s	1077 w	1075 vs 1079 vs	1075 m	a_1
1164 dp	1163 w	1164 vw	1158 m 1161 m	1159 w 1162 vw	
		1182 vw	1181 vw	1181 m	
			1186 w	1185 w	
				1190 w	
	1218 vw		1215 w 1221 w	1214 w 1217 w	
1236 pp	1236 m	1237 s	1233 s	1232 s	C-C-H and CH$_2$ deformations
	1238 m, sh		1237 m, sh 1239 m	1236 s 1240 s, sh	
			1245 m		
1250 p	1249 m	1250 w	1250 w 1254 w	1250 m, sh 1253 s	a_1
1254 dp	1258 w	1256 m	1257 w, sh		
1330 p	1331 s	1330 m	1327 s 1329 s	1327 s 1330 m	a_1
		1348 vw	1344 w	1341 m 1343 m	
1360	1365 w				
	1441 m	1439 vw	1438 w 1443 m	1438 w 1443 w	
1454 dp	1454 m	1452 vw	1451 m 1455 m	1451 w 1454 w	
2861 p	2858 m	2859 s	2856 m	2858 vs	a_1, methylene C H str
		2910 w, sh	2904 w 2907 w	2905 m	b_2, methylene C-H str
2932 p	2929 m	2931 s	2917 s 2925 s	2918 vs 2926 vs	a_1, $C_{2(4)}$-H str
2938 pp	2942 m, sh	2938 m, sh	2944 m 2949 m	2944 s 2949 m, sh	b_1, $C_{2(4)}$-H str
		3050 m, br	3047 s 3050 s 3053 s	3048 s 3054 m	
3055 dp	3059 m, br		3056 s	3057 m	
		3071 s	3063 m 3067 s	3064 s 3069 m	cyclobutane C H str.
3083 p	3080 s		3074 m 3079 m 3084 s 3096 s	3073 m, sh 3079 m 3097 w	a_1

[a] dp = depolarized, pp = partially polarized, and p = polarized.

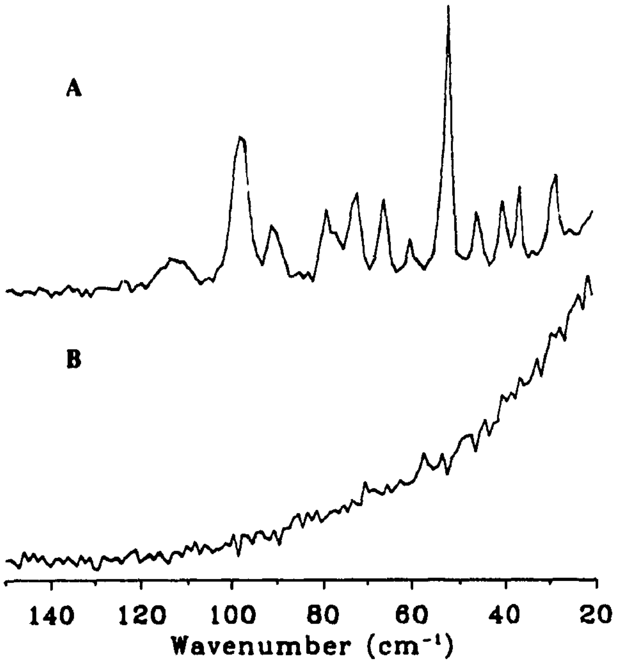

Figure 5.2.4. Low-frequency regions of the Raman spectrum of quadricyclane at (A) 43 K and (B) 185 K.

768 cm^{-1} band of phase I splits into three peaks in phase II, which occur at 765, 767, and 770 cm^{-1}. No obvious cases of any IR peaks splitting further than doublets are apparent in the spectra. Under the conditions that the IR bands are split into two, whereas the Raman peaks are split into two or three by the crystalline lattice, the correlation method can aid in specifying the structure of phase II.

Since combinations and overtones of external modes can also occur, the thirteen peaks observed in the low-frequency Raman spectrum may not all be fundamental transitions. A simple survey of these band positions indicates that at least five, and possibly up to eight, of these bands are true lattice fundamentals (the remainder being combinations or overtones), and it can be concluded that the unit cell of phase II contains more than one quadricyclane moiety. Moreover, the unit cell is noncentrosymmetric due to the high degree of coincidence between IR and Raman peaks throughout the low-temperature spectra. As with the cases of NBA and NBD, the site symmetry of the molecules in the lattice can be C_{2v}, C_2, C_s or C_1. Correlation with all the possible crystal symmetries results in three types of site and factor group combinations: (1) D_2 crystal with a C_2 site, or C_{2v} crystal with either a C_2 or C_s site; (2) D_{2d} crystal with a C_s site; or (3) S_4 or C_4 crystal with a C_1 site. The first group of possibilities should result in some of the IR peaks splitting into two, and all of the Raman peaks doubling. The second class should cause some of the IR peaks to double, while the Raman peaks split into two or three. The third set should result in all peaks in the IR doubling and all peaks in the Raman tripling. Since only a few possible triplets were observed in the Raman spectrum, even as low as 45 K, the third set of site and factor group combinations is unlikely. The structure of phase II of quadricyclane is most likely, therefore, orthorhombic (D_2 or C_{2v}) with Z = 2, or tetragonal (D_{2d}) having four molecules per unit cell. It is interesting to note that the ordered phase of quadricyclane does not have the same structure as those of NBA or NBD, which also have C_{2v} molecular symmetry, but it could be isostructural with the possible orthorhombic lattice of NBE, although the latter molecule has lower symmetry (C_s).

5.3 High-Pressure Vibrational Spectra

To complete the investigation of the phase behaviour of quadricyclane, vibrational spectra under pressure were measured. Initially, high-pressure Raman spectroscopy was performed, and, while the phase transition was clearly determined to occur at 10.7 ± 1.0 kbar, only one peak in phase I and two in phase II could be observed due to the low signal-to-noise ratio of the experiment. Thus, high-pressure IR spectroscopy was performed in order to obtain pressure dependences for a greater number of spectral peaks Infrared spectra were measured at several pressures up to 13.4 kbar, and the spectral changes characteristic of the phase transition were observed to occur at 9.3 ± 0.5 kbar This confirms that, within the errors of pressure calibration, the high-pressure IR and Raman data are consistent, and the phase transition pressure is just below 10 kbar Upon decompression, the phase transition was observed at approximately 7 kbar This pressure hysteresis indicates that the volume change, using equation 4.3.1, is close to 4.0 cm^{3} mol^{-1}, which is significantly higher than for other pure hydrocarbon cages. This would explain the poor fit of the thermodynamic data to equation 5.2.2, because the calculated "excess entropy" should be higher due to the larger ΔV_t. Figures 5.3.1 and 5.3.2 show the two spectral regions at varying pressures, upon compression. The spectral changes characteristic of the phase transition occur suddenly within a one kbar range, with phase I existing below 8.8 kbar, and phase II occurring above 9.8 kbar. The C-H stretching vibrations in Figure 5.3.1 also display characteristic splitting patterns, but broadening caused by nonhydrostatic pressure precluded the measurement of their fine structure. In general, the band profiles of the high-pressure phase resemble those of the ordered phase formed by lowering the temperature, thereby confirming the equivalence of the low-temperature and high-pressure phases. An exception to this rule is that the intensities of some bands at high pressure are more intense than their low-temperature counterparts, for example, the peaks at 983, 986, 998, and 1025 cm^{-1} (peak positions extrapolated to 0

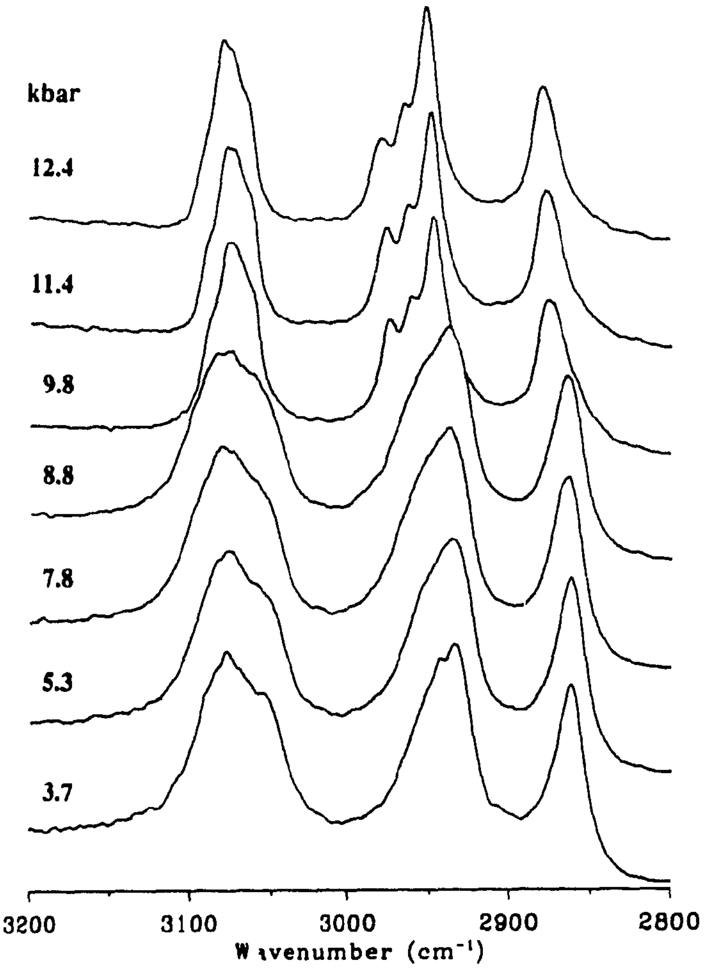

Figure 5.3.1. Infrared spectra of the C-H stretching region of quadricyclane at the indicated pressures upon compression.

kbar). These higher intensities can be attributed to small distortions of the quadricyclane cage, resulting in changes in the transition dipole moments and therefore in IR band intensities, and also by relaxation of symmetry selection rules.

Several peaks could be measured in both phases of quadricyclane; the shifting of several bands are shown in Figure 5.3.3, and the pressure dependences for all peaks are represented numerically in Table 5.3.1. The pressure dependences of the modes in either solid phase are generally very high, and they do not, as a rule, decrease from phase I to phase II. This is a peculiar observation, especially since the volume change is suspected to be unusually high. As with the ordered phases of other compounds, in phase II, the

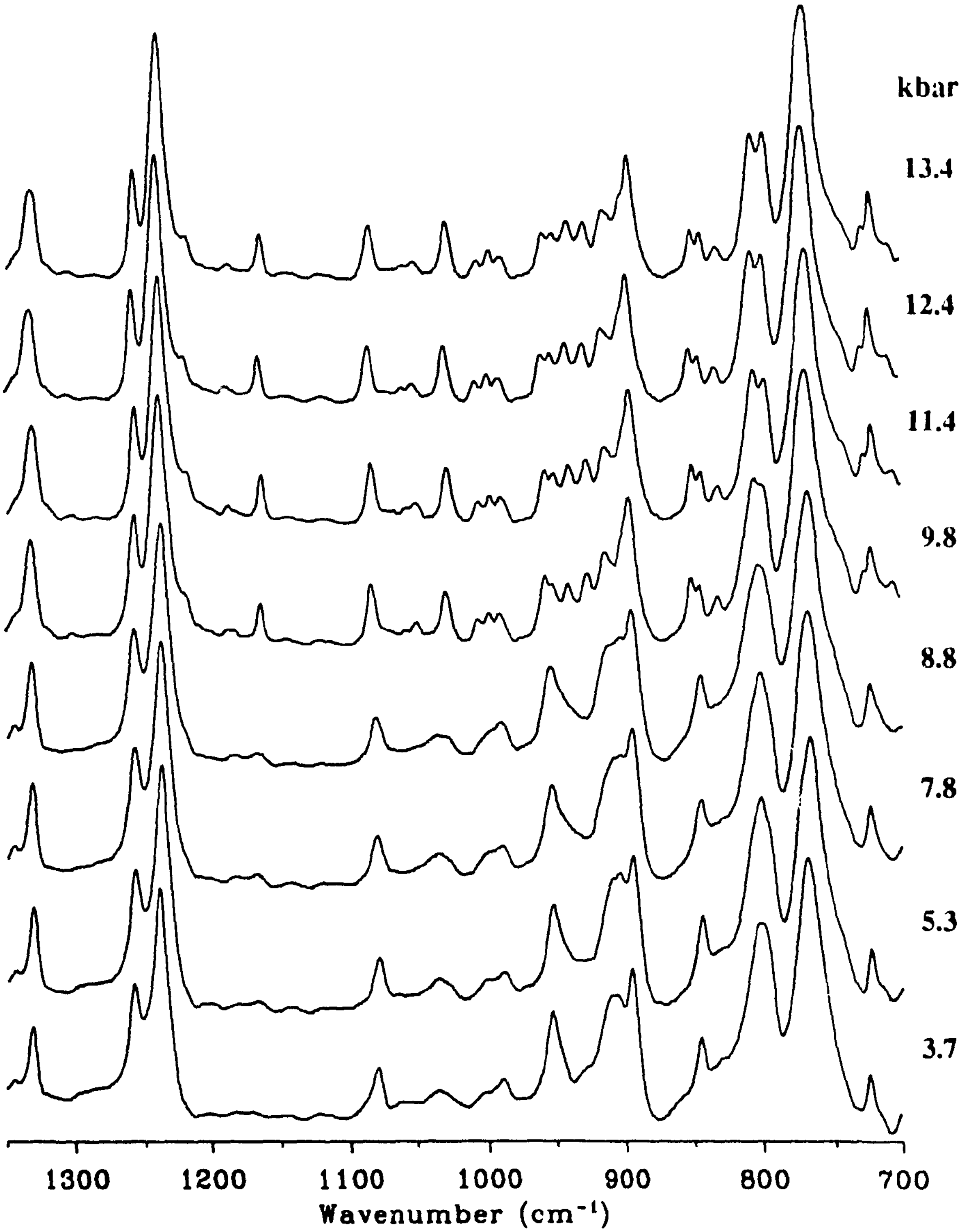

Figure 5.3.2. Infrared spectra of quadricyclane at the indicated pressures upon compression.

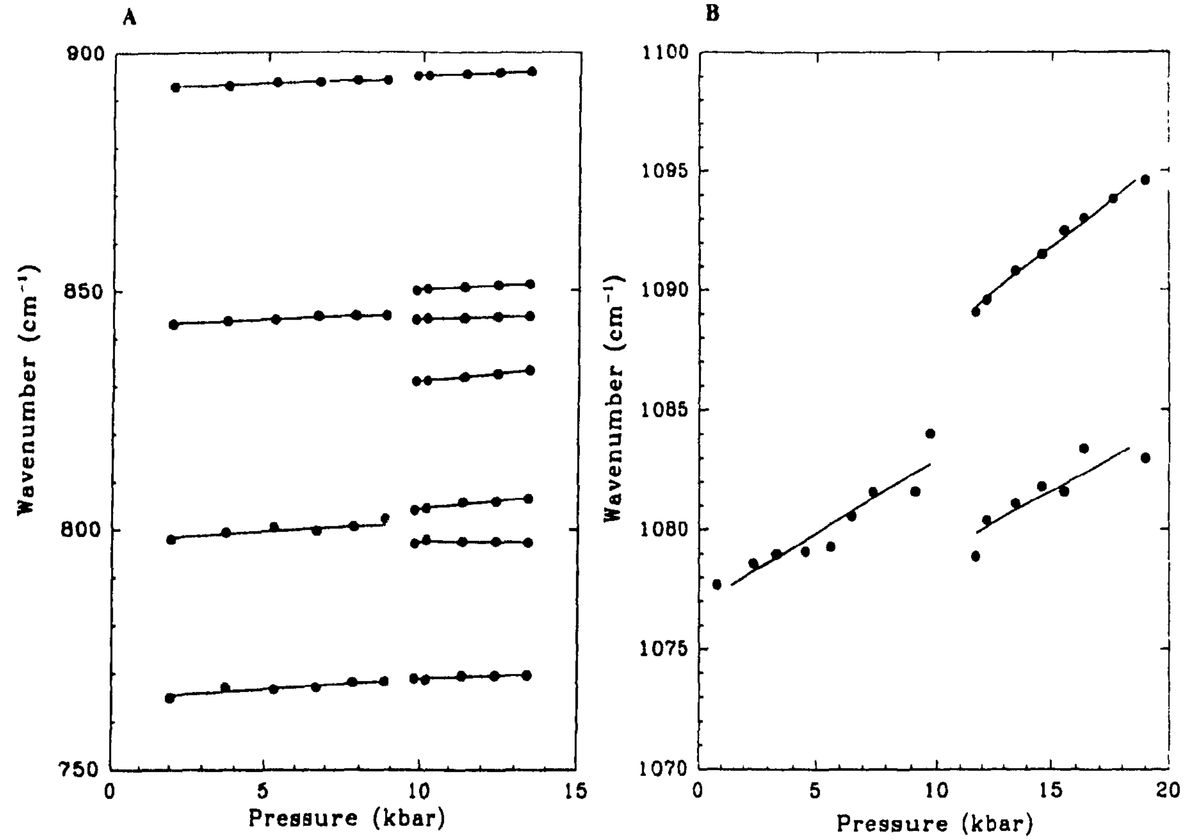

Figure 5.3.3. Pressure dependences of several vibrational bands of quadricyclane measured in (A) the IR spectrum and (B) the Raman spectrum. Note the factor group splittings which occur at the phase transition.

diverging behaviour observed to be typical of components of solid-state split bands was again exhibited, *e.g.*, by those peaks at 845 and 847 cm^{-1}, and 1075 and 1079 cm^{-1}.

The calculated force field in the literature was not adequate on its own to make vibrational assignments since the *ab initio* frequencies were often too far off from the observed band positions.[18] However, a combination of these computational data and the dlnv/dp values measured in this thesis can be used to begin assigning the vibrational spectra of quadricyclane. Stretching modes generally have higher pressure dependences than do deformation modes, and of the bands measured in the high-pressure phase, the peaks at 804, 823, 911, 950, 998, and 1075 cm^{-1} all have particularly high pressure dependences compared to the remaining spectral bands. These bands may all be

Table 5.3.1. Pressure Dependences of Vibrational Peaks of Quadricyclane *

phase I			phase II			
ν (cm^{-1})	dν/dp (cm^{-1}kbar^{-1})	dlnν/dp (kbar^{-1}x10^{4})	ν (cm^{-1})	dν/dp (cm^{-1}kbar^{-1})	dlnν/dp (kbar^{-1}x10^{4})	assignment
766	0.4	5	767	0.2	3	
797	0.4	5	798	-0.04	-0.6	
			804	0.67	8.3	C-C str.
			823	0.6	8	C-C str.
843	0.27	3.2	845	0.17	2.0	
			847	0.34	4.0	
892	0.20	2.2	891	0.26	2.9	
903	-0.5	-6				
(903)	0.67	7.4	911	0.60	6.5	C-C str
			915	0.92	9.9	
			922	0.41	4.4	
950	0.56	5.9	941	0.28	3.0	
			950	0.66	6.9	C-C str
985	0.53	5.4	983	-0.004	-0.04	
			986	0.1	1	
			998	0.52	5.2	C-C str
			1025	0.21	2.0	
1032	0.2	2				
1077	0.55	5.1	1075	0.63	5.8	C-C str., a_1
			1079 (R)	0.76	7.0	
1164	0.3	-3	1159	0.29	2.5	
			1214	0.35	2.9	
1237	0.11	0.89	1236	0.36	2.9	
1256	0.30	2.4	1253	0.25	1.9	
1330	0.29	2.2	1327	0.2	1	
2859	0.62	2.2	2858	0.96	3.3	CH_2 str., a_1
2931	0.76	2.6	2926	1.37	4.7	$C_{2(4)}$-H str., a_1
			2944	1.52	5.1	$C_{2(4)}$-H str., b_1
			2949	1.69	5.7	
3071	1.2	4.0	3069	0.75	2.4	cyclobutane C-H str

*All peaks are from the IR spectrum, except for that marked with an R.

attributed to skeletal stretching modes, and their frequencies correspond relatively well with the totally calculated band positions of 811 (partial contribution), 901 (partial contribution), 937 (partial contribution), 975, 1008, and 1034 cm^{-1} [18] Further assignment of the skeletal, CH_2, and C-C-H deformations is not yet possible, since only general trends have been observed. Concerning the pressure behaviour of the C-H stretching modes, in light of the previous discussion of NBA NBE, and NBD, it is expected that the cyclobutane C-H stretches would have the highest pressure dependences, followed by the two $C_{2(4)}$-H, and lastly, the methylene stretches. Unfortunately, the unavoidable broadening of the peaks caused by uneven pressure in the DAC obscured the measurement of all but a few of the C-H stretching modes. Despite this problem, in phase I, the three broad peaks corresponding to one of each type of stretching mode do follow this prediction. In phase II, the methylene and $C_{2(4)}$-H stretches maintain this trend, but the highest frequency band measured, occurring at 3069 cm^{-1}, had a very low pressure dependence. This peak is actually a pressure-broadened average of eight single bands, however, and its behaviour should not be considered typical of any of its components.

References

1. S J. Cristol and R. L. Snell, J. Am. Chem. Soc., **80**, 1950 (1958).
2. W G. Dauben and R. L. Cargill, Tetrahedron, **15**, 197 (1961).
3. G. S. Hammond, N. J. Turro, and A. Fischer, J. Am. Chem. Soc., **83**, 4674 (1961).
4. L. R. Canas and D. B. Greenberg, Solar Energy, **34**, 93 (1985).
5. T. Arai, T Oguchi, T. Wakabayashi, M. Tsuchiya, Y Nishimura, S. Oishi, H. Sakuragi, and K. Tokumaru, Bull Chem. Soc. Jpn., **60**, 2937 (1987).
6. R. R. Hautala, J. Little, and E. Sweet, Solar Energy, **19**, 503 (1977).
7. A. Basu, A. R. Saple, and N. Y Sapre, J Chem. Soc., Dalton Trans., 1797 (1987).
8. L. A. Paquette, H Kunzer, and M. A Kesselmayer, J Am. Chem. Soc., **110**, 6521 (1988).
9. See for example, (a) R. B Taylor and P. W. Jennings, Inorg. Chem., **20**, 3997 (1981); (b) C. Kutal, C K. Kelley, and G. Ferraudi, Inorg Chem , **26**, 3258 (1987); (c) N. Colin Baird, A. M. Draper, and

P. de Mayo, Can J Chem., **66**, 1579 (1988), (d) E. S Kirkor, V M. Maloney, and J Michl, J Am. Chem Soc., **112**, 148 (1990).

10 K. Maruyama, H Tamiaki, and S Kawabata, J Chem Soc , Perkin Trans. II, 543 (1986)

11. P. G. Gassman and J W Hershberger, J. Org Chem , **52**, 1337 (1987).

12. W. V Steele, J Chem. Thermodynamics, **10**, 919 (1978).

13. D. S. Kabakoff, J -C G Bunzli, J. F M. Oth, W. B. Hammond, and J. A. Berson, J Am Chem Soc , **97**, 1510 (1975)

14. B. Vogelsanger and A Bauder, J. Mol Spectrosc., **136**, 62 (1989).

15. K Mizuno, T Fukuyama, and K. Kuchitsu, Chem Lett., 249 (1972).

16. E. Osawa, G Szalontai, and A. Tsurumoto, J Chem Soc., Perkin Trans. II, 1209 (1983)

17. C. Van Alsenoy, J. N. Scarsdale, and L Schafer, J Comput. Chem , **3**, 53 (1982)

18. L. Doms, H. J. Geise, C. Van Alsenoy, L. Van Den Enden, and L. Schafer, J Mol. Struct , **129**, 299 (1985).

19. D. G. Lishan, K. V. Reddy, G. S. Hammond, and J. E. Leonard, J. Phys. Chem , **92**, 656 (1988).

20. J. B. Guthrie and J. P McCullough, J. Phys Chem Solids, **18**, 28 (1961)

21. T. Clark, M. A McKervey, H. Mackle, and J. J. Rooney, J. Chem. Soc , Faraday Trans I, **70**, 1279 (1974).

22. T. Clark, T. Mc. O. Knox., H. Mackle, and M. A. McKervey, J Chem. Soc., Faraday Trans I, **73**, 1224 (1977).

CHAPTER 6. BICYCLOOCTENE

6.1 Introduction

Bicyclo[2.2.2]oct-2-ene (BCOE), C_8H_{12}, is an organic cage compound which is also known to exhibit orientational disorder in the solid state. Electron diffraction studies[1] have shown that BCOE is a rigid structure, having C_{2v} symmetry, and possesses a strain energy of 40.5 kJ mol^{-1}. The parent alkane, bicyclo[2.2.2]octane (BCO), is dynamic because the eclipsed CH_2 groups cause an internal twisting motion. This type of torsional motion is absent in BCOE due to the presence of the double bond. Thus, BCOE is a rigid bicyclic structure, and can be considered as an extension of the seven-carbon systems described in Chapters 4 and 5.

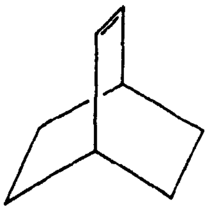

BCOE

Adiabatic calorimetry has shown that BCOE undergoes two phase transitions below the melting temperature, at 176.5 (phase I → phase II) and 110.5 K (phase II → phase III).[2] The upper transition was shown to be first order with a large entropy change (32 J K^{-1} mol^{-1}), while the lower has a very small transition entropy (3.3 J K^{-1} mol^{-1}) and was suspected to be higher than first order due to its broad shape. Although it has been suggested that the second phase transition may be related to the presence of impurities,[3] no proof has been provided in the literature. Proton NMR measurements have been reported on the various solid phases of BCOE.[3] In the same study, x-ray diffraction on the powder determined that the highest temperature phase, phase I, was face-centred cubic (a = 9.08 ± 0.02 Å). In phase I, which was observed to supercool by 6 K, rapid endospherical reorientation occurs with an activation enthalpy of 7.4 ± 0.6 kJ mol^{-1} Below the phase I → II transition point, anisotropic reorientation appears to occur, with an activation enthalpy of 17.3 ± 1.2 kJ mol^{-1} Comparison of the data obtained for BCOE and BCO revealed that, despite the differences in symmetries, they are comparable in shape, and BCOE undergoes very similar behaviour as BCO In phases II and III, therefore, reorientation was thought to occur along the pseudo three-fold axis of BCOE. At the phase II → phase III transition point, no discontinuities were observed in the T_1, $T_{1\rho}$ or T_2 measurements, indicating that the structures of these phases are very similar.

There are no vibrational spectroscopic studies of BCOE at all in the literature A limited high-pressure IR study has been reported which, surprisingly, did not detect any phase changes up to 45 kbar,[4] however no spectroscopic data were provided. A complete investigation of the solid phases of BCOE by vibrational spectroscopy was therefore warranted, to obtain structural information, and to confirm or disprove the absence of a pressure-induced phase transition.

6.2 Variable-Temperature Studies

Preliminary to the vibrational spectroscopic measurements, the phase transition temperatures were measured in both heating and cooling directions by DSC. A typical thermogram is shown in Figure 6.2.1. In agreement with the calorimetric and NMR results, the major transition displayed only a slight hysteresis, occurring at 176 K on heating and 169 K on cooling. The transition peak was broad in both directions, and slowing the scanning speed to 2.5 K min^{-1} did not reduce this broadening. The lower temperature transition was not observed within the limits of the calorimeter (103 K). This implies that this phase can supercool by at least 7 K. The average enthalpy and entropy changes for the phase I → phase II transition were 5.4 kJ mol^{-1} and 31.4 J K mol^{-1}, which are also in good agreement with the literature values.

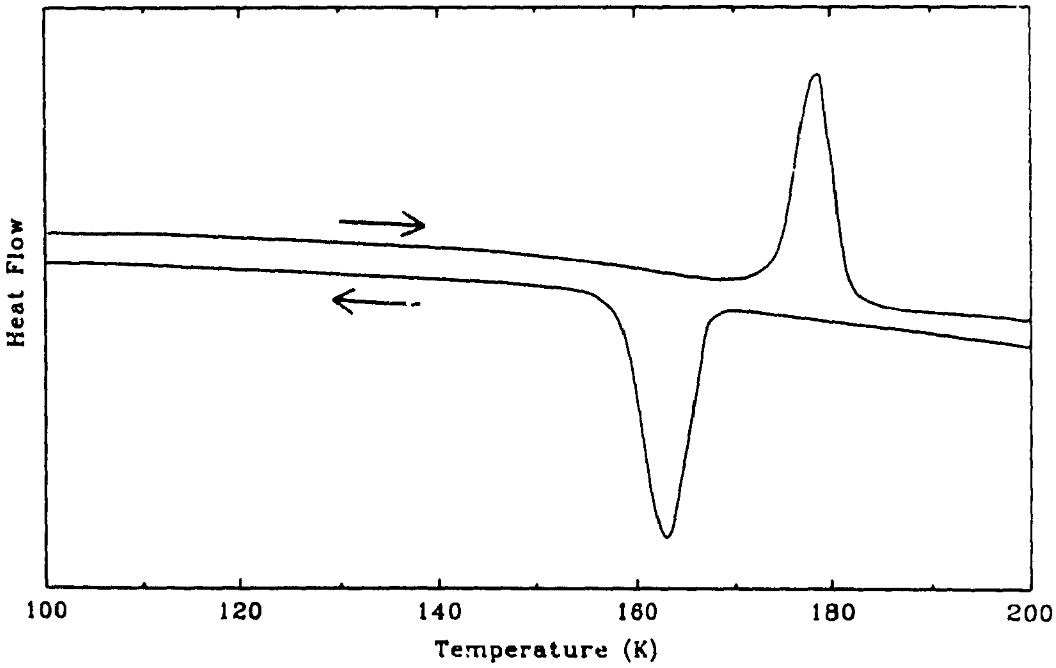

Figure 6.2.1. Differential scanning calorimetric thermogram of bicyclooctene, scanning at 5 K min^{-1}.

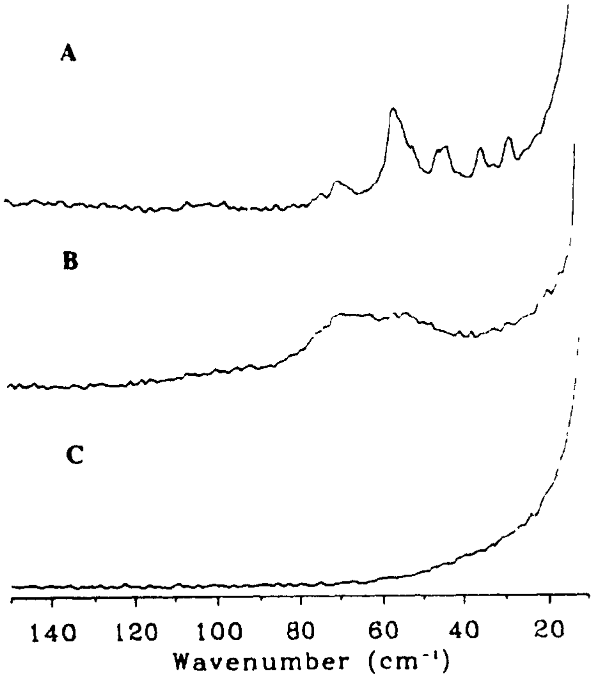

Figure 6.2.2. Low-frequency Raman spectra of bicyclooctene at (A) 70 K, (B) 150 K, and (C) 200 K

Since the cryogenic apparatus used in the vibrational spectroscopic measurements could reach temperatures far below those of the DSC instrument, the second phase transition could be followed by spectroscopic measurements Upon cooling from room temperature (phase I), the first phase transition was observed easily in both IR and Raman measurements as a sudden narrowing of peaks throughout the spectral region Further cooling, as low as 70 K, did not reveal any other obvious changes, except for in the lattice region. Consider the low-frequency Raman spectra of Figure 6 2 2. In phase I, isotropic reorientation (in the face-centred cubic lattice) is confirmed by the broadened Rayleigh line. After passing through the first phase transition, two broad bands indicate that anisotropic reorientation is occurring within the lattice. This is consistent with the results of the NMR data,[3] although the axis of rotation cannot be determined. Between 100 and 90 K, these broad librational bands give way to several sharp peaks, indicative of an ordered lattice structure The existence of the second phase transition was therefore confirmed by spectroscopic rather than calorimetric methods The absence of any major changes in the IR and Raman spectra at the phase II $\rightarrow$ phase III transition confirms that the crystal structures of the two are very similar, and probably the same. Figures 6 2.3 and 6 2.4 exhibit representative IR and Raman spectra of each phase of BCOE. The IR and Raman band positions in all three solid phases, as well as the Raman spectrum in CCl_4 solution, are given in Table 6 2.1

The sample of BCOE was shown to be > 99.9% pure by GC analysis, which is equal to or higher in purity than the samples of NBA, NBE, NBD, and quadricyclane. It is unlikely, therefore, that the second phase transition is an impurity effect, given that these four other compounds did not exhibit similar effects.

Bicyclooctene, consisting of 20 atoms, has 54 normal modes The majority of peaks observed in the IR and Raman spectra, therefore, are still mostly fundamentals ($\Gamma_{vib}^{int} = 16a_1 + 12a_2 + 15b_1 + 11b_2$). Anisotropic reorientation obscures any solid-state splittings in the spectra of phase II, and structural information cannot be deduced solely from its spectra. However, it is reasonable to assume that the space group of phase II is identical to that of phase III given the overall similarities of their spectra. and in light of the NMR results reported in the literature [3] In phase III, though, a few cases of peaks splitting into doublets due to solid-state effects were observed in the Raman spectrum, and these are bracketed in Table 6.2.1 Since only one possibility of solid-state splitting was observed in the IR spectrum (3025 and 3029 cm^{-1}), this behaviour was considered atypical While there are many coincidences of bands in the IR and Raman spectra, the fraction of overlap is about half, and a centrosymmetric space group for phase III (and phase II) cannot be eliminated. The factor group analysis, therefore, is identical to that of NBD in

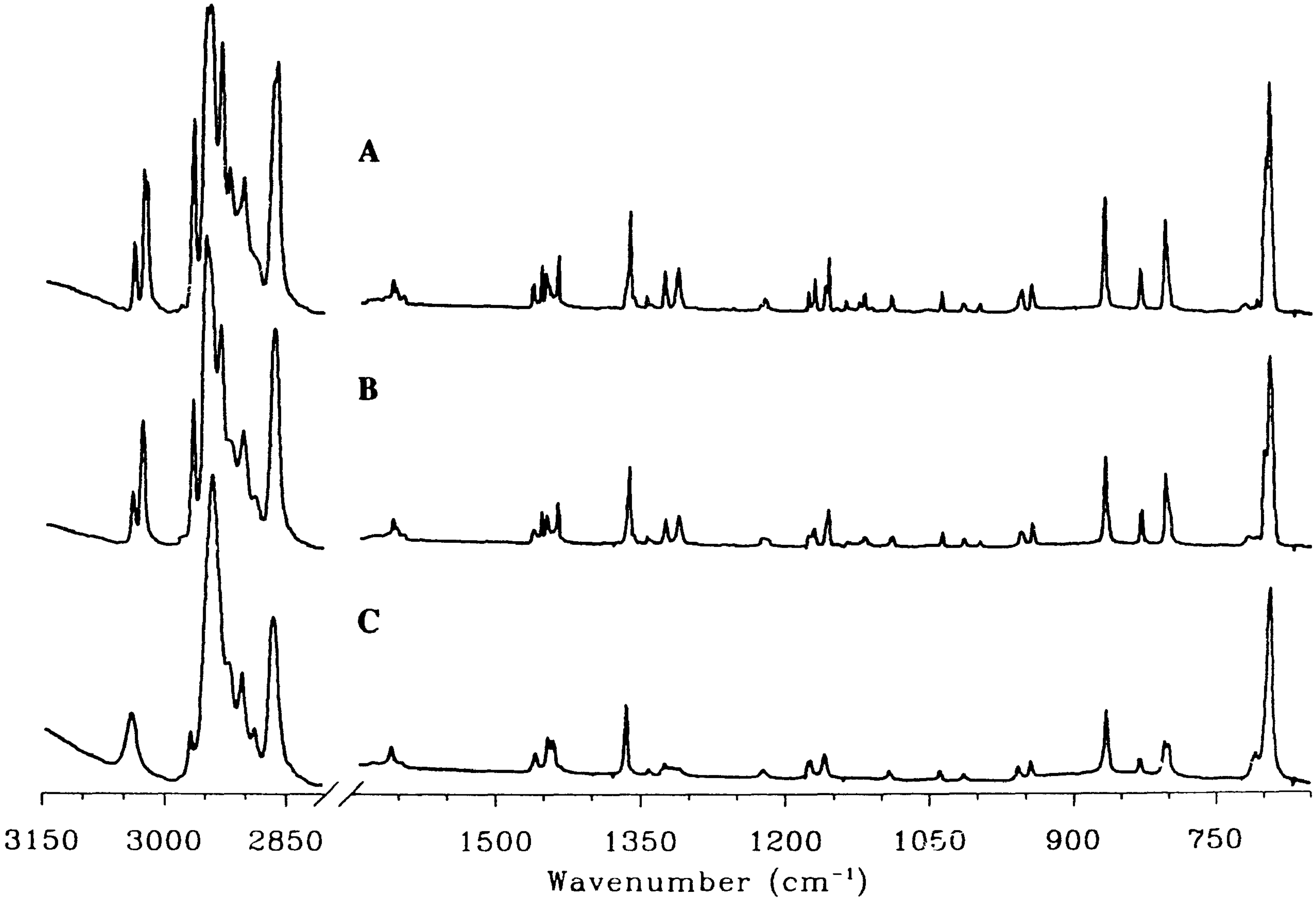

Figure 6.2.3. Infrared spectra of bicyclooctene at (A) 70 K, (B) 150 K, and (C) 200 K

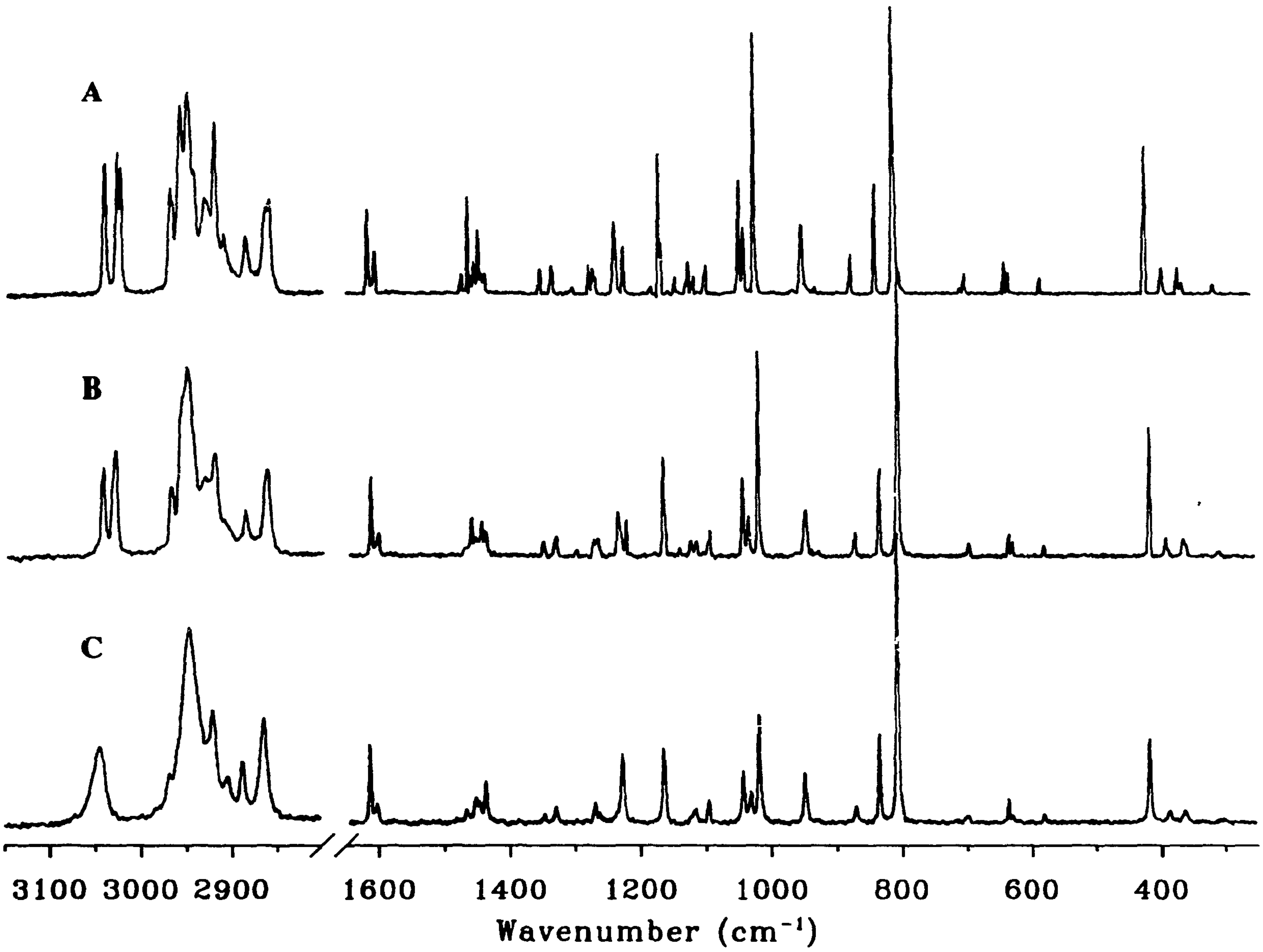

Figure 6.2.4. Raman spectra of bicyclooctene at (A) 70 K, (B) 150 K, and (C) 200 K.

Table 6.2.1. Vibrational Data (cm^{-1}) for Bicyclooctene

sol./CCl_4	phase I		phase II		phase III			
Raman[a]	Raman (200 K)	IR (200 K)	Raman (150 K)	IR (150 K)	Raman (70 K)	IR (70 K)		assignment
					38 w			lattice modes
			54 w, br		49 w			
					64 w			
			66 w, br		67 w			
					78 w			
					85 m			
					109 w			
	297 vw		305 vw		308 w			C=C-C def + C C-C def
358 w, dp	358 w		356 w		356 w			
			361 w, sh		363 m			
383 vw, dp	383 w		388 w		388 m			
414 m, dp	413 m		413 s		413 s 416 m			
574 vw	576 vw		576 vw		577 w			
	625 vw		625 w		626 w			C C C def + C C str
631 w	632 w		631 w		632 m			
697 vw	695 vw	693 s	692 w	693 s	694 w	695 w		
				700 m, sh	700 w	699 m, sh		
	708 m			707 vw		707 w		
				716 vw		719 vw		
	801 m							
802 s, p	804 s	805 m	804 vs	804 m	805 vs	805 m	a_1	
831 m, p	832 m	830 w	832 s	830 w	833 s	831 w	a_1	
868 w, dp	868 w	867 m	870 m	869 m	870 m	869 m		
946 m, pp	947 m	946 w	946 m	946 w	946 s 948 m	946 w		
		959 w		958 w		957 w		
						959 w		
				1001 w		1001 w		
1017 m, pp	1018 m	1017 w	1019 s	1018 w	1020 vs	1018 w		
1032 w	1031 m		1034 m		1035 m			
1041 w, dp	1043 m	1042 w	1043 s	1041 m	1043 s	1042 w		C-C str + C=C H def + C C-H def + CH_2 def
1097 w, pp	1097 w	1095 w	1095 m	1094 w	1095 m 1097 m	1094 w		
	1117 w, br		1115 w		1114 w 1116 w, sh	1115 vw		
			1123 w	1122 w	1122 m 1125 w, sh	1123 w		
						1128 w		
			1140 vw		1143 w	1142 w		
					1153 vw	1152 vw		
						1161 m		
1165 m, pp	1165 m	1164 m	1166 s	1162 m	1164 m, sh 1168 s	1164 w		
				1176 w		1175 w		
		1179 m		1182 w, sh	1179 vw	1182 w		
1229 m, dp	1230 m	1229 w	1224 m	1226 w	1222 m	1226 w		
				1229 w, sh		1228 w, sh		
					1233 w, sh	1232 w, sh		
			1236 m, br		1236 m 1238 w, sh			
	1265 vw		1268 w	1266 w				C-C H def + CH_2 def + C-C str
				1269 w				
1271 w, p	1272 w		1274 w		1276 m		a_1	
			1300 vw		1300 vw			
		1317 vw, sh		1319 w		1319 m		
		1326 vw, sh						
1332 w, p	1332 w	1331 w	1333 w	1333 w	1333 m	1334 m	a_1	

Table 6.2.1. (cont'd).

sol./CCl_4	phase I		phase II		phase III		
Raman[a]	Raman (200 K)	IR (200 K)	Raman (150 K)	IR (150 K)	Raman (70 K)	IR (70 K)	assignment
1349 vw	1349 vw	1348 w	1351 w	1347 vw, sh	1351 m	1346 vw	CH_2 def + C=C-H def.
				1351 vw		1352 w	
		1373 m		1370 m		1371 m	
					1437 w		
1442 w, dp	1440 m	1440 w, sh	1442 w	1444 m	1442 w	1445 m	
1445 w, dp			1446 m		1446 m	1451 vw	
	1450 w	1449 m			1454 w	1454 w	
	1456 w	1454 m	1458 w	1457 m	1459 w	1458 m	
			1462 m	1462 m	1463 m	1462 m	
1469 vw	1469 w	1467 m	1471 w	1470 w	1473 w	1470 m	
1606 w, pp	1608 w	1608 w	1606 w	1606 w	1606 m	1606 w	A_1, 2 x 804 cm^{-1}
				1613 w, sh		1614 w	
1618 m, p	1619 m	1618 m	1617 s	1618 m	1618 m	1618 m	a_1, C=C str.
				1622 w, sh		1625 w	
		1635 w		1632 w		1633 vw	804 + 832 cm^{-1}
						1642 vw	
2866 m, p	2863 m	2862 s	2862 m	2861 s	2860 s	2860 s	a_1 CH_2 and bh Č-H str
					2865 s	2864 s, sh	
2890 w, p	2887 m	2886 m	2886 m	2886 m	2886 m	2886 m	a_1
2906 w	2903 w	2901 s	2909 w	2902 m	2910 m	2902 m	
2922 m, p	2920 m	2918 s	2920 m	2917 m	2921 s	2920 m	a_1
			2931 m	2931 s	2931 m	2932 s	
				2942 s, sh	2944 m, sh	2945 s	
2946 s, pp	2945 s	2941 vs, br	2950 s	2948 s	2951 s	2950 s	
			2957 s, sh		2959 s		a_2
2967 w	2967w	2967m	2968 m	2966 m	2968 m, sh 2970 m	2966 m	
			3030 m	3030 m	3025 s 3029 s	3025 m 3028 m	a_1, vinyl C-H str.
3046 m, pp	3045m	3042m	3045 m	3042 s	3042 s	3041 m	b_1, vinyl C-H str

[a] dp = depolarized, pp = partially polarized, p = polarized.

Chapter 4, and the crystal structures of both phases II and III of BCOE are tetragonal with either two or four molecules per unit cell.

The IR and Raman spectra of both cyclohexene[5] and BCO[6,7] have been assigned in the literature according to force-field calculations. Even with this information, the complete assignment of all the vibrational bands of BCOE is not trivial since the geometry and symmetry of the cage differ from BCO, and the strain on the rings is higher than in cyclohexene. The assignments of peaks in Table 6.2.1 are therefore on an elementary level. Among the C-H stretching modes, the vinyl C-H stretches can be easily identified as the peaks at 3030 and 3041 cm^{-1}, but the methylene and methine vibrations are numerous and overlap too much to be differentiated. Of the three polarized bands, however, occurring at 2860, 2886, and 2920 cm^{-1}, one is a bridgehead C-H stretch while the other two are methylene C-H stretches.

6.3 High-Pressure Infrared Studies

Figure 6.3.1 shows the skeletal mode region of bicyclooctene at various pressures, up to 27 kbar. In this first set of high-pressure IR data, only the skeletal modes were measured because the C-H stretching peaks are much more intense and many of these latter peaks were offscale. The first phase transition, phase I → phase II, was reached at 7.9 ± 1.0 kbar upon compression, and appeared extended over a 1 kbar pressure range. This transition range was anticipated since the phase change was broadened over temperature in the DSC thermograms as well. The second transition was not as easily detected, since the spectral changes are minimal. Spectra were measured at nine pressures after the phase I → phase II transition, and they could be fit to linear dependences (Figure 6.3.2). This line, however, could also be fit quite well to two separate lines with a break at about 15 kbar. In order to confirm this second phase transition pressure, and also to measure the dependences of the C-H stretching modes, a second set of high-pressure IR data was obtained. The IR spectra of the C-H stretching region of BCOE at different pressures is shown in Figure 6.3.3, and these frequencies are plotted in Figure 6.3.4. The phase I → phase II transition was clearly observed once again. Unfortunately, no systematic break in the pressure dependences above 9 kbar could be determined, and thus the second phase transition was not confirmed. It can be concluded, though, that the behaviour of the IR peaks under pressure in phases II and III are very similar. The pressure dependences of all the bands measured are shown in Table 6.3.1.

Analogous to the results of the seven-carbon systems, the pressure dependences of many peaks in phases II and III are lower than those of phase I. There are exceptions, however, and the larger slopes measured for the high-pressure phases may have been caused by the combination of points from two different solids. It was noted that if the lines were divided at 15 kbar, *i.e.*, if the second phase transition was assumed to occur,

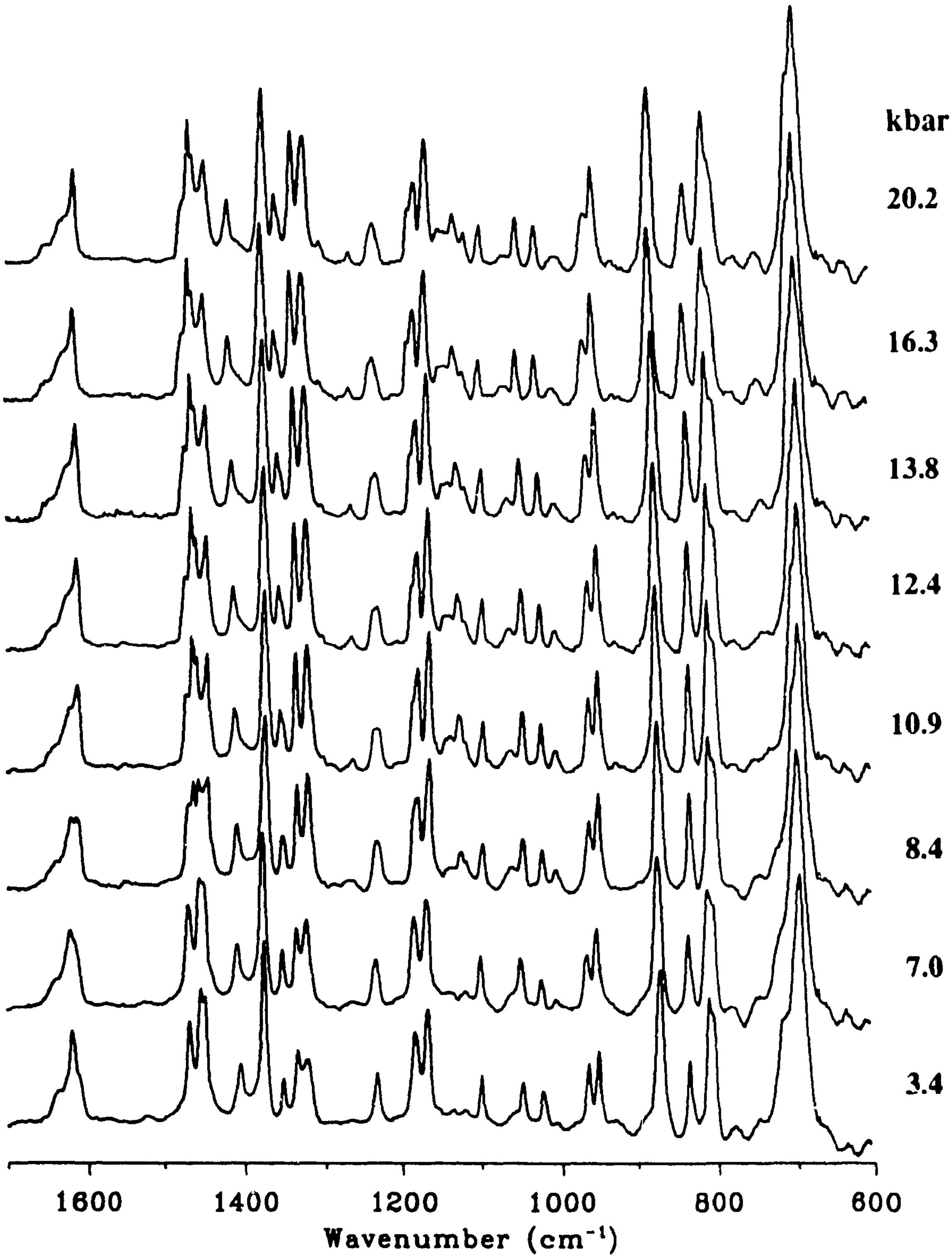

Figure 6.3.1. The skeletal mode region of the IR spectrum of bicyclooctene at the indicated pressures upon compression.

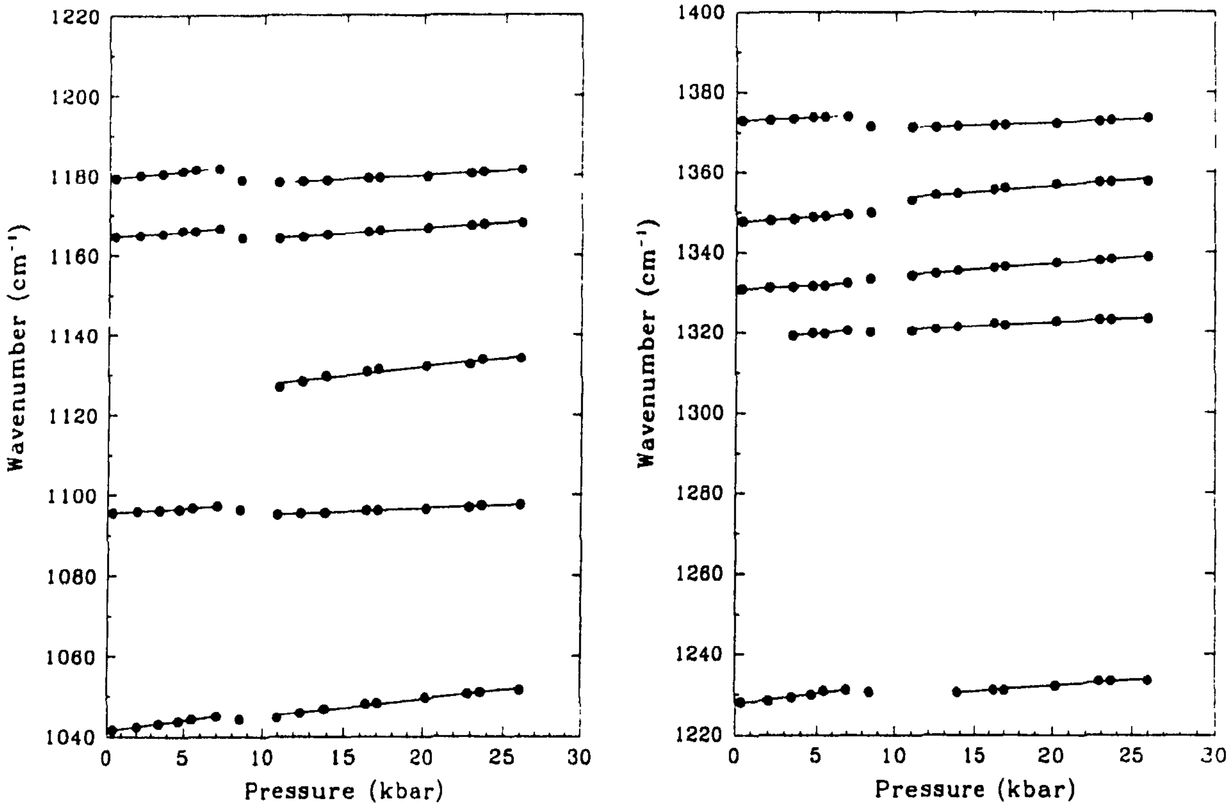

Figure 6.3.2. Representative plots of the pressure dependences of several bands in the skeletal mode region of the IR spectrum of bicyclooctene.

there was a general trend of a slight increase in slopes at the first phase transition (phase I → phase II), and then a decrease in slopes from phase II → phase III. This would infer that an anisotropic rotator phase is more compressible than an isotropic phase, but less compressible than the ordered phase. The latter point is expected in light of the behaviour of other disordered compounds; however, the former implies that the greatest volume change occurs at the second phase transition, and not at the first. The major contribution to the phase II → phase III transition entropy is therefore due to the decrease in crystal volume, and the ΔS_t of the first transition is largely orientational entropy loss.

Among the skeletal vibrations of BCOE, the dlnv/dp values are similar, and it is not possible to use these pressure dependences to make spectral assignments beyond those in

Table 6.2.1. However, the IR peaks having higher pressure dependences are probably skeletal stretching modes rather than deformations. For example, of the many peaks in this region with much lower pressure dependences, the peak at 869 cm^{-1} is more likely to be a C-C stretching vibration. The C=C stretching mode, at 1618 cm^{-1}, has a dlnv/dp value similar to those of the four CH$_2$ scissoring vibrations between 1445 and 1461 cm^{-1}, this trend was also noted for NBE, although the actual dlnv/dp values for these vibrations are higher in BCOE. In fact, the pressure dependences for all the skeletal modes of BCOE, generally ranging from 2 to 5 x 10^{-4} kbar^{-1}, are higher than the values for NBE.

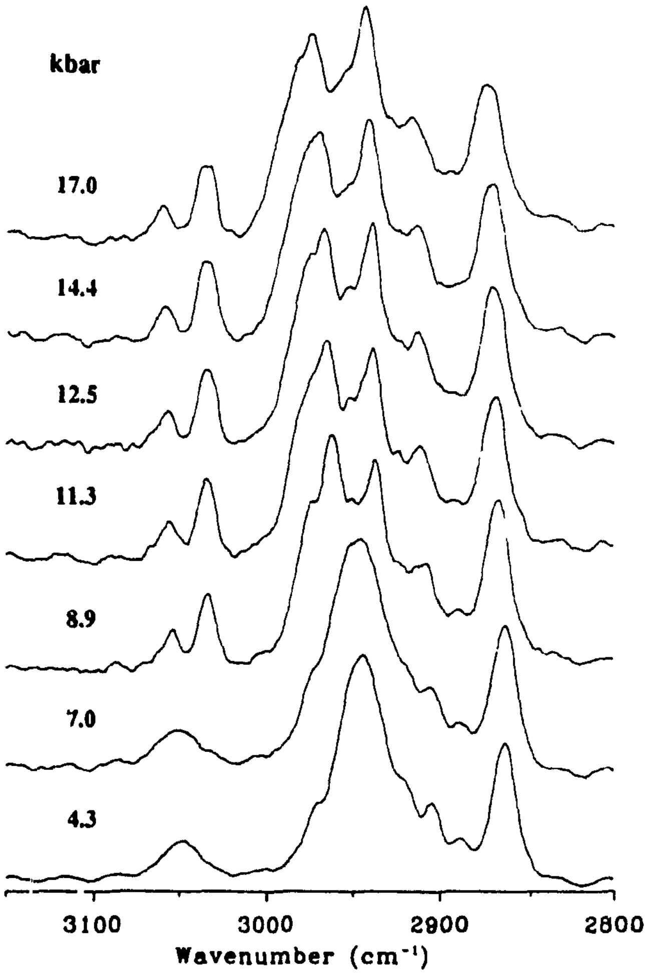

Figure 6.3.3. Infrared spectra of the C-H stretching region of bicyclooctene at the indicated pressures upon compression.

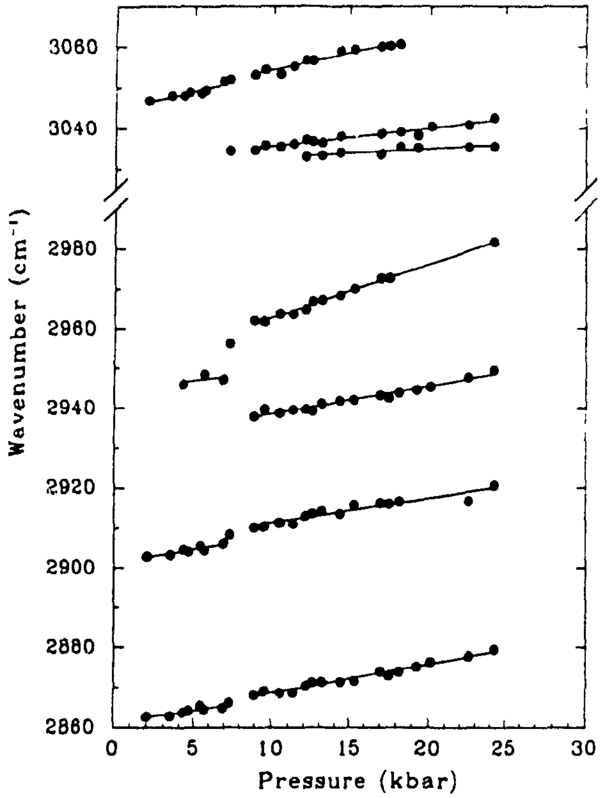

Figure 6.3.4. Pressure dependences of the IR peaks in the C-H stretching region of bicyclooctene.

This implies that the compressibilities of phases II and III of BCOE are higher than that of phase II of NBE. The pressure dependences of only seven C-H stretching modes could be measured, and of these, the peak at 2950 cm^{-1} has a significantly higher dlnv/dp value, and was assigned as a bridgehead C-H stretch, having b_1 symmetry. Since the frequencies of the two bridgehead C-H stretches are expected to be similar, the polarized band at 2920 cm^{-1} can now be assigned as the a_1 bridgehead C-H stretch.

The method of using pressure dependences to assign the vibrational spectra of BCOE was not as successful compared to the results on the seven-carbon cage compounds. Nevertheless, the phase I → phase II transition, and probably the phase II → phase III transition, were successfully induced by pressure and observed by IR spectroscopy. The

Table 6.3.1. Pressure Dependences of Infrared Peaks of Bicyclooctene

phase I			phases II & III			
ν (cm^{-1})	dν/dp (cm^{-1}kbar^{-1})	dlnν/dp (kbar^{-1}x10^4)	ν (cm^{-1})	dν/dp (cm^{-1}kbar^{-1})	dlnν/dp (kbar^{-1}x10^4)	assignment
693	0.3	4	695	0.36	5.1	C-C str + C-C-C def + C=C-H def
805	0.56	7.0	805	0.37	4.6	
830	0.35	4.2	831	0.34	4.0	
867	0.53	6.1	869	0.55	6.3	
946	0.48	5.0	946	0.39	4.1	
959	0.40	4.2	957	0.2	2	
1017	0.52	5.1	1018	0.43	4.2	
1042	0.54	5.2	1042	0.44	4.2	
1095	0.25	2.3	1094	0.15	1.4	
			1123	0.43	3.5	
1164	0.31	2.6	1164	0.27	2.3	
1179	0.40	3.4	1182	0.21	1.8	
1229	0.49	4.0	1226	0.28	2.3	
1317	0.35	2.6	1319	0.20	1.5	
1331	0.20	1.5	1334	0.31	2.3	
1348	0.28	2.1	1352	0.30	2.2	C-C-H def
1373	0.17	1.3	1371	0.15	1.1	
1449	0.2	1	1445	0.17	1.2	
1454	0.1	4	1458	0.37	2.6	
1467	0.09	0.6	1462	0.29	2.0	
			1470	0.35	2.4	
1618	0.42	2.6	1618	0.31	1.9	a_1,C=C str
2862	0.6	2	2860	0.70	2.4	a_1,CH_2 str
2901	0.7	2	2902	0.6	2	CH_2 str
2941	0.5	2	2932	0.68	2.3	CH_2 str
			2950	1.3	4.5	b_1,bridgehead C-H str
			3025	0.2	0.7	a_1,vinyl C-H str
			3028	0.44	1.4	
3042	0.9	3	3042	0.82	2.7	b_1,vinyl C-H str

difficulty in observing the phase II → phase III transition was expected, since the structures of the two were determined to be very similar, and most likely identical, by the low-temperature vibrational spectroscopic measurements. The pressure dependences did provide information that could be used to assign a few of the vibrations, particularly in identifying the bridgehead C-H stretching modes, which would have been difficult to assign even with force-field calculations. Finally, the compressibilities of phases II and III of BCOE were determined to be higher than those of the ordered phases of NBE and NBD, and considerably higher than that of phase III of NBA.

References

1 A. Yokozeki and K. Kuchitsu, Bull. Chem. Soc. Jpn., **44**, 1783 (1971).

2 W.-K. Wong and E. F. Westrum, Jr , J. Phys. Chem., **74**, 1303 (1970).

3. S. McGuigan, J H Strange, J. M. Chezeau, and M. Nasr, J. Phys. (Orsay, Fr.), **46**, 271 (1985).

4. S. D. Hamann, High Temp.-High Pressures, **10**, 445 (1978).

5. N. Neto, C. Di Lauro, E. Castellucci, and S. Califano, Spectrochim. Acta, **23A**, 1763 (1967).

6. P. Bruesch, Spectrochim. Acta, **22**, 867 (1966).

7. P Bruesch and Hs H. Gunthard, Spectrochim Acta, **22**, 877 (1966).

CHAPTER 7. 1-FLUOROADAMANTANE

7.1 Introduction

The investigations of many derivatives of adamantane, tricyclo[3.3.1.1]decane, have been reported in the literature in an attempt to correlate phase behaviour with molecular structure. There are two positions on the cage where single substitution can occur: the 1-position, where the molecule retains a three-fold rotation axis, and the 2-position, where a plane of symmetry remains intact. The behaviour of the 1-substituted adamantanes varies according to the substituent. Methyladamantane exhibits two phase transitions to achieve a crystalline, ordered phase.[1] The 1-chloro and 1-bromoadamantanes exhibit one and two phase transitions, respectively.[1] The 1-iodo derivative also exhibits a solid-solid phase transition, however, the high-temperature phase is not plastically-crystalline.[1,2] The behaviour of 1-cyanoadamantane is drastically different from the other derivatives.[3] Upon cooling, the plastic crystal, phase I, undergoes a transition to phase II, which can be quenched to a glassy crystal, phase I_g. Upon heating, this glassy phase can be annealed to form a metastable phase, phase I', which will then undergo an irreversible transition to phase II. Several adamantane derivatives have been investigated in our laboratory by vibrational and NMR spectroscopy, including 1-adamantanol,[4] 1-adamantanecarboxylic acid,[5,6] 1-adamantanaminehydrochloride,[7] 2-adamantanone,[8] 1-bromoadamantane,[6,9] 1-chloroadamantane,[9] 2-bromoadamantane,[9] and 2-chloroadamantane.[10] As a continuation of these studies of adamantane derivatives, and organic cage compounds in general, an investigation of the phase behaviour of 1-fluoroadamantane is included in this thesis.

Several studies have been reported specifically on the phase behaviour of 1-fluoroadamantane. Differential scanning calorimetric measurements[1] revealed a phase transition at 222 K, with an enthalpy and entropy of transition of 1.50 kJ mol^{-1} and 6.77 J K^{-1} mol^{-1}, respectively. The melting temperature in a sealed tube was measured to be 525 K. The high-temperature phase has been the subject of a number of studies by a

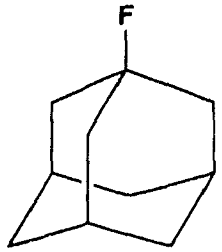

1-fluoroadamantane

group of investigators at the University of Lille in France. Single-crystal x-ray diffraction[11] was used to determine the structure as face-centred cubic (Fm3m), having four molecules per unit cell, with a = 9.535(4) Å. Although the entropy of fusion is not known, the cubic structure suggests that the high-temperature phase of fluoroadamantane is plastic. The molecular motions in the plastic phase were investigated by ^{1}H, ^{19}F, and ^{13}C NMR spectroscopy, by measuring T_1 relaxation times,[12] by IQNS,[13] from dielectric properties,[14] and by Raman scattering from a single crystal.[15] The reorientational motions of fluoroadamantane could be separated into two components: rotation about the three-fold molecular axis, and a tumbling motion of the molecular axis about eight distinguishable equilibrium orientations along the $\langle 111 \rangle$ directions of the cubic lattice. The results of the different techniques agreed very well with each other; the correlation times of the motions could be described by Arrhenius laws:[13]

$$\tau_{C4} = 9.3 \times 10^{-15} \exp(2960/T) \text{ s} \qquad [7.1.1]$$

$$\tau_{M3} = 5.9 \times 10^{-13} \exp(1560/T) \text{ s} \qquad [7.1.2]$$

where τ_{C4} is the correlation time of the tumbling motion, and τ_{M3} is that of molecular rotation The activation energies for the tumbling and rotational motions are therefore 24.6 and 13.0 kJ mol^{-1}, respectively These barriers are comparable to those in the plastic phase of 1-chloroadamantane,[16] reflecting the structural similarities of the two solids Only the ^{1}H wideline NMR and dielectric experiments were successfully carried out below the phase transition temperature. According to proton second moment measurements, the phase transition does not qualitatively change the reorientational motions, which slow down progressively until a rigid lattice is formed near 80 K ($\tau < 10^{-5}$ s).[12] The crystal structure of the phase below 222 K could not be determined precisely because the single crystals cracked upon cooling through the transition; however, the low-temperature phase was shown to be non-cubic even at 4 K.[14] The dielectric measurements suggested that the low-temperature lattice is tetragonal, as in adamantane,[17,18] with one of the $\langle 001 \rangle$ directions of the cubic lattice remaining as a four-fold axis. The overall reorientational correlation times below and above the phase transition were determined by dielectric relaxation to be:

$$\tau_r = 9.73 \times 10^{-16} \exp(3502/T)\ \text{s} \quad \text{if } T < 222\ \text{K} \qquad [7.1.3]$$

and

$$\tau_r = 3.6 \times 10^{-14} \exp(2282/T)\ \text{s} \quad \text{if } T > 222\ \text{K} \qquad [7.1.4]$$

The knowledge of the structure and the degree of order of fluoroadamantane below 222 K, therefore, remains elusive. This phase also appears to form a glass upon cooling. The existence of another phase transition is expected, and it is suspected to be highly dependent upon cooling rate. Recently, a "symmetry departure" model has been used to explain glass transitions in molecular crystals such as cyclohexanol and 1-cyanoadamantane,[19] and an analysis of the available data on fluoroadamantane led to the prediction of a glass transition, upon heating, near 90 K.

The IR spectrum, measured in solution, has been reported, but with virtually no assignments,[20] and, except for the few bands measured from the single crystal,[15] the full Raman spectrum has yet to be described. The behaviour of fluoroadamantane under pressure also remains unexplored, and, due to the apparent disorder down to 4 K, may be different from the effects that arise from lowering the temperature. Thus, as an addition to the chloro- and bromo-derivatives under study in our laboratory, the phase behaviour of fluoroadamantane was investigated by low-temperature and high-pressure vibrational spectroscopy.

7.2 Variable-Temperature Studies

Differential scanning calorimetric measurements of fluoroadamantane confirmed the presence of a single phase transition (phase I → phase II) at 227 K on cooling, with enthalpy and entropy changes of 1.7 kJ mol^{-1} and 7.6 J K^{-1} mol^{-1}. Upon heating, the transition displayed a slight hysteresis, occurring at 231 K, with ΔH_t and ΔS_t of 1.6 kJ mol^{-1} and 6.9 J K^{-1} mol^{-1}. This transition temperature is higher than the value of 222 K (on heating) reported in the literature.[1] Since impurities depress the temperature of first-order phase transitions, it may be concluded that the sample used in the earlier studies, although specified to be near 99.8% pure, is less pure than the present sample. No other phase transitions were observed by DSC, and repeated cycling of the sample between 298 and 123 K did not affect the phase I → phase II transition temperature.

Variable-temperature IR and Raman spectra were measured at every 5 K on cooling and on heating between 250 and 200 K, *i.e.*, through the phase I → phase II transition temperature. Spectra of each phase are shown in Figures 7.2.1 and 7.2.2. Upon comparison of these spectra, very few differences are apparent, but a definite narrowing of peaks did occur suddenly at the transition point. Figure 7.2.3 is a plot of linewidths (FWHH) of an IR and of a Raman band versus temperature, in the cooling direction. In both cases, there is a distinct decrease in the linewidths at the phase transition. Although the spectral characteristics of each phase are not easily discernible upon simple inspection, the C-H stretching region is particularly informative. In both the IR and Raman spectra, phase I is characterized by a peak at 2857 cm^{-1} and then a broad agglomeration of peaks centred at about 2928 cm^{-1}. In phase II, the narrowing of peaks is sufficient to resolve the band at 2891 cm^{-1}, and the other higher-frequency C-H stretching bands appear as a more rounded envelope centred at about 2930 cm^{-1}. The low-frequency regions of the Raman spectra of both phase I and phase II do not contain

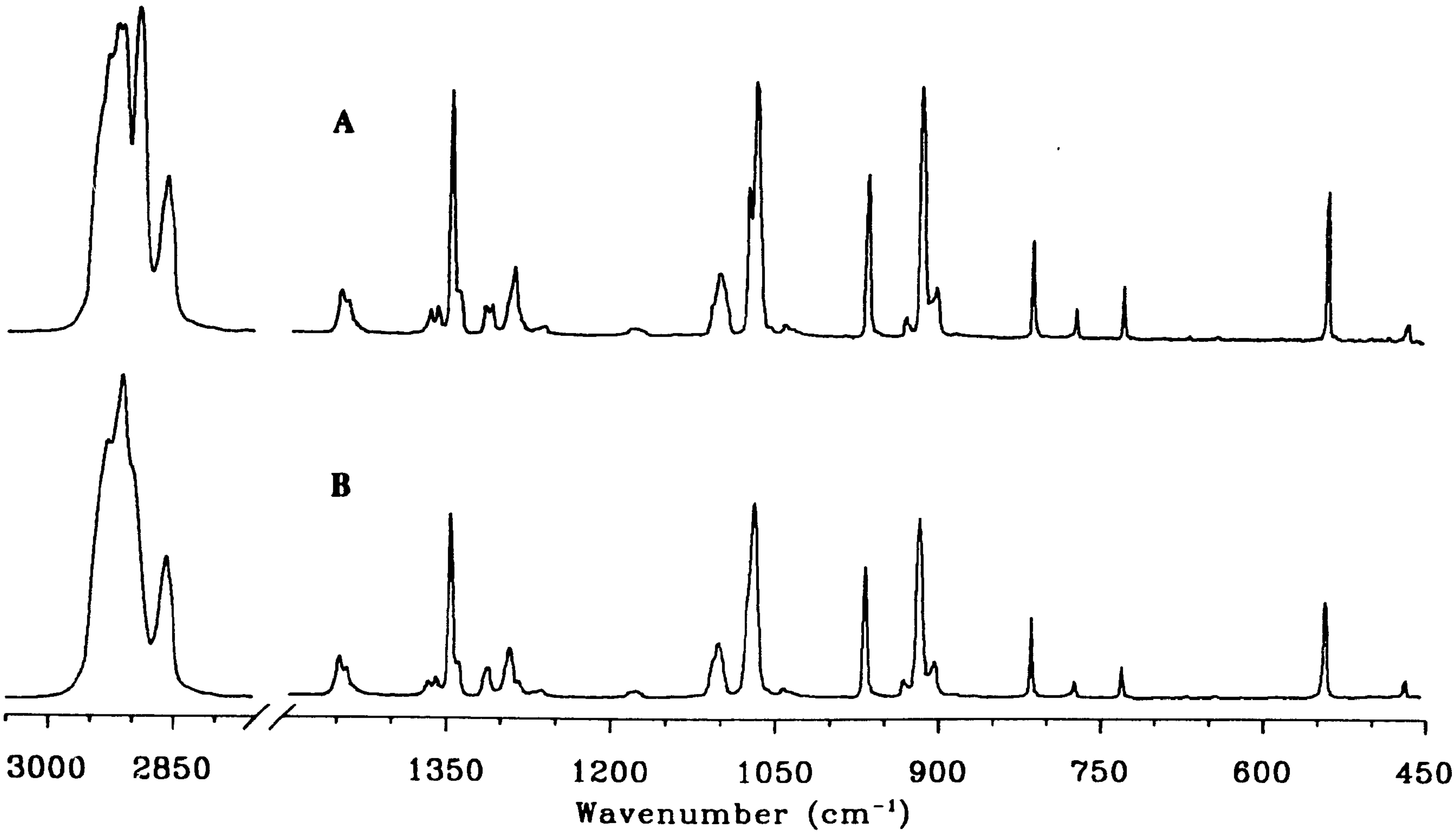

Figure 7.2.1. Infrared spectra of 1-fluoroadamantane at (A) 200 K and (B) 250 K

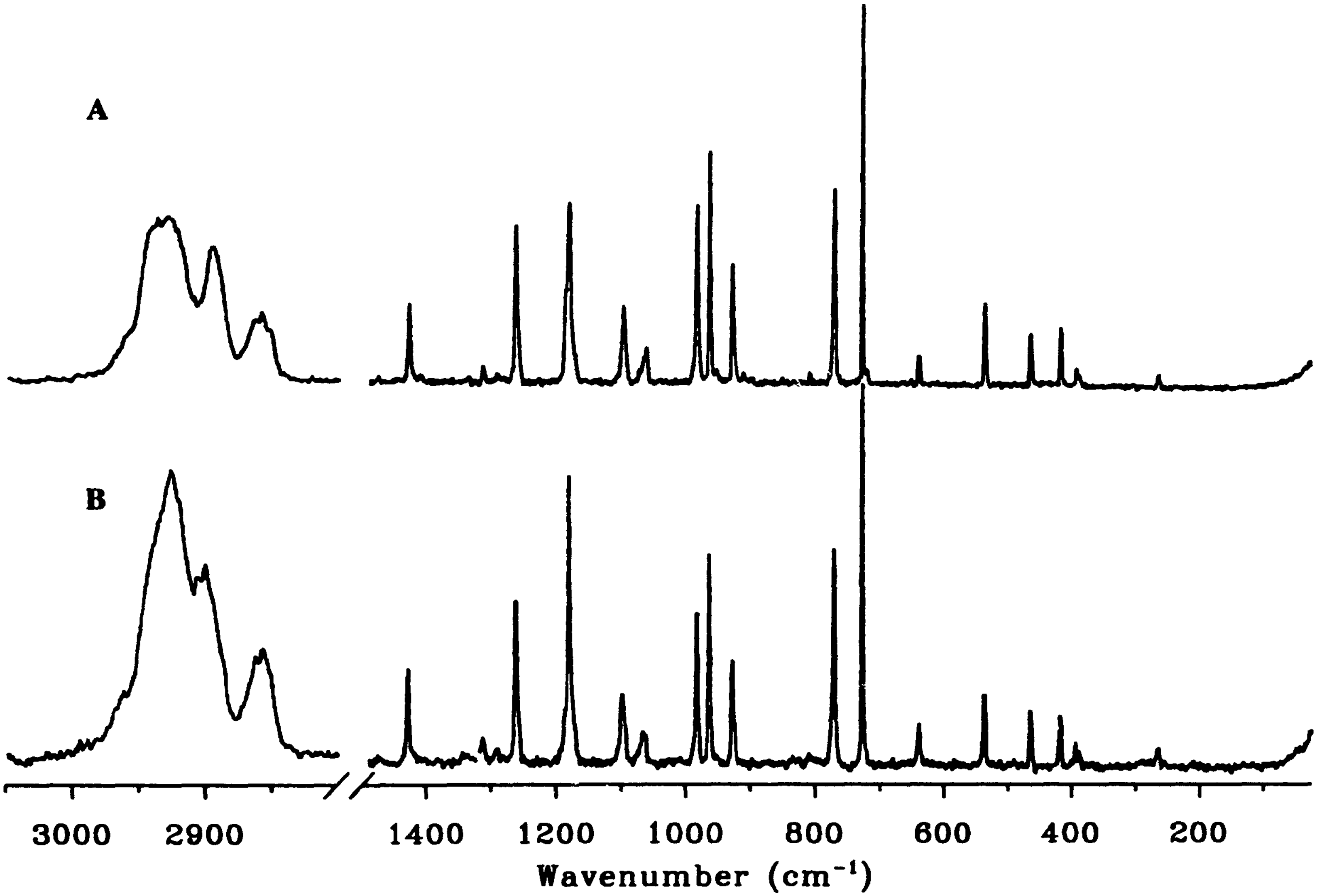

Figure 7.2.2. Raman spectra of 1-fluoroadamantane at (A) 205 K and (B) 250 K.

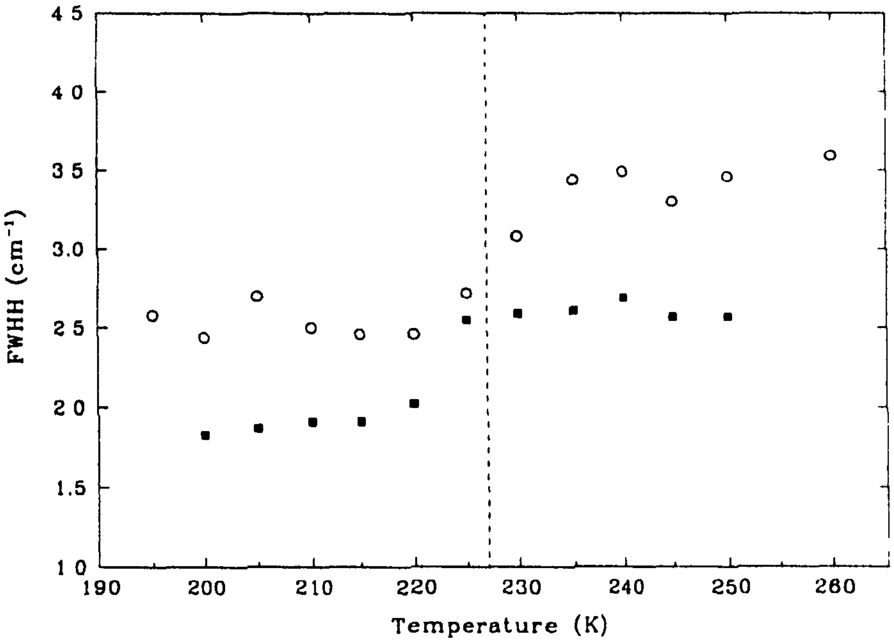

Figure 7.2.3. Full width at half height (FWHH) of two vibrational peaks of 1-fluoroadamantane: ○ 420 cm^{-1} Raman band, ■ 731 cm^{-1} IR band. The dashed line represents the phase transition temperature as measured by DSC (227 K on cooling).

any peaks, indicating that, on the timescale of the Raman measurements, the molecular motions are isotropic. The broadening of the Rayleigh line, however, was not as extensive as in the disordered phases of the compounds described in Chapters 4 through 6; therefore, at the same temperature, the fluoroadamantane molecules are moving slower than the smaller cage molecules in their disordered phases. Further cooling of phase II down to 60 K did not induce any other observable phase transitions. Another approach to induce this transition would be tc cool the sample to about 60 K and then to heat it very slowly above the predicted glass transition temperature. If the sample then underwent an annealing process from the glass, it may be possible to observe it spectroscopically. This was attempted by Raman spectroscopy; the temperature of the sample was increased from 60 to 120 K by approximately 5 K every hour. If the glassy phase transformed to an ordered, crystalline phase, line narrowing and the appearance of sharp external modes would be expected. Such effects, however, were not observed in the Raman spectrum. The rate of heating and slight temperature instability of the cryostat at very low temperatures may have been responsible for the failure to crystallize a new phase. Ideally, this slow heating should have been performed by DSC, where the heating rate and temperature of the sample can be controlled precisely and accurately, and the thermogram would display this glass transition as an exotherm. The commercial DSC apparatus, however, was not able to reach temperatures lower than 100 K.

The vibrational peaks of phases I and II of fluoroadamantane are listed in Table 7.2.1. Raman polarization measurements were measured in CS_2 solution. While the spectra of adamantane itself have been assigned according to force-field calculations,[21] other 1-substituted derivatives have been assigned simply by comparison with other molecules. The vibrational spectra of fluoroadamantane, $C_{10}H_{15}F$, should contain 72 normal modes. Under C_{3v} molecular symmetry, however, these transform as $\Gamma_{vib}{}^{int} = 17\ a_1 + 7\ a_2 + 24\ e$, where only the a_1 and e modes are IR and Raman active, and the a_2 modes are totally inactive. These can be separated into 15 C-H stretching modes ($\Gamma_{v(CH)} = 4\ a_1 + a_2 + 5\ e$), and 57 non-CH modes ($\Gamma_{non\text{-}CH} = 13\ a_1 + 6\ a_2 + 19\ e$). Therefore, there should be a total of 41 peaks coincident in the IR and Raman spectra, with nine of these in the C-H stretching region. A total of 50 bands were observed in the IR and Raman spectra of phase II, which should not display any solid-state effects, but where the linewidths are narrowed sufficiently to resolve close-lying bands. The vibrational spectrum was assigned with the aid of assignments for adamantane[21,22] and other 1-substituted derivatives,[20] and seven a_1 bands could be identified from the polarization measurements. Although C-F stretching bands usually occur between 1000 and 1400 cm^{-1},[23] it has been reported that, when adjacent to a C-C single bond, the C-F and C-C

Table 7.2.1. Vibrational Data (cm^{-1}) for 1-F-adamantane.

sol'n/CS$_2$	phase I		phase II		
Raman[a] (295 K)	Raman (250 K)	IR (250 K)	Raman (205 K)	IR (200 K)	assignment
264 dp	267 vw		266 w		C-C-F bend, e
	391 vw		391 vw		C-C-C def
	396 vw		395 vw		
420 pp	420 w	419 w	420 w	419 w	
		463 w		463 w	
465 dp	467 w		467 w		
540 p	540 w	539 s	539 m	538 s	
	642 w	640 vw	643 w	641 vw	
		668 vw		668 vw	
			724 vw		
730 p	731 s	729 w	731 vs	729 w	C-F str, a_1
774 p	775 m	773 w	775 s	773 w	C-C str, a_1
		814 m	814 vw	814 m	C-C str + CH$_2$ and CH def
		904 m		904 m	
920 pp		918 s	918 vw	918 s	
931 dp	934 w	932 w	935 m	933 w	
			959 vw		
		969 s		968 s	
970 dp	970 m		970 s	970 m, sh	
988 dp	989 m		990 s		
		1044 vw		1045 vw	
			1070 w		
1076 dp	1072 vw	1072 s	1074 vw, sh	1072 s	
			1080 vw, sh	1079 s	
1102 dp	1105 w	1105 m	1105 m	1105 m	
		1111 w, sh		1113 w, sh	
		1183 vw, br		1184 vw, br	
1180 dp	1189 s		1190 s		
	1195 w, sh		1195 m, sh		
1265 dp	1271 m	1268 vw	1273 m	1268 vw	
		1290 w			
		1297 m		1295 m	
	1301 vw		1302 vw	1299 w, sh	
		1318 m		1316 w	
	1323 w		1324 w	1322 w	
		1345 m		1346 m	CH$_2$ and CH def
		1353 s		1354 s	
		1366 w		1366 w	
		1373 w		1373 w	
1439 dp	1439 w		1439 m		CH$_2$ scissor
		1449 w		1449 w	
		1456 m		1456 m	
2851 p	2852 m, sh		2852 m, sh	2851 m, sh	C-H str, CH$_2$, a_1
2857 pp	2857 m	2857 s	2858 m	2857 s	CH$_2$, e
2864 dp	2863 m, sh		2863 m, sh	2862 m, sh	CH$_2$, e
2886 p					(2 x 1456 cm^{-1}, A_1)
2901	2901 m	2898 s, sh	2896 m	2891 vs	CH, a_1
2909	2907 m	2910 vs		2911 vs	CH, e
				2917 vs	CH$_2$, e
2925 p	2928 s, br	2928 vs, sh	2931 m	2930 vs	CH$_2$, a_1
			2938 m, sh		CH$_2$, e
2958 p	2962 w, sh		2959 w, sh		CH$_2$, a_1

[a] dp = depolarized, pp = partially polarized, and p = polarized.

stretching vibrations become mixed and the lower frequency band is higher in C-F character.[24] For example, in $(CH_3)_3CF$, the C-F stretching band occurs at 751 cm^{-1} whereas the symmetric and antisymmetric C-C stretches are observed at 892 and 1260 cm^{-1}, respectively.[25] From comparisons with other 1-substituted adamantanes, the symmetric cage-breathing mode was assigned to the strong, polarized band at 774 cm^{-1}. Therefore, the C-F stretching vibration could be assigned to the polarized band at 730 cm^{-1}, and the peak at 1265 cm^{-1} is probably a skeletal stretching mode having e symmetry. As a consequence of the cage structure, the majority of the other bands between 800 and 1400 cm^{-1} are coupled, and involve contributions from skeletal stretching, and from methylene and methine C-C-H deformations. According to valence force-field calculations for adamantane,[21] the symmetric and antisymmetric methine C-H stretching modes could be assigned to the bands occurring at 2891 and 2911 cm^{-1}, respectively. The remaining C-H stretches were assigned to the methylene hydrogens, and their symmetries were determined according to the polarization measurements.

7.3. High-Pressure Vibrational Spectra

In the cases of the seven- and eight-carbon molecules described in the previous chapters, the behaviour of the compounds under pressure mimicked their low-temperature results. These molecules, however, all displayed phase transitions to ordered, crystalline solids. The effects of pressure on fluoroadamantane, therefore, may or may not be analogous to the low-temperature experiments.

Initially, Raman spectra were measured over a wide pressure range of 59 kbar. Figure 7.3.1 shows the C-H stretching region through a range of moderate pressures. Below 1.7 kbar, the spectrum resembles those observed for phase I in the variable-temperature experiments. Between 1.7 and 4.5 kbar, however, the shoulder at about 2945 cm^{-1} becomes better separated from the remainder of the higher-frequency C-H bands.

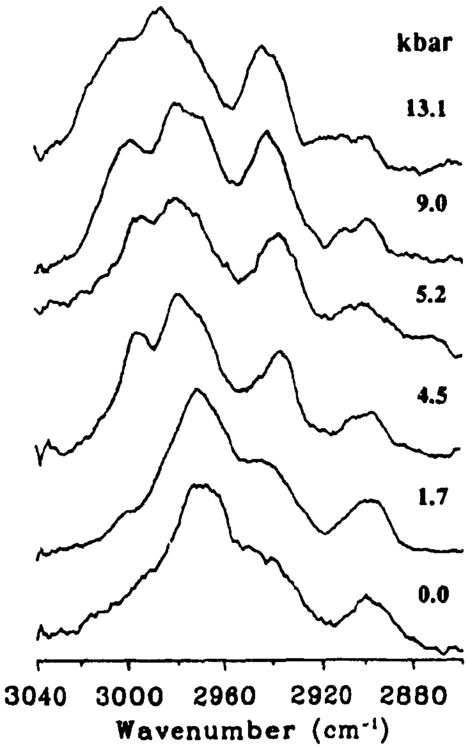

Figure 7.3.1. The C-H stretching region of the Raman spectrum of 1-fluoroadamantane at the indicated pressures upon compression.

This is analogous to the observations of the phase I → phase II transition under low-temperature conditions. The additional application of pressure, even as high as 59 kbar, did not induce any other phase transitions. This was demonstrated by the measurement of several peaks throughout the spectral region, which did not show any abrupt line narrowing or solid-state splitting in the Raman spectrum. It is concluded, therefore, that the glassy phase also forms upon compression, and will not spontaneously crystallize even under very high pressure.

High-pressure IR experiments were performed on fluoroadamantane as well, but at smaller pressure increments and over a narrower range of pressures. Figure 7.3.2 shows the C-H stretching region of the IR spectrum at various pressures. Although the line-narrowing effect is not as obvious as in the Raman spectra, the phase I → phase II transition can be observed to occur between 2.8 and 3.9 kbar. The IR experiments were also used to measure the spectral changes which occur to the peak at 1318 cm^{-1}, which is a combination of C-C stretching and various C-C-H and CH_2 bending modes. In Figure 7.3.3(A), the splitting of this peak due to sudden line narrowing is observed between 2.8 and 3.9 kbar. This is analogous to the effect which occurred upon lowering the temperature, and offers further proof of the occurrence of the phase transition at 3.3 ± 1.0 kbar; the band at 1318 cm^{-1}, which appears sharp in phase I, is resolved into two bands at 1316 and 1322 cm^{-1} in phase II, as shown in Figure 7.3.3(B). In another attempt to induce the second phase transition, the sample was left under 22 kbar of pressure for a period of 36 h, and then left at 18 kbar for an additional 36 h. From our experience, these pressures correspond roughly to cooling the sample at 20 K and then around 80 K, respectively. As in the low-temperature experiments, a crystalline phase of fluoroadamantane did not form.

The pressure dependences of several modes were measured in both the IR and Raman spectra. Since more data points were obtained in the IR spectra at moderate

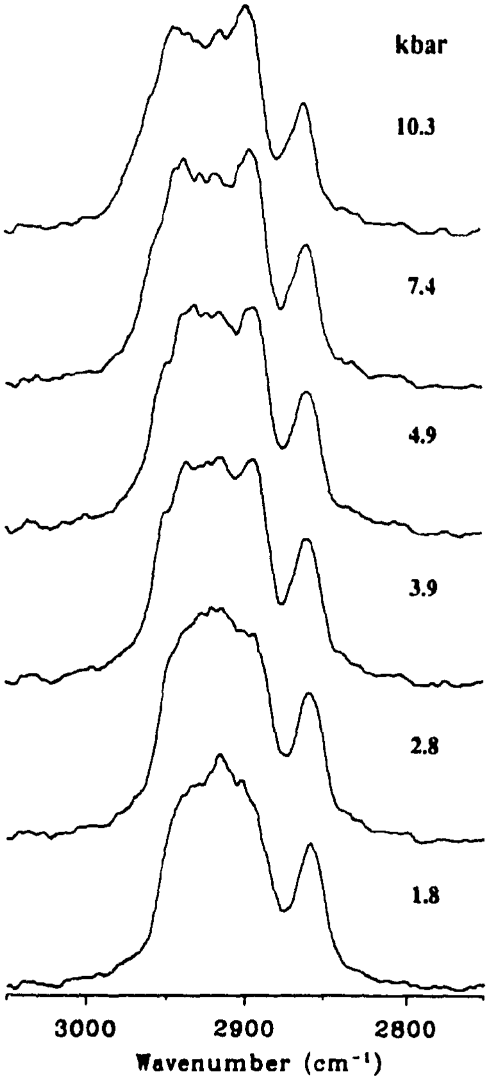

Figure 7.3.2. Infrared spectra of the C-H stretching region of 1-fluoroadamantane at the indicated pressures upon compression

pressures, the dv/dp values were measured from the IR rather than the Raman whenever possible. Figure 7.3.4 shows the pressure dependences of several peaks in the IR spectrum, and Table 7.3.1 lists the pressure dependences of all the vibrational peaks measured. Overall, the dlnv/dp values of both phases are quite high, which is consistent with the disordered nature of phases I and II. The pressure dependences of several Raman bands of adamantane itself have been reported,[26] and these dlnv/dp values are also very high, ranging from -0.5 to 14 x 10^{-4} kbar^{-1} for the skeletal modes, and from 1.1 to 3.2 x 10^{-4} kbar^{-1} for the C-H stretching vibrations. The totally symmetric, cage-breathing vibration in adamantane, occurring at 759 cm^{-1}, has the highest pressure dependence of 14 x 10^{-4} $kbar^{-1}$. The symmetric cage-breathing mode was also reported in the high-pressure Raman spectroscopic studies of 1-chloroadamantane[9], where the band at 773 cm^{-1} exhibited a pressure dependence of approximately 20 x 10^{-4} and 6 x 10^{-4} $kbar^{-1}$ in the disordered and ordered phases, respectively. The value in the disordered phase, however, was based on only four data points. These pressure dependences can be compared to the dlnv/dp values for the 773 cm^{-1} peak of fluoroadamantane (9.2 x 10^{-4} and 7.0 x 10^{-4} $kbar^{-1}$ in phases I and II, respectively). The

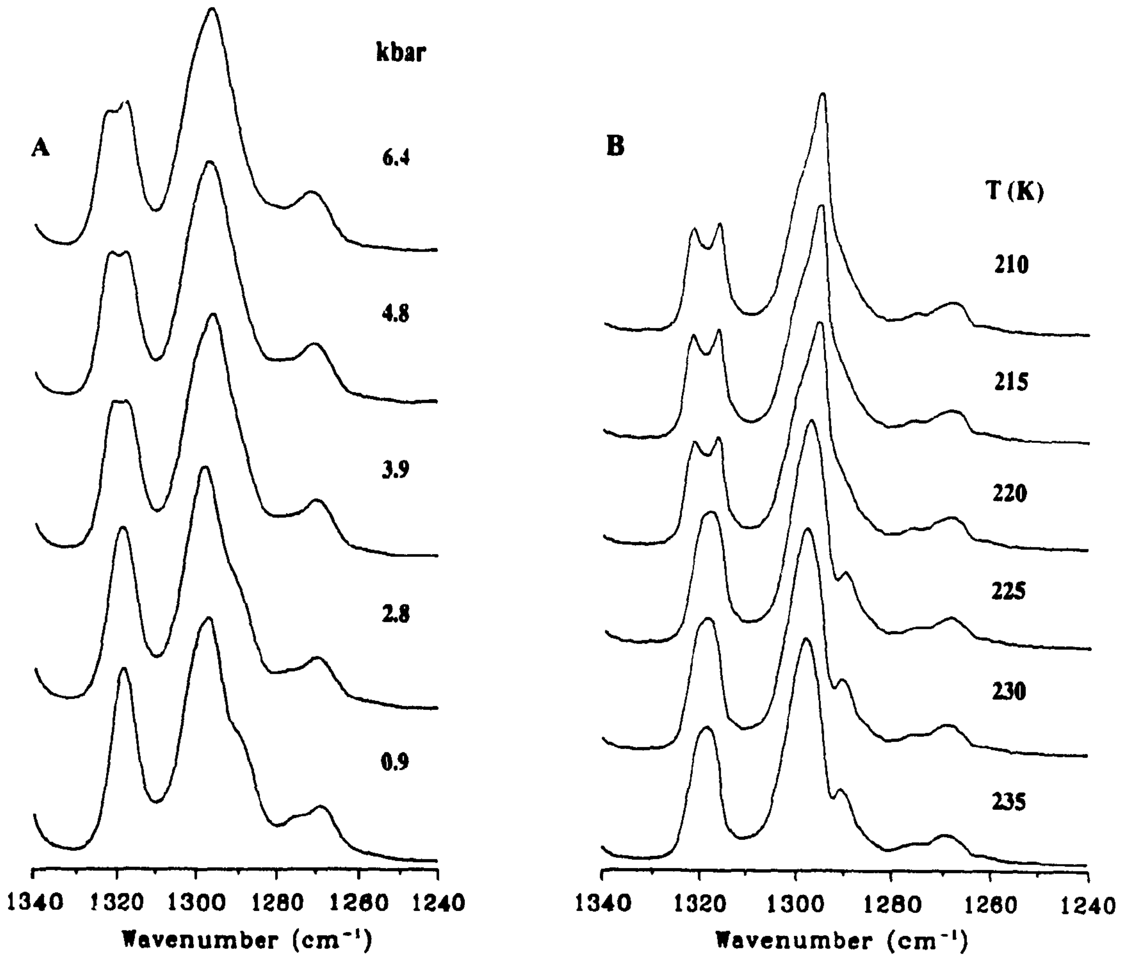

Figure 7.3.3. The resolution of the 1318 cm^{-1} IR band into two bands at 1316 and 1322 cm^{-1} at the phase transition of 1-fluoroadamantane, (A) under pressure, and (B) at low temperature.

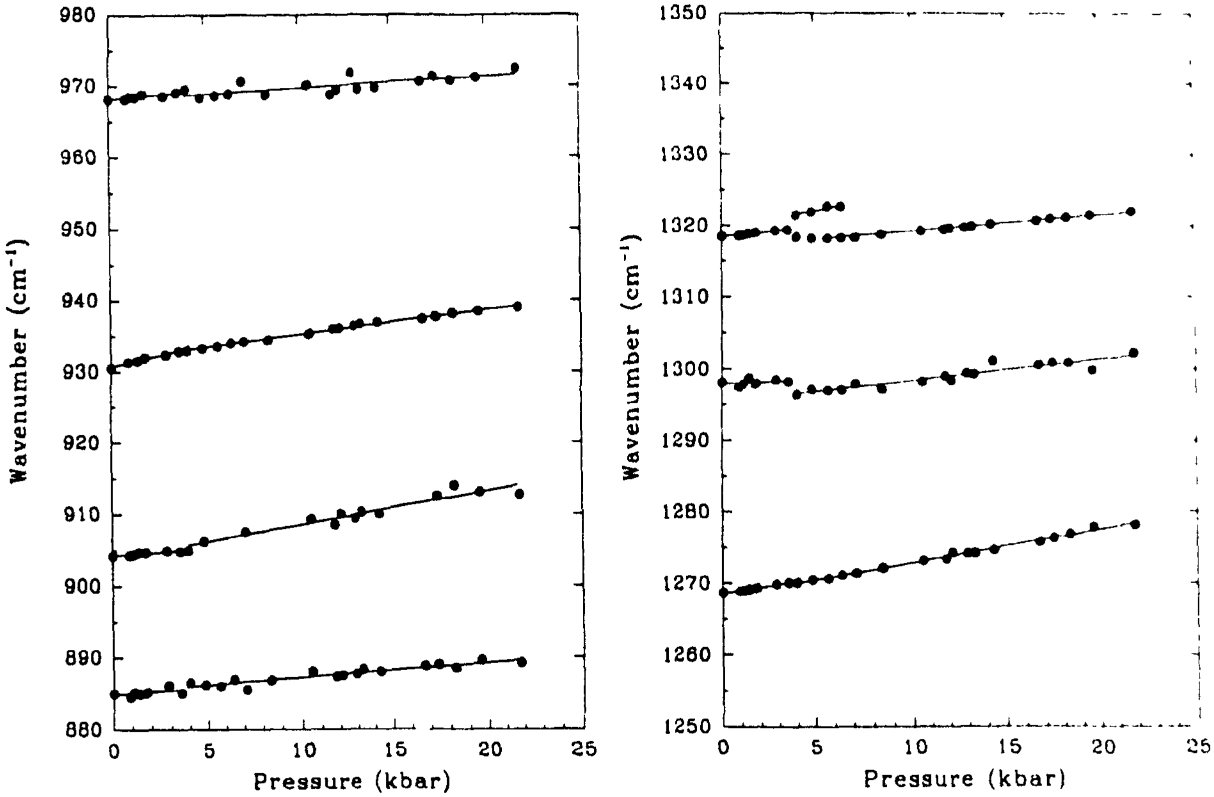

Figure 7.3.4. Pressure dependences of several IR bands of 1-fluoroadamantane

disordered phases of these adamantane derivatives all belong to the same space group, Fm3m, Z = 4, where a = 9.445 Å for adamantane,[27] a = 9.97 Å for 1-chloroadamantane,[28] and a = 9.53 Å for fluoroadamantane.[11] From these unit cell dimensions, the densities of these solids are calculated to be 1.07, 1.14, and 1.18 g cm^{-3}, respectively. It is reasonable, therefore, that the pressure dependence of the cage-breathing mode of adamantane has the highest value compared to the other two derivatives, because its crystal density is the lowest, and its lattice should be the most compressible. The same vibrational mode in fluoroadamantane, which has the highest crystal density, should have the lowest pressure dependence, and this was confirmed experimentally. The behaviour of the disordered phase of 1-chloroadamantane is puzzling, however, since its crystal density is closer to that of fluoroadamantane, but its

Table 7.3.1. Pressure Dependences of Vibrational Peaks of 1-F-adamantane *

phase I			phase II			
v (cm^{-1})	dv/dp (cm^{-1}kbar^{-1})	dlnv/dp (kbar^{-1}x10^{4})	v (cm^{-1})	dv/dp (cm^{-1}kbar^{-1})	dlnv/dp (kbar^{-1}x10^{4})	assignment
			419	0.2	4	C-C-C def.
			463	0.1	2	
			538	0.2	3	
640	0.2	3	641	0.18	2.8	
729	0.46	6.2	729	0.42	5.8	C-F str.
773	0.71	9.2	773	0.54	7.0	C-C str.
814	0.78	9.6	814	0.57	6.9	C-C str. + CH_2 and CH def.
904	0.2	2	904	0.47	5.2	
			918	0.32	3.5	
932	0.64	6.9	933	0.35	3.7	
969	0.4	4	968	0.2	2	
970 (R)	0.31	3.2				
989 (R)	0.3	3	990 (R)	0.6	6	
1044	0.60	5.7	1045	0.58	5.6	
1072	0.2	2	1071	0.1	1	
1105	0.8	7	1105	0.5	5	
1183	1	11	1184	0.38	3.2	
1268	0.44	3.4	1268	0.47	3.7	
			1295	0.3	2	
1318	0.29	2.2	1316	0.23	1.7	
			1322	0.5	4	
1353	0.37	2.8	1354	0.26	1.9	
1366	0.40	2.9	1366	0.38	2.8	
1373	0.56	4.1	1373	0.48	3.5	
2857	1	4	2857	0.2	0.7	methylene C-H str.
			2891	0.3	1	methine C-H str.

*All peaks are from the IR spectrum, except for those marked with an R.

behaviour under pressure is more akin to that of adamantane. The dlnv/dp value for the same skeletal mode should be between those of adamantane and fluoroadamantane. Assuming that all of the x-ray structures are correct, it is probable that the pressure dependence reported for the skeletal-breathing peak in 1-chloroadamantane should be closer to the value measured presently for fluoroadamantane, *i.e.*, ~10 x 10^{-4} kbar^{-1}. The discrepancy in the dlnv/dp value in 1-chloroadamantane is most likely imprecision due to the shortage of data points.

Upon examination of the pressure dependences within the fluoroadamantane molecule, those of the 729 and 773 cm^{-1} peaks are particularly high. This is expected since these bands have been assigned in section 7.2 as the symmetric C-F and C-C stretching modes, respectively. This C-C stretching mode has a higher pressure dependence compared to the C-F stretch in both phases I and II; the C-F bond length in fluoroadamantane was reported to be 1.370 ± 0.004 Å by microwave spectroscopy,[29] and the C-F stretching force constant is typically 6.0 x 10^{-5} dyn cm^{-1}.[30] Thus, the higher force constant causes the C-F bond to be less compressible, and the pressure dependence is slightly lower than that of C-C vibrations, even though the former also has a shorter bond length. The peaks at 814, 904, and 1045 cm^{-1} also have relatively large pressure dependences, and these bands can therefore be assigned to modes which have significant contributions from skeletal stretching vibrations The peaks which have very low dlnv/dp values are largely deformation modes, *i e*. those at 1316 and 1354 cm^{-1} are CH_2 twisting or wagging vibrations. Although the C-H stretching region could not be fully explored, due to the extensive overlap of these peaks, the two bands which were measured suggest that their pressure dependences are relatively low. This can be attributed to the absence of ring strain in the fluoroadamantane molecule.

References

1. T. Clark, T. Mc. O. Knox, H. Mackle, and M. A. McKervey, J. Chem. Soc., Faraday Trans. 1, 73, 1224 (1977).
2. M. Foulon and C. Gors, Acta Crystallogr., **B44**, 156 (1988).
3. M. Foulon, J. P. Amoureux, J. L. Sauvajol, J. Lefebvre, and M. Descamps, J. Phys. C. Solid State Phys., **16**, L265 (1983).
4. P. D. Harvey, D. F. R. Gilson, and I. S. Butler, Can J. Chem., **65**, 1757 (1987)
5. (a) P. D. Harvey, D. F. R. Gilson, and I. S. Butler, J. Phys. Chem., **90**, 136 (1986); (b) F. Belanger-Ganepy, F. Brisse, P. D Harvey, D. F. R. Gilson, and I. S. Butler, Can J Chem., **68**, 1163 (1990)

6. Y. Huang, D. F R. Gilson, I. S. Butler, and F. A. Morin, J. Phys. Chem., in press.

7. (a) P. D. Harvey, D F. R. Gilson, and I. S Butler, J. Phys. Chem., **91**, 1267 (1987); (b) F. Belanger-Gariepy, F. Brisse, P D Harvey, I. S. Butler, and D F. R. Gilson, Acta Crystallogr., **C43**, 756 (1987)

8. (a) I. S. Butler, H B. Cole, D. F R. Gilson, P. D Harvey, and J. D. McFarlane, J. Chem. Soc., Faraday Trans 2, **82**, 535 (1986); (b) P D. Harvey, I. S. Butler, D F. R. Gilson, and P. T. T. Wong, J. Phys Chem., **90**, 4546 (1986).

9. R. M. Paroli, Ph.D. Thesis, McGill University, Montreal, Quebec, Canada, 1988.

10. R. M. Paroli, N. T Kawai, I. S. Butler, and D F. R Gilson, Can. J. Chem., **66**, 1973 (1988).

11. J. P. Amoureux, M. Bee, and J. L. Sauvajol, Acta Crystallogr., **B38**, 1984 (1982).

12. J. P. Amoureux, R. Decressain, and M. Castelain in *Dynamics of Molecular Crystals*, (J. Lascombe, ed.), Studies in Physical and Theoretical Chemistry, **46**, Elsevier Science Publishers B.V , Amsterdam, 1987, p. 559.

13. M. Bee and J. P. Amoureux, Mol. Phys., **50**, 585 (1983).

14. J. P. Amoureux, M. Castelain, M. Bee, M. D. Benadda, and M. More, Mol. Phys., **55**, 241 (1985).

15. Y. Guinet, J L. Sauvajol, and M. Muller, Mol. Phys., **65**, 723 (1988).

16. M. Bee and J. P Amoureux, Mol. Phys., **48**, 63 (1983).

17. C. E. Nordman and D. L. Schmitkons, Acta Crystallogr., **18**, 764 (1965).

18. J. Donohue and S. H Goodman, Acta Crystallogr., **22**, 352 (1967).

19. H. Szarc, Thermochim Acta, **109**, 91 (1986).

20. T. J. Broxton, L. W. Deady, M. Kendall, and R. D. Topsom, Appl. Spectrosc., **25**, 600 (1971).

21. R. G. Snyder and J. H. Schachtschneider, Spectrochim. Acta, **21**, 169 (1965).

22. R. T. Bailey, Spectrochim. Acta, **27A**, 1447 (1971).

23. F. L. Dollish, W. G. Fateley, and F. F. Bentley, *Characteristic Raman Frequencies of Organic Compounds*, Wiley-Interscience, New York, 1974, p. 23.

24. E. C. Tuazon, W G. Fateley, and F. F. Bentley, Appl. Spectrosc., **25**, 374 (1971).

25. W. Huttner and W. Zeil, Spectrochim. Acta, **22**, 1007 (1966).

26. G. Burns, F. H. Dacol, and B. Welber, Solid State Commun., **32**, 151 (1979).

27. J. P Amoureux, M. Bee, and J. C. Damien, Acta Crystallogr., **B36**, 2633 (1980).

28. P. Zielinski and M. Foulon in *Dynamics of Molecular Crystals*, (J. Lascombe, ed.), Studies in Physical and Theoretical Chemistry, **46**, Elsevier Science Publishers B.V., Amsterdam, 1987, p. 201.

29. D. Chadwick, A. C. Legon, and D. J Millen, J. Chem. Soc. A, 1116 (1968).

30. G Herzberg, *Molecular Spectra and Molecular Structure Vol II Infrared and Raman Spectra of Polyatomic Molecules*, D. Van Nostrand Company, Princeton, 1945, p. 193.

CHAPTER 8. A STRUCTURAL STUDY OF 1,4-DIIODO- AND 1,4-DIBROMOCUBANE IN THE SOLID STATE

8.1 Introduction

The synthesis of cubane, pentacyclo[$4.2.0.0^{2,5}.0^{3,8}.0^{4,7}$]octane, was first reported by Eaton and Cole in 1964,[1] and the crystal structure of this novel cage molecule was determined to be trigonal/rhombohedral, $R\bar{3}$, Z = 1, with the body diagonal of the cube along a three-fold rotation axis of the crystal.[2] Due to the high symmetry and "globular" shape of this molecule, it is expected to form an orientationally-disordered solid phase, evidence of a phase transition at 393 K (just below the fusion temperature of 404 K) has been recently reported in the literature.[3] The crystal structure of the 1,4-dinitrocubane molecule has also been reported; in this case, the unit cell is monoclinic, $P2_1/c$, and the two molecules in the unit cell are located at centres of inversion.[4] A phase transition in this derivative of cubane has also been suggested to occur at about 315 K.[5]

During the synthesis of cubane by Prof. P. G. Farrell and co-workers, several 1,4-substituted derivatives were prepared, including the dibromo and diiodo compounds. Differential scanning calorimetric studies were performed on the cubane derivatives, above and below room temperature. No phase transitions were observed between 103 K and the sublimation or decomposition temperature (> 500 K), and it was apparent that these cubane derivatives did not form orientationally-disordered solids This result was surprising since these molecules are ellipsoidal in shape and have a three-fold rotation axis similar to, for example, 1-chloro- and 1-bromoadamantane. To confirm the absence of disorder, and to investigate the molecular and crystal structures of these interesting cage compounds, single-crystal x-ray diffraction studies were performed on 1,4-dibromo- and 1,4-diiodocubane.

8.2 Experimental: Single-Crystal X-Ray Diffraction

During the course of this work, the crystal structure of 1,4-diiodocubane was reported in the literature,[6] and the study was discontinued. The structure of the dibromo analogue, however, remained uninvestigated, and is reported here.

The sample of 1,4-dibromocubane, freshly recrystallized from CH_2Cl_2, contained an adequate selection of single crystals needed for the x-ray diffraction measurements. Firstly, the density of a crystal was measured by the flotation method in an aqueous solution of $ZnBr_2$; the density of 1,4-dibromocubane was measured to be 2.13 Mg m^{-3}. Unit cell parameters were initially defined according to Buerger precession photographs, and the space group was determined to be $P2_1/c$. A single crystal of 1,4-dibromocubane, approximately 0.2 mm in all directions, was chosen for the x-ray diffraction measurements. Diffraction data were collected at room temperature on an Enraf-Nonius CAD4 diffractometer with Mo-$K\alpha$ radiation ($\lambda(K\alpha_1) = 0.70930$, $\lambda(K\alpha_2) = 0.71359$). Unit cell parameters were refined with 24 reflections ($2\theta = 40 - 50^{o}$). Crystal data are: $C_8H_6Br_2$; f.w. = 261.94; monoclinic, a = 6.878(1), b = 6.9600(7), c = 8.793(2) Å, β = 113.08(2); V = 387.2(1) Å^3; Z = 2; ρ_c = 2.247 Mg m^{-3}; F(000) = 247.96; μ = 102.8 cm^{-1}. Systematic absences occurred at: $h, 0, l$: $h + l = 2n + 1$; $0, k, 0$: $k = 2n + 1$; $h, 0, 0$: $h = 2n + 1$; and $0, 0, l$: $l = 2n + 1$, indicating the space group $P2_1/n$ ($P2_1/c$ with an alternate choice of cell, #14)[7], with the molecules located at special positions. Intensity data were collected using the $\theta/2\theta$ scan mode up to $2\theta = 44.7^{o}$. Two octants were measured within the index range h, k, l = -6 to 6, 0 to 6, and 0 to 9. Three standard reflections, measured 46 times during the data collection, showed a maximum instability of 2.83%, and were used to make corrections in the data reduction. Of the 475 unique reflections measured, 415 had intensities greater than $2.5\sigma(I)$.

The structure was solved by Patterson methods using the NRCVAX software.[8] Halogen atom positions were determined from a Patterson map, and the carbon atoms were positioned from an electron-density difference map. The lowest and highest peaks in the difference map were -1.4 e Å^{-3} and 0.65 e Å^{-3}. Hydrogen atoms were initially located according to the carbon atom framework. Spherical absorption corrections were performed. Refinement of the non-hydrogen atoms was made with anisotropic temperature factors, while hydrogen atoms were refined with isotropic factors. Final atomic coordinates are given in Table 8.2.1, and thermal parameters are listed in Table 8.2.2. The final extinction coefficient was 0.1867. Convergence was reached at R = 0.055, R_w = 0.063 for the 415 significant reflections, where $R = \Sigma (F_0 - F_c) / \Sigma F_0$, $R_w = [\Sigma (K (F_o - F_c)^2) / \Sigma (KF_0^2)]^{1/2}$. Refinement was based on 59 variables, with a weight modifier K in KF_0^2 of 0.00005. Bond lengths and angles are presented in Table 8.2.3.

Table 8.2.1. Atomic Coordinates and Equivalent Isotropic Temperature Factors (B_{iso} in Å^3) for 1,4-Dibromocubane.

atom	x	y	z	B_{iso}
Br	0.2758(2)	0.3117(2)	0.1522(2)	4.52(9)
C1	0.411(2)	0.126(2)	0.063(1)	2.7(6)
C2	0.518(2)	0.180(2)	-0.054(2)	3.4(7)
C3	0.292(2)	-0.046(2)	-0.050(1)	3.2(6)
C4	0.595(2)	-0.007(2)	0.168(2)	3.4(7)
H1	0.49(2)	0.32(2)	-0.09(1)	5(3)
H2	0.14(2)	-0.14(2)	-0.04(1)	6(3)
H3	0.65(1)	-0.00(1)	0.28(1)	1(2)

Table 8.2.2. Temperature Factors for 1,4-Dibromocubane.[a]

atom	u_{11}	u_{22}	u_{33}	u_{12}	u_{13}	u_{23}
Br	0.064(1)	0.050(1)	0.081(1)	-0.0036(8)	0.0525(9)	-0.0103(5)
C1	0.041(7)	0.038(8)	0.033(7)	-0.003(6)	0.025(6)	-0.007(5)
C2	0.047(8)	0.034(8)	0.061(9)	-0.003(7)	0.034(7)	0.006(7)
C3	0.038(7)	0.049(8)	0.041(7)	-0.003(6)	0.023(6)	0.000(7)
C4	0.042(8)	0.06(1)	0.037(8)	-0.007(6)	0.024(7)	-0.002(7)
H1	0.06(4)[b]					
H2	0.07(4)					
H3	0.02(3)					

[a] Anisotropic temperature factors are of the form: $T = -(2\pi^2) \Sigma \Sigma u_{ij} a_i^* a_j^* a_i a_j$.
[b] Isotropic temperature factors, U, are given for the hydrogen atoms.

Table 8.2.3. Bond Lengths (Å) and Angles (°) for 1,4-Dibromocubane.[a]

Br-C1	1.93(1)	C3-C2'	1.57(2)
C1-C2	1.54(2)	C3-C4'	1.57(2)
C1-C3	1.56(2)	C3-H2	1.3(1)
C1-C4	1.55(2)	C4-C2'	1.56(2)
C2-C3'	1.57(2)	C4-C3'	1.57(2)
C2-C4'	1.56(2)	C4-H3	0.9(1)
C2-H1	1.0(1)		

Br-C1-C2	123.1(8)	C1-C3-C2'	88.8(9)
Br-C1-C3	123.9(8)	C1-C3-C4'	88.5(8)
Br-C1-C4	125.0(8)	C1-C3-H2	126(5)
C2-C1-C3	91.5(8)	C2'-C3-C4'	90.6(9)
C2-C1-C4	92.6(9)	C2'-C3-H2	101(5)
C3-C1-C4	91.2(9)	C4'-C3-H2	142(5)
C1-C2-C3'	88.5(9)	C1-C4-C2'	89.7(9)
C1-C2-C4'	89.5(9)	C1-C4-C3'	88.3(9)
C1-C2-H1	111(7)	C1-C4-H3	121(5)
C3'-C2-C4'	90.4(9)	C2'-C4-C3'	90.5(9)
C3'-C2-H1	139(7)	C2'-C4-H3	129(6)
C4'-C2-H1	122(7)	C3'-C4-H3	125(5)

[a]The atoms indicated by primes (') are symmetry equivalents related by the operator 1-x, -y, -z.

8.3 Results and Discussion

The structure of 1,4-dibromocubane was determined to be isomorphous to the diiodocubane crystal, and also to the 1,4-dinitrocubane structure. The final x-ray structure of 1,4-dibromocubane, depicted in Figure 8.3.1, did not show any significant distortion of the cubic carbon skeleton. The packing of the unit cell is shown in Figure 8.3.2. There are no exceptional differences between the carbon skeletons of the dibromo and the diiodo analogues. The C-Br bond length was determined to be 1.93(1) Å. This is shorter than the C-Br bond in t-butyl bromide, which was reported to be 1.975(5) Å,[9] and probably shorter than the C-Br bond in 1-bromoadamantane (C-Br = 1.947(6) Å).[10] This decrease in C-Br bond length from t-butyl- to adamantyl- to cubyl- structures is expected, since the bond angles at the halogen-bonded carbon also decrease in this order. The C-I bond length of 1,4-diiodocubane was reported to be 2.123(6) Å in the single-crystal x-ray structure determination.[6] This is also significantly shorter than the C-I bond length in 1-iodoadamantane, which is 2.207(5) Å.[11]

The 1,4-dihalocubanes belong to the D_{3d} point group, and the normal modes transform according to $\Gamma_{vib}^{int} = 6a_{1g} + a_{2g} + 7e_g + 2a_{1u} + 5\ a_{2u} + 7e_u$. Symmetry selection rules result in the a_{1g} and e_g modes being Raman active, while the a_{2u} and e_u modes are IR active. The a_{2g} and a_{1u} modes are totally inactive. From the x-ray structure determination, the site symmetry of the molecule in the crystal is C_i, and the factor group is C_{2h}; a correlation diagram for the isomorphous dibromo- and diiodocubane derivatives is given in Figure 8.3.3. According to this diagram, the a modes are split into two by the factor group, while the e modes are doubled first by site splitting, and then doubled again by factor group splitting. As a result of these couplings, the a_{1g} modes in the Raman spectrum, and the a_{2u} modes in the IR spectrum, are doubled. Similarly, the e_g modes in the Raman spectrum, and the e_u modes in the IR

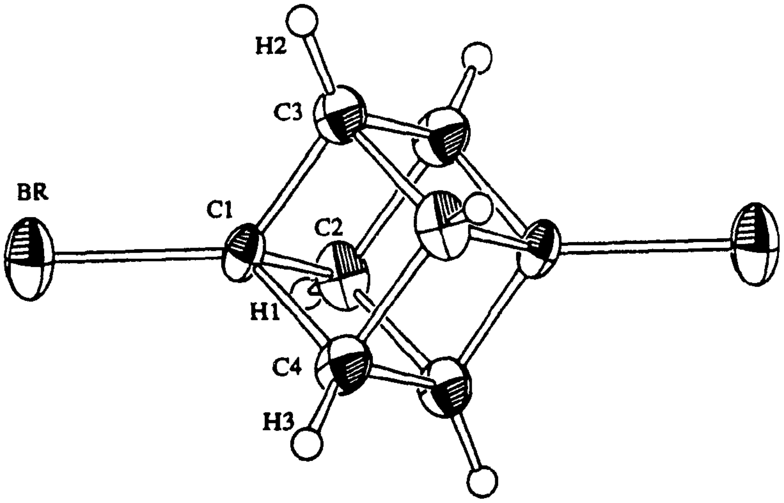

Figure 8.3.1. ORTEP[12] diagram of 1,4-dibromocubane, with thermal ellipsoids represented at 30% probability for the carbon and bromine atoms, and as arbitrary spheres for the hydrogen atoms.

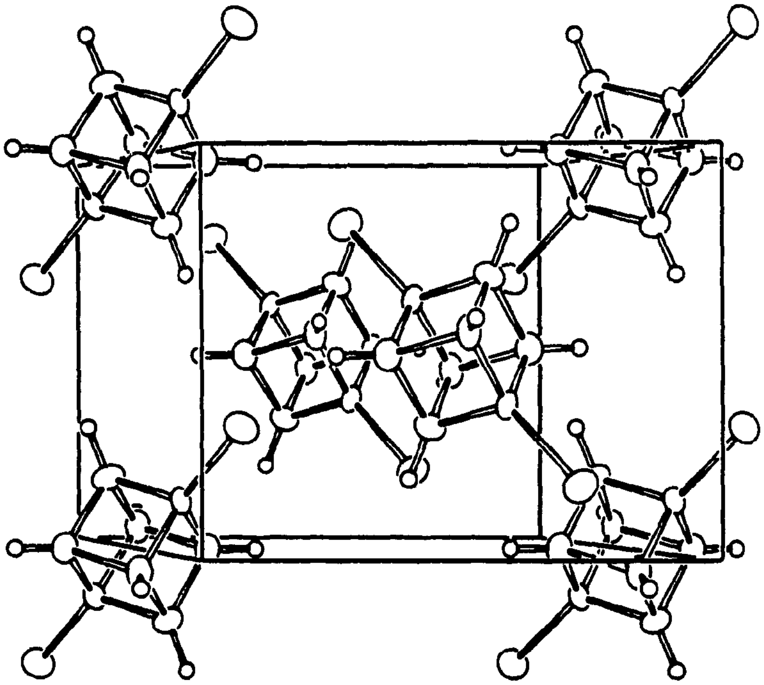

Figure 8.3.2. Packing diagram of the monoclinic unit cell of 1,4-dibromocubane, $P2_1/n$, looking down the a^* axis, with **c** parallel to the bottom of the page. Note the centre of symmetry in the molecule, site and crystal.

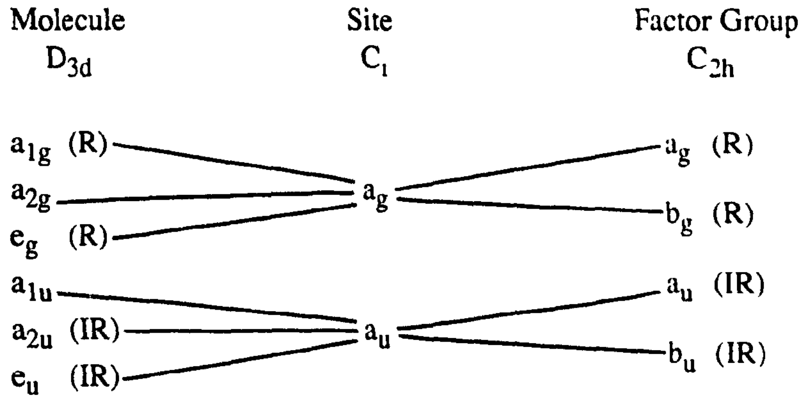

Figure 8.3.3. Correlation diagram for crystalline 1,4-dibromo- and 1,4-diiodocubane (R = Raman active, IR = IR active).

spectrum, are doubled twice, or quadrupled. Since the point, site, and factor group are all centrosymmetric, the rule of mutual exclusion should be followed quite rigorously.

Solid-state IR and Raman spectra were obtained for both 1,4-dibromo- and 1,4-diiodocubane (Figures 8.3.4 and 8.3.5), and the frequencies of the peaks are summarized in Table 8.3.1. The Raman spectrum of the bromo derivative in CS_2 solution was also measured, however the iodo derivative decomposed in this solvent, and its spectrum had to be measured in $CHCl_3$. Raman polarization measurements aided in making assignments of the totally symmetric a_{1g} modes. The similarities observed between the IR and Raman spectra of 1,4-dibromo- and 1,4-diiodocubane are not surprising since the two solids are isostructural. Almost all of the bands observed in the vibrational spectra of both compounds exhibited the predicted solid-state splitting patterns, although not all of the components could be observed since the spectra were measured at room temperature. In addition, the bands in the IR and Raman spectra are almost totally noncoincidental, again as expected according to the symmetry properties of the molecule and crystal.

The external vibrations of the molecules in the monoclinic lattice transform as $\Gamma_{vib}{}^{ext} = 3a_g + 3b_g + 2a_u + b_u$, resulting in three IR and six Raman bands which are again

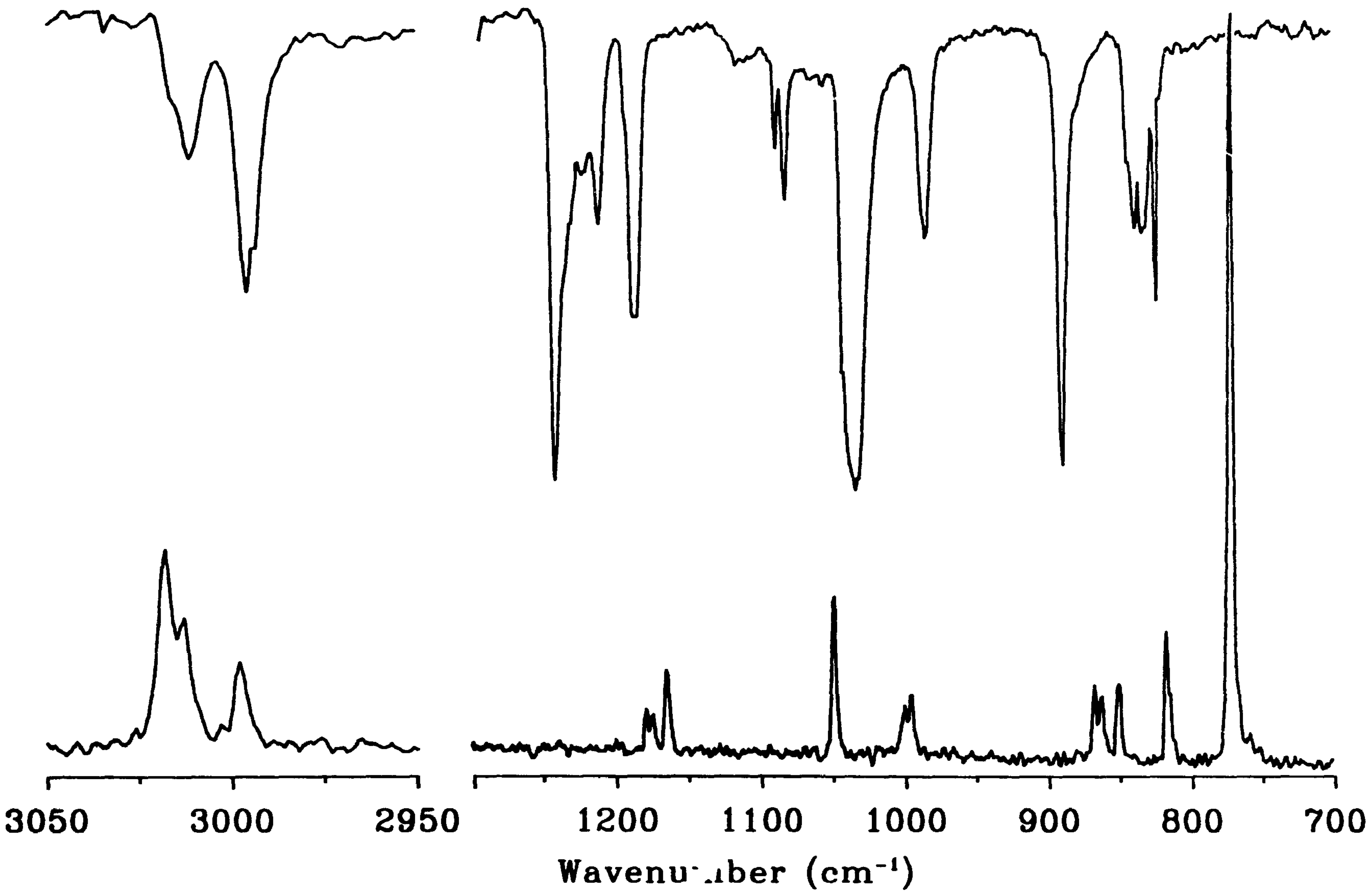

Figure 8.3.4. Solid-state vibrational spectra of 1,4-dibromocubane: IR spectrum in % transmittance (upper curve), and Raman spectrum in total counts (lower curve).

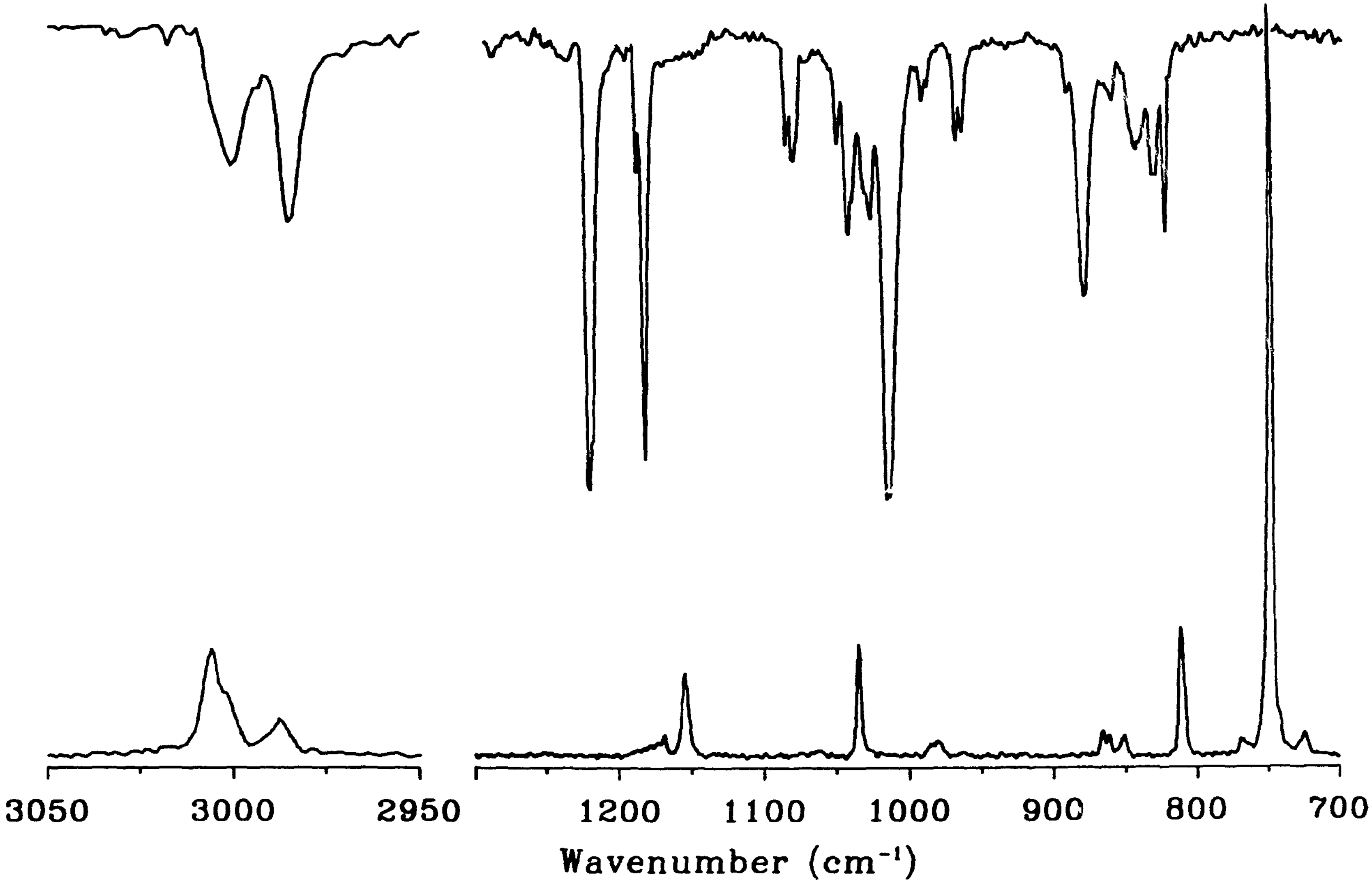

Figure 8.3.5. Solid-state vibrational spectra of 1,4-diiodocubane. IR spectrum in % transmittance (upper curve), and Raman spectrum in total counts (lower curve).

Table 8.3.1. Solid-State Vibrational Data (cm^{-1}) for 1,4-X_2-Cubane.

X = Br		X = I	
Raman	IR	Raman	IR
28 s		28 s	
33 s		35 s	
45 s		40 m	
204 vs		151 vs	
		152 vs, sh	
236 m		212 m	
240 m		215 w	
		219 vw	
		725 w	
770 vs		748 s	
		767 w	
816 m		811 m	
	824 m		825 m
	831 w		832 w
	834 w		843 w, sh
	838 m		845 w
849 w		850 vw	852 w, sh
861 w		861 vw	862 w
866 w		866 vw	
	890 s		881 s
	985 m		894 w
	987 m, sh		968 m
			972 m
994 w		980 vw	
999 w		985 vw	
			993 vw
			995 w
	1026 s, sh		1019 vs, sh
	1036 vs		1021 vs
	1045 m, sh		1032 m
1048 m		1035 m	1035 m, sh
	1086 m		1043 m, sh
	1092 w		1046 m
			1054 m
			1083 w, sh
			1087 m
			1190 m
1165 w		1155 m	
1175 w		1170 vw	
1179 w			
	1186 m		1189 s
	1189 m, sh		1194 m
	1217 m		
	1227 w		1225 s, sh
	1236 w, sh		1229 vs
	1247 s		
	2995 m, sh		2986 m
	2997 m		
2998 m		2988 w	
3003 w			
	3011 w		3001 m
3013 m		3002 m	
	3017 w, sh		3003 m, sh
3018 m		3006 m, sh	

mutually exclusive. In the low-frequency region of the Raman spectra of both compounds, three strong bands were present. The other three bands are either too weak to be measured or are unresolved from the other strong peaks.

Due to the strain on the substituted carbon, the C-halogen stretching mode is expected to have a higher frequency compared to other molecules such as in t-butyl bromide ($\nu_{(C\text{-}Br)}$ at 516 cm^{-1})[13], t-butyl iodide ($\nu_{(C\text{-}I)}$ at 492 cm^{-1})[14] and 1-bromoadamantane ($\nu_{(C\text{-}Br)}$ at 676 cm^{-1}).[15] The totally symmetric C-Br and C-I stretching vibrations can thus be assigned to the strong, polarized peaks at 770 and 748 cm^{-1}, respectively. The C-C-Br bending vibrations can be assigned to the solid-state peaks at 204, 236, and 240 cm^{-1}, whereas the C-C-I bending modes can be attributed to the bands between 150 and 220 cm^{-1}. The frequency of the totally symmetric cage-breathing mode in cubane has been reported as 1002 cm^{-1}, however this vibration shifts to lower frequency even in the 1,4-dideuterocubane derivative, occurring at 990 cm^{-1} [16] It is reasonable, therefore, to assign the cage-breathing mode to the medium intensity, polarized peaks at 816 and 811 cm^{-1} in 1,4-dibromo- and 1,4-diiodocubane, respectively The remaining bands between 820 and 1250 cm^{-1} are mostly C-C-H deformation modes, with some contributions from C-C stretches. The peaks below 900 cm^{-1} also have contributions from C-C-C deformations. Two IR and two Raman C-H stretching bands are predicted for the isolated molecule of each compound ($\Gamma_{\nu(C\text{-}H)} = (a_{1g} + e_g + a_{2u} + e_u$), with each of these split into two according to the solid-state structure. All eight of these bands were observed in the bromo derivative, while six of them were measured for the iodo derivative. According to the Raman polarization measurements, the pair of bands with the highest energy in the Raman spectrum of either compound correspond to the totally symmetric C-H stretching vibration.

References

1. P. Eaton and T. Cole, J. Am. Chem. Soc., **86**, 3157 (1964).
2. E. B. Fleischer, J. Am. Chem. Soc., **86**, 3889 (1964).
3. R. A. Dalterio and F. J. Owens, Solid State Commun., **67**, 673 (1988).
4. P. E. Eaton, R. Shankar, G. D. Price, J. J. Pluth, E. Gilbert, J. Alster, and O. Sandus, J. Org. Chem., **49**, 185 (1984).
5. F. J. Owens and R. A. Dalterio, J. Phys. Chem. Solids, **51**, 989 (1990).
6. H. L. Ammon, C. S. Choi, and S. Reddy, Acta Crystallogr., **C44**, 1671 (1988).
7. T. Hahn, ed., *International Tables for Crystallography*, D. Reidel Publishing Company, Dordrecht, Holland, 1983.
8. E. J. Gabe, F. L. Lee, and Y. Lepage, J. Appl. Crystallogr., **22**, 384 (1989).
9. A. C. Legon, D. J. Millen, and A. Samsam-Baktiari, J. Mol. Struct., **52**, 71 (1979).
10. D. Chadwick, A. C. Legon, and D. J. Millen, J. Chem. Soc. A, 1116 (1968).
11. M. Foulon and C. Gors, Acta Crystallogr., **B44**, 156 (1988).
12. C. K. Johnson, ORTEP-II, Report ORNL-5138, Oak Ridge National Laboratory, Oak Ridge, TN, 1976.
13. J. E. Bertie and S. Sunder, Can. J. Chem., **51**, 3344 (1973).
14. F. L. Dollish, W G. Fateley, and F. F. Bentley, *Characteristic Raman Frequencies of Organic Compounds*, Wiley-Interscience, New York, 1974, p. 19.
15. T. J Broxton, L. W. Deady, M. Kendall, and R. D. Topsom, Appl. Spectrosc., **25**, 600 (1971).
16. E. W. Della, E. F McCoy, H. K. Patney, G. L. Jones, and F. A. Miller, J. Am. Chem. Soc., **101**, 7441 (1979).

CHAPTER 9. CONCLUSIONS

The phase behaviour of six organic cage compounds, norbornane, norbornylene, norbornadiene, quadricyclane, bicyclooctene, and 1-fluoroadamantane, has been studied by vibrational spectroscopy at variable temperatures and pressures. The transformations of the seven- and eight-carbon compounds from high-temperature (or low-pressure) disordered phases to low-temperature (or high-pressure) ordered phases were observed. Bicyclooctene formed an additional phase, which was anisotropically disordered The structures of the ordered phases could be postulated from the observed solid-state splittings in the vibrational spectra. The fluoroadamantane molecule proved to be different in many ways from the smaller cage molecules. This compound underwent only a small-entropy phase transition, and the motions remained isotropic as observed at the vibrational timescale. Further cooling resulted in the formation of a glassy phase, and attempts to anneal the glass were unsuccessful. The behaviour of this fluoro-derivative of adamantane proved to be very different even from those of the bromo- and chloro-derivatives, the latter exhibiting phase transitions to ordered, crystalline phases.

In all cases, the phases formed by the application of pressure were the same as those caused by lowering the temperature. The phase transition pressures were measured for all compounds in the compression direction, and additionally for NBA, NBE and quadricyclane upon decompression. The measured pressure hystereses enabled the calculation of the volume changes at the phase transitions; quadricyclane was shown to have a high ΔV_t, while NBE has a value comparable with those of phase transitions in other hydrocarbon cages. A summary of the transition temperatures and pressures for all six compounds is given in Table 9.1.

The pressure dependences of the vibrational frequencies for the isotropically disordered phases of NBA, NBE, NBD, and BCOE were consistent from compound to

Table 9.1. Summary of the Phase Transition Temperatures and Entropies Measured by DSC, and the Phase Transition Pressures Determined by Vibrational Spectroscopy.

compound	transition	T_t (K)	ΔS_t ($J\ K^{-1}\ mol^{-1}$)	p_t (kbar)
norbornane	II → III	129	31.7	16.4
	III → II	130	32.3	16.1
norbornylene	I → II	114	35.8	14.9
	II → I	127	35.9	13.3
norbornadiene	I → II	175	40.4	6.4
	II → I	201	42.8	--
quadricyclane	I → II	153	45.0	10.7
	II → I	180	40.0	9.3
bicyclooctene	I → II	169	31.2	7.9
	II → I	176	31.5	--
	II → III	~95*	--	~15
	III → II	--	--	--
fluoroadamantane	I → II	227	7.6	3.3
	II → I	231	6.9	--

*Phase transition temperature measured by low-temperature Raman spectroscopy.

compound, in the range of 1 to 5 x 10^{-4} $kbar^{-1}$ for the skeletal modes. This indicates that these disordered phases have very similar compressibilities. The ordered phases of NBE, NBD, and BCOE were also determined to have similar compressibilities, but lower than those of the disordered phases. Phase III of NBA is significantly less compressible than the ordered phases of NBE, NBD, and BCOE. The peaks of quadricyclane in both phases had relatively high pressure dependences spanning a wider range of values, and these effects are probably due to the extra strain in the cage. The pressure dependences of the peaks of fluoroadamantane were higher than those of the smaller molecules. Upon comparison with the disordered phases of adamantane and 1-chloroadamantane, though, the pressure dependence of the skeletal-breathing mode of fluoroadamantane was observed to be very low. The behaviour of these molecules under pressure was explained according to their differences in crystal density.

The pressure dependences of different IR and Raman modes have proven to be useful in making further assignments of the vibrational spectra. As an outcome of the cage structures of these compounds, many modes are coupled to one another. Nevertheless, peaks which had significantly higher dlnν/dp values could be assigned to normal modes which have a large contribution from C-C stretching vibrations. Band splittings attributed to correlation coupling were confirmed by the diverging behaviour of the different components under pressure. The peaks due to C-H stretching motions usually exhibit a large range of pressure dependences. As a general rule, the dlnν/dp values of C-H stretching vibrations are higher than those of skeletal modes because the former are highly anharmonic. For the different types of C-H bonds in the bicyclic or polycyclic molecules, assignments of several C-H stretching bands could be made for NBE, quadricyclane, and BCOE. This analysis was possible because C-H stretching modes are normally pure in nature, and the vibration can be modelled as a single hydrogen atom bonded to a large sphere. Fermi resonance effects were also investigated as a function of pressure, and two bands in the Raman spectrum of NBD were assigned as a Fermi resonance pair according to the pressure dependences of their peak positions and the shift in intensity from one to the other.

In this thesis, the method of using pressure dependences of vibrational bands to assist in making spectral assignments has been introduced into the field of high-pressure vibrational spectroscopy. Attempts to explain numerically the effect of pressure on molecular bonds have been reported in the literature; however the results have been of limited value, and additional information (such as crystal compressibility) is required.[1,2] The observed shift in vibrational frequency with applied pressure depends not only upon the compressibility of the bond, but also the fractional change in bond length. In the qualitative analysis used in this thesis, the absolute reductions in interatomic distances were assumed to be constant for different types of bonds. The high dlnv/dp values for C H stretching modes were explained in light of the very short C-H bond lengths (~1.08 Å in cage molecules)[3] compared to C-C bonds (~1.53 Å). The short bond length appears to be the governing factor over the pressure dependence of the C-H stretching modes since the force constant of C-H (4.5 x 10^{-5} dyn cm^{-1}) is comparable with that of C-C (4.4 x 10^{-5} dyn cm^{-1}).[4] The C=C double-bond stretches have very low pressure dependences compared to C-C single bond, and this is due to the much higher force constant (6.8 x 10^{-5} dyn cm^{-1}) rather than the shorter bond length (1.33 Å).[4] In the case of C-F stretching vibrations, the high force constant of the bond (6.0 x 10^{-5} dyn cm^{-1})[5] and the short bond length (1.370 Å)[6] appear to balance each other, resulting in a pressure dependence slightly lower than those of the C-C stretches. The behaviour of bending modes is very complicated, although it was observed that the pure bending vibrations, such as the CH_2 scissoring modes, have the lowest pressure dependences within a given molecule.

A semiquantitative method for predicting pressure dependences can be derived from the trends observed in this thesis. The C-C stretching vibration will be regarded as the reference point, and other stretching force constants and bond lengths will be described relative to this standard. Using the force constants and bond lengths mentioned above, the force constants of C=C, C-F, and C-H are 54, 36, and 2% higher than C-C, and the bond lengths are 13, 10, and 30% shorter, respectively. The ratios of the relative change in force constant to bond length are, therefore, 4.2, 3.6, and 0.07, respectively, for C=C, C-F, and C-H. From potential energy calculations of diatomic molecules, it has been approximated that a 1% decrease in bond length will result in a 6% increase in vibrational force constant, and thus a 3% increase in vibrational frequency.[1,7] From these numbers, in order for another stretching mode to have the same pressure dependence as a C-C stretch, the ratio of the force constant increase to the bond length shortening should be approximately 6:1. Any smaller ratio would result in a higher pressure dependence, and a larger ratio would result in a lower pressure dependence, compared to C-C. This ratio does not agree with that deduced from the pressure behaviour observed for C=C, C-F, and C-H stretching vibrations. For the molecules reported in this thesis, the experimentally determined ratio of change in force constant to change in bond length, in order for the relative pressure dependences to be the same, appears to be around three as opposed to six.

It is hoped that the data compiled in this thesis will provide a basis for the extension and improvement of the analysis of high-pressure vibrational spectroscopic measurements to other types of molecules.

References

1. W. F. Sherman and G. R. Wilkinson in *Advances in Infrared and Raman Spectroscopy*, vol. 6, (R. J. H. Clark and R. E. Hester, eds.), Heydon and Son, London, 1980, Chap. 4, p. 158.
2. D. Salmon, V. L. Shannon, and H. L. Strauss, J. Chem. Phys., **90**, 773 (1989).
3. C. R. Castro, R. Dutler, A. Rauk, and H. Wieser, J. Mol. Struct. (Theochem), **37**, 241 (1987).
4. T. G. Lenz and J. D. Vaughan, J. Phys. Chem., **93**, 1588 (1989).
5. G. Herzberg, *Molecular Spectra and Structure Vol II Infrared and Raman Spectra of Polyatomic Molecules*, D. Van Nostrand Company, Princeton, 1945, p. 193.
6. D. Chadwick, A. C. Legon, and D. J. Millen, J. Chem. Soc. A, 116 (1968)
7. G. Herzberg, *Molecular Spectra and Structure Vol I Spectra of Diatomic Molecules*, 2nd ed., Van Nostrand Reinhold Company, New York, 1950, p. 457.

SUGGESTIONS FOR FUTURE WORK: HIGH-PRESSURE FT-RAMAN SPECTROSCOPY

In this thesis, several high-pressure vibrational spectroscopic experiments, using both IR and Raman spectroscopy have been described. Although the diamond anvils proved to be satisfactory windows over the IR region useful for hydrocarbons, they are not transparent in the 2700 - 1800 cm^{-1} region, which is important for many other compounds. Also, the cutoff of most infrared instruments in the mid-IR region is 400 cm^{-1}, which seriously curtails the study of metal-ligand vibrations and does not allow the observation of lattice modes. In theory, Raman spectroscopy should allow the observation of the complete vibrational spectrum through the diamond anvils. Raman spectroscopy is also more useful since the spectra are less complicated by combinations and overtones, and trace amounts of water do not interfere with the observed spectra. The external modes can also be observed, which is highly important in structural studies. In practice, however, these Raman studies are not free from interferences; the diamonds which are the most transparent in the IR region, type IIA, are also those which generally exhibit high fluorescence when excited by a visible-laser source. Most commercially-available DAC's are not tested for a low fluorescent background, only IR transparency, and it is difficult to purchase a cell which satisfies both specifications.

The development of high-pressure FT-Raman spectroscopy is therefore proposed, to alleviate the problems and combine the advantages of both IR and Raman techniques. The combination of an open spectroscopic region, the elimination of the fluorescent background by using a near-IR laser as the excitation source, and the speed of Fourier transform interferometry can result in a powerful new method of high-pressure spectroscopic analysis. The development of this technique consists of several stages: first, the measurement of a spectrum in the cell must be achieved; second, a pressure calibrant must be developed since the near-IR laser will not excite the ruby fluorescence which is used in conventional Raman spectroscopy; third, the problem of sample heating must be addressed. Preliminary work on stage one was attempted at Bomem Inc. (Ste-Foy, Quebec) using their DA3 and DA8 spectrometers.

Alignment of the DAC is the most difficult and the most crucial part of the experiment, because the actual sample size is only 400 μm in diameter, and 400 μm in thickness. The set-up used in the IR experiments already described in this thesis was employed; the cell was mounted onto an XYZ translator which has 2 cm of movement in all directions. Once the cell was aligned, it could be mounted and dismounted quickly and easily without disrupting its position. The positioning of the cell in the near-IR laser beam was initially achieved by placing a power meter behind the cell, and adjusting the vernier translators to maximize the laser power through the diamond anvils. With an empty gasket mounted in the DAC, the intensity of the strong diamond Raman peak (1333 cm^{-1}) was measured while moving the cell in small increments in a direction parallel to the laser beam. The intensity of this peak was observed to systematically decrease and then increase as the focal point of the near-IR laser passed from one diamond, to the empty gasket, to the other diamond anvil. Thus, the focussing of the excitation source onto the gasket hole had been successful.

Due to time constraints, no further progress could be made on the high-pressure FT-Raman experiments. However, the following steps should be addressed in sequence

(1) Once the DAC is roughly aligned, a strongly scattering substance, such as MoO_3, should be loaded into the cell, and the alignment should be fine-tuned.

(2) A suitable calibrant must be chosen, and it must then be calibrated against the R_1 ruby fluorescence line in a conventional Raman experiment. Quartz is suggested as a calibrant with which to begin.

(3) Since the DAC is equipped with a flow-through purge line, sample heating by the high-powered near-IR laser can be counteracted by flowing cool nitrogen gas through the DAC. The ability to control the sample temperature can lead to the development of simultaneous variable-temperature, variable-pressure FT-Raman spectroscopy.

Once these problems have been addressed, high-pressure FT-Raman spectroscopy will become a routine experiment to study the behaviour of a wide range of organic and inorganic systems under high-pressure conditions.

CONTRIBUTIONS TO KNOWLEDGE

(1) Variable-temperature and variable-pressure IR and Raman spectroscopy have been shown to be useful methods to study the phase behaviour of several orientationally-disordered organic cage molecules: norbornane, norbornylene, norbornadiene, quadricyclane, bicyclooctene, and 1-fluoroadamantane. Solid-solid, order-disorder phase transitions have been monitored spectroscopically, and the site and factor group symmetries of the crystalline phases have been deduced from the observed solid-state splitting effects.

(2) For all the cage compounds, the phases formed with respect to pressure were identical to those induced by lowering the temperature. The measurement of the pressure hysteresis in quadricyclane and norbornylene enabled the calculation of the volume change at the phase transition. According to the general range of pressure dependences in the various phases, comparisons concerning the compressibilities of the different structures and compounds could be made.

(3) A qualitative method of using pressure dependences of vibrational bands to make spectral assignments has been developed. This procedure has been used to assign specific C-H stretching bands in several of the cage molecules, as well as identifying modes which have large contributions from skeletal stretching motions. Previously, the assignment of these peaks would have necessitated force-field calculations or selective deuteration of the molecules. The behaviour of different types of bonds under pressure has been discussed according to comparisons of force constants and bond lengths. The effect of pressure on vibrational peaks coupled by Fermi resonance has been used to reassign two bands in the Raman spectrum of norbornadiene.

(4) The phase transitions in three structurally-related seven-carbon compounds, norbornane, norbornylene, and norbornadiene, have been explored, and the vibrational spectra of the different solid phases have been described in full.

(5) The solid-state vibrational spectra of an eight- and of a ten-carbon disordered cage compound, bicyclooctene and 1-fluoroadamantane, have also been characterized. There are three solid structures of bicyclooctene: two disordered phases, and an ordered, crystalline solid. Fluoroadamantane undergoes a single solid-solid phase transition, but the lower-temperature phase is not ordered. Further cooling of fluoroadamantane results in the formation of a glass.

(6) The phase behaviour of quadricyclane has been extensively investigated by differential scanning calorimetry and infrared and Raman spectroscopy. Quadricyclane has been shown to undergo a single solid-solid phase transition from a plastically-crystalline phase to an ordered solid. The spectral bands have been reported and partially assigned.

(7) The crystal structure of 1,4-dibromo-cubane has been determined by single-crystal x-ray diffraction. The solid-state infrared and Raman spectra have been shown to correspond very well with group-theoretical predictions based on the crystal structure.

The results of the investigations of norbornylene and norbornadiene have been published in the following journal articles:

N. T. Kawai, I. S. Butler, and D. F. R. Gilson, J. Phys. Chem., **95**, 634 (1991).

N. T. Kawai, D. F. R. Gilson, and I. S. Butler, J. Phys. Chem., **94**, 5729 (1990).